Electromagnetic Properties of Baryons

Dissertation

zur

Erlangung des Doktorgrades (Dr. rer. nat.)

der

Mathematisch-Naturwissenschaftlichen Fakultät

der

Rheinischen Friedrich-Wilhelms-Universität Bonn

vorgelegt von

Christian Haupt

aus

Bonn

Bonn 2006

Angefertigt mit Genehmigung der Mathematisch-Naturwissenschaftlichen Fakultät
der Rheinischen Friedrich-Wilhelms-Universität Bonn.

1. Referent: Prof. Dr. H.-R. Petry
2. Referent: Prof. Dr. U.-G. Meißner

Tag der Promotion: 28.06.2006

Erscheinungsjahr: 2006

to my family

Contents

Introduction and overview

Describing the properties of strongly interacting particles is among the most challenging tasks for modern physics. While it is believed, that quantum chromo dynamics (QCD) is the underlying theory of hadron physics, its application still poses severe problems due to its non-abelian nature. Unlike quantum electro dynamics (QED), QCD exhibits the phenomenon of asymptotic freedom, which leads to the picture of free quarks in the high-energy regime, where perturbative methods are applicable. At low energies, which is the regime of strongly bound states, the running coupling constant of QCD becomes large, which forestalls a naive perturbative treatment. This region is nevertheless accessible through methods, of which the most important we briefly want to review.

In the limit of massless quarks, the Lagrangian of QCD exhibits an additional symmetry. It becomes invariant under chiral transformations. By spontaneously breaking this symmetry, Goldstone bosons appear, which correspond to the light meson octet and constitute the effective degrees of freedom of the theory. A systematic construction of an effective Lagrangian in powers of momenta or derivatives constrained by chiral symmetry becomes possible (see ref. [1]). The theory has been extended to also include baryons in ref. [2]. However being an effective theory, in each order a set of free parameters, so-called low energy constants are introduced, which encode short-distance or higher energy effects and have to be fitted to experimental data.

An attempt to solve QCD from first principles is lattice QCD, which tries to compute the partition function of QCD in a discretized Euclidean space-time numerically. Since this approach makes use of a considerable amount of computational power, simplifying assumptions have been made to reduce computational costs. One of these is the so-called quenched approximation, where vacuum polarization effects are removed from the QCD vacuum. In recent years also unquenched calculations have become available, giving estimates for the errors induced by neglecting fermion dynamics. Since computations become more expensive with light quark masses, the calculation of light baryon properties also poses a problem. Efforts have been made, to connect lattice calculations with chiral perturbation theory by so-called chiral extrapolations, which extrapolate lattice results obtained with large quark masses to the physical masses.

Although both approaches are able to describe certain hadron properties starting from the underlying QCD Lagrangian, they currently do not give a consistent global picture of strong interaction phenomena. By this we mean the simultaneous description of hadron spectra as well as decay observables and electromagnetic properties like charge radii, magnetic moments and form factors. One of the earliest developments in this direction is the nonrelativistic quark model. A phenomenologically motivated lin-

early rising confinement potential accounts for the gross features of the hadron spectra, whereas the fine structure is tuned by a residual interaction inspired by the one-gluon exchange. Surely the nonrelativistic ansatz is doubtful to describe deeply bound states correctly as well as highly excited states and electromagnetic observables at high momentum transfer. Moreover the one-gluon exchange is motivated perturbatively, but in the energy regime of hadrons the strong coupling strength is not small. Also a flavor-independent interaction is likely to fail in the description of the $\pi-\eta-\eta'$ mass splitting. There is however a residual interaction, inspired by instantons (see refs. [3, 4]), which are classical solutions of the Yang-Mills equations, that is able to successfully reproduce the observed mass splitting within a nonrelativistic quark model.

It is thus the next step to incorporate the instanton interaction in a fully relativistic quark model as has been done in refs. [5, 6, 7] in case of baryons and which is the basis for the numerical computations done in this work. It is based on the Bethe-Salpeter equation, which is a suitable starting point in quantum field theory for the description of bound states (see ref. [8] for the original paper) and also is the theoretical foundation for the analytical derivations performed in the present work. The Bethe-Salpeter equation, as being an eight-dimensional integral equation in case of three fermions, poses however conceptional problems, which are due to retardation effects. Neglecting these, results in the Salpeter equation, which was originally derived to compute the fine structure of hydrogen-like atoms (see ref. [9]). In the last years it has served as a basis to formulate quark models, which incorporate the residual instanton force and successfully describe meson and baryon spectra. Within these models also decay observables (see ref. [10]) as well as form factors and transition amplitudes could be computed (see refs. [11, 12]) and led to quite satisfactory results without the introduction of further parameters. These models however predict more states as have been observed in nature, a feature that it shares with other quark models. There are however first hints (see ref. [13]) that these states only couple weakly to the favored production channel, which is πN such that they are not seen in this process.

The aim of this work is to get new access to static properties of relativistic three-fermion systems. We are especially interested in the charge radii and magnetic moments of baryons. Access to this bound state properties is usually gained through the calculation of form factors. The charge radius is defined as the slope of the electric form factor at vanishing four-momentum transfer squared, whereas the magnetic moment is defined as the value of the magnetic form factor at the photon point. This is the usual method for the computation of these quantities (see *e.g.* refs. [11, 12]), but it obscures the underlying structure. It is for example well known how a fermion produces a magnetic moment through both its spin and its angular motion, but how does this translate into the magnetic moment of a bound state, *e.g.* a baryon composed of three quarks? On the other hand static properties in nonrelativistic quantum mechanics can be formulated by means of expectation values involving essentially scalar products of wavefunctions. We seek a synthesis of both approaches, expressing static observables as expectation values with respect to Salpeter amplitudes, which are the intrinsically defined wavefunctions of the Salpeter equation. The emerging operators will show an interesting physical structure and allow for a sensible interpretation. We also expect that this method is numerically more reliable, since no extrapolation of a form factor is necessary and moreover symmetries of the Salpeter amplitudes, which enter the matrix

elements in the rest frame of the baryon, may be fully exploited. Although the analytic results of this work can be extended to arbitrary three-fermion systems in an obvious way, we focus our attention mainly on the study of static baryon properties.

The first chapter of this work is devoted to the introduction of the Bethe-Salpeter formalism. Starting from the six-point Green's function of three fermions interacting among themselves, we introduce an integral equation for the six-point function whose iterative solution consists of a sum of infinitely many Feynman diagrams, needed in order to describe bound states, which show up as poles in the six-point function. By fixing a specific time-ordering, we identify bound states as poles in the total energy variable, thus introducing the so-called Bethe-Salpeter amplitudes. From a Laurent series expansion one simultaneously obtains the Bethe-Salpeter equation and the normalization condition for its solutions, the Bethe-Salpeter amplitudes. Since retardation effects pose severe conceptional problems to the solution of this equation, one introduces the instantaneous approximation, which assumes that the interaction kernels do not depend on the relative energy variables. In addition, the full fermion propagators are replaced by the free ones, thus introducing effective fermion masses. Both approximations allow for a reduction of the eight-dimensional Bethe-Salpeter equation to the six-dimensional Salpeter equation. We also briefly touch upon the problems and its solutions stemming from the unconnected pieces within the two-particle interaction kernels. Since we are mainly concerned with static properties of baryons, a prescription is needed to derive current matrix elements in the present formalism. We show that the six-point function in the presence of an external electromagnetic field leads to a modification of the fermion propagators accounting for the external coupling. By isolating the poles in the total energy variable of the modified six-point function, we derive the desired current matrix element. Since the numerical calculations of this work are devoted to static baryon properties, we briefly introduce the quark model, that we build upon. We show the interaction kernels that have been used, namely a confinement kernel and an instanton induced residual interaction accounting for the fine structure. The discussion of the resulting nucleon spectrum will close this chapter.

In the second chapter we then turn to charge radii of relativistic three-fermion systems in general and especially — concerning the numerical application — to those of baryons. The analytic derivation is based on the formalism developed in the first chapter. The aim is to formulate the charge radius as an expectation value with respect to Salpeter amplitudes. We have at least two options to start from, the first being a definition of the radius of a charge distribution in classical electrodynamics, and the second being the definition of the charge radius as the slope of the electric form factor at the photon point. Common to both approaches is, that the connection to the Bethe-Salpeter formalism is made via the current matrix element derived in the first chapter. We will however see, that both approaches are identical on a generic level, *i.e.* without turning to a specific formalism. Consequently the subsequent derivations are similar. In the first approach we first obtain the Laplacian of the current matrix element with respect to the momentum transfer, which we evaluate before we take the static limit. After integrating out the dependence on the relative energy variables, replacement of the vertex functions with Salpeter amplitudes and symmetrizing over the three fermions, we obtain the desired expression, *i.e.* an expectation value with respect to Salpeter amplitudes. Before we interpret this result, we also follow the sec-

ond approach, by considering the expansion of the boosted Salpeter amplitude, which enters the current matrix element, as an exponential. We are thus able to easily extract the linear term in Q^2 which is relevant for the slope of the form factor at the photon point. The remaining part of the derivation is similar to the first approach and also leads to the same result. We then give a sensible physical interpretation of the resulting expression. It turns out to be the canonical relativistic generalization of the nonrelativistic result. The center of mass motion is accounted for in a natural way. An application of the analytic result is performed within the quark model described in the first chapter. We compute the charge radii of the baryon octet and compare our results to experiment as well as to form factor calculations. The dependence of the nucleon charge radii on the particular choice of the instanton cutoff size and coupling strength are discussed. Whereas the spectrum is almost insensitive to a variation of these parameters, we expect a larger effect on the radii, which we indeed see. Since with the original parameter set the neutron charge radius is too large, we propose new parameters, which describe both the proton as well as the neutron charge radius quite well. We close this chapter with a short comparison of our results with other models.

The third chapter is devoted to magnetic moments of relativistic three-fermion systems. Since a derivation of this observable as an expectation value with respect to Salpeter amplitudes has already been successfully given in ref. [16] — starting however from the energy of a magnetic dipole in an external magnetic field — we want to add a different approach here, that is inspired by the derivation of the charge radius from form factors. We start with the definition of the magnetic moment as the value of the magnetic form factor at the photon point. Since the current matrix element in this definition is divided by $\sqrt{Q^2}$ we need to know the Q^2-dependence of the current matrix element. Following the idea, that was developed in the alternative treatment of the charge radius, we expand the boost of the incoming vertex function as an exponential. We isolate the lowest order term in $\sqrt{Q^2}$ to safely take the static limit. The subsequent steps are similar to the charge radius calculation, *i.e.* integrating out the relative energy variables, replacement of the vertex functions by Salpeter amplitudes and symmetrizing over the three fermions. Because the result turns out to be identical to the one of ref. [16] and is discussed in detail there, we only give a short physical interpretation. The most striking feature of the resulting expression, besides its fully relativistic form and inherent center of mass correction, is the decomposition of the total magnetic moment in contributions originating from the fermion spins and their orbital angular momenta. We apply the result to compute the magnetic moments of the octet and decuplet ground states as well as some selected nucleon excitations, which will be covered by experiment in the future as mentioned in ref. [14]. In case of the octet ground states, the experimental situation according to ref. [15] is good and the model is able to reproduce the empirical values quite accurately. Since the analytic result allows for a separation of spin and orbital angular momentum contributions, we study the magnitude of these. It will turn out, that by far the largest part of roughly 90 % for the baryon octet originates from the quark spins. For the nucleon magnetic moments we then study the evolution of both contributions with smaller quark masses. As we will see, both will become comparable in magnitude, for quark masses nearly as small as the current masses. For the decuplet magnetic moments one also has to include mixed energy contributions as was shown in ref. [16], but not numerically implemented

there. The computation shows, that the contribution of these mixed energy terms is equal in magnitude as compared to the pure energy contributions. Experiments were so far performed to measure the magnetic moments of the Δ^+, Δ^{++} and Ω^-. In case of the Δ resonances, the experimental errors and theoretical uncertainties are however too large at present to allow for a conclusive comparison. Refined experiments are in preparation.

In the fourth chapter we extent the method that was successfully applied to compute charge radii and magnetic moments to arbitrary moments. Since experimental measurements are sparse, we restrict ourselves to an analytical exploration and work exemplary with the charge distribution of a three-fermion system. We introduce an arbitrary moment of this distribution resembling our starting equation for the charge radius but being more general and including the charge radius as a special case. Then by performing similar steps as in the case of the charge radius, we are able to express an arbitrary moment of the electric charge distribution as an expectation value with respect to Salpeter amplitudes. If the moment under consideration has a greater order than two, we also find terms between mixed energy contributions to the vertex functions, which are presumably small in magnitude. The successful extension to higher moments then leads to the question, whether the formalism may be applied to the calculation of form factors as well. The idea is to expand the boost of the incoming Salpeter amplitude as an exponential as it has already been done to derive the charge radius and magnetic moment. The resulting series expansion in powers of the rapidity separates the momentum dependence from static matrix elements in every order. The computation of static matrix elements benefits from simplifications which are due to symmetries of the entering rest-frame Salpeter amplitudes. To check if such an expansion is applicable to the computation of form factors, we take the usual dipole parameterization of the electric proton form factor and expand it in powers of the rapidity. Unfortunately it will show, that the coefficients rise exponentially with the order, such that the expansion cannot be used to calculate the form factor over a large Q^2-range. Nevertheless the expansion shows, that higher orders are determined by static matrix elements similar to the charge radius, which motivates us to study the influence of the instanton cutoff parameter on the form factors. The analysis of the charge radii revealed a strong dependence of the neutron radius on this parameter, whereas the proton radius was only slightly affected. We will see a similar behavior for the form factors. The proton form factor barely depends on the instanton parameters, but the neutron form factor becomes noticeably smaller with an increased cutoff, thus describing the experimental data much better. We also study the impact of a parameter variation on the description of the nucleon-delta transition, which commonly poses a problem to quark models. Unfortunately we see no improvement of this situation.

Chapter 1

Three-particle bound states in the Bethe-Salpeter approach

The aim of the present work is to find new access to static properties of three-particle systems in general and — because of the empirical situation — especially of baryons. In this chapter we therefore present the formalism which is the foundation of the following discussions on static properties. Since the formalism has been intensively discussed in ref. [5], we restrict ourselves to a short description and only put some emphasis on aspects that are important for the subsequent treatment of static properties.

1.1 Introduction and overview

Bound states in nonrelativistic quantum mechanics are described by wavefunctions. To compute observable quantities from those one simply takes the expectation value of suitable operators, which can most easily be deduced from the correspondence principle. Since we however are interested in systems that behave relativistically this is not a suitable starting point. A sounder foundation is given by relativistic quantum field theory. Here the basic quantity which describes the propagation of three fermions interacting among themselves is given by the so-called six-point Green's function. Since bound states show up as poles of this function in the total energy, one is forced to find a way to sum up an infinite number of Feynman diagrams. Indeed the six-point function can be written as an integral equation whose iterative solution consist in a summation of an infinite number of simpler irreducible diagrams. Fixing a specific time-ordering one is able to isolate bound state contributions to the six-point function thus defining the Bethe-Salpeter amplitude. By expanding the six-point function in the vicinity of bound state poles in a Laurent series both the Bethe-Salpeter equation for the Bethe-Salpeter amplitudes as well as a normalization prescription for the Bethe-Salpeter amplitudes emerge. The foregoing will be the content of section 1.2.

In order to solve the Bethe-Salpeter equation in physical cases, relevant for *e.g.* the structure of hadrons, one applies two approximations. First by replacing the full fermion propagators by their free counterparts one introduces effective fermion masses and second by neglecting retardation effects in the interaction kernels the time compo-

nents of the relative four-momentum variables may be integrated over. We will however see that the inclusion of two-particle interaction kernels leads to difficulties stemming from its unconnected peaces. As was shown in ref. [5] this may be overcome by the introduction of an effective three-body interaction kernel which accounts for the effects of the problematic contributions of the two-body interaction. The approximations to the Bethe-Salpeter equation, the effective inclusion of two-particle kernels and the resulting Salpeter equation are the subject of section 1.3. The solutions to the Salpeter equation, describing the bound state, are the so-called Salpeter amplitudes, which may in some sense be viewed as the generalization of the nonrelativistic Schrödinger wavefunctions.

To compute electromagnetic observables in general and especially static properties of the system under consideration we need a prescription of how to compute the electromagnetic vector current from the Salpeter amplitudes. In section 1.4 we will see that this actually consists of two steps, the first of which being the derivation of the current matrix element of the so-called vertex functions and the second being the reconstruction of the vertex functions from the Salpeter amplitudes. We will then transform the resulting current matrix element such that it is better suited to derive static properties from it.

Since we are interested in an application of our analytical results to baryons, we present a quark model in section 1.5, which is based on the Bethe-Salpeter formalism sketched in sections 1.2 and 1.3, and discussed in detail in refs. [6, 7]. We introduce the model interactions, consisting of a linearly rising confinement potential with an appropriate Dirac structure and a residual interaction — based on an effective instanton Lagrangian — accounting for the fine structure of the mass spectra. With only seven parameters this model is able to describe the mass spectra of light baryons up to the highest orbital and radial excitations remarkably well.

1.2 From Green's function to the Bethe-Salpeter equation

1.2.1 The six-point Green's function

The propagation of three fermions interacting among themselves is described by the vacuum expectation value of a time-ordered product of fermion field operators and their adjoints:

$$G_{a_1a_2a_3;a_1'a_2'a_3'}(x_1,x_2,x_3;x_1',x_2',x_3') := -\langle\Omega|T\psi^1_{a_1}(x_1)\psi^2_{a_2}(x_2)\psi^3_{a_3}(x_3)\overline{\psi}^1_{a_1'}(x_1')\overline{\psi}^2_{a_2'}(x_2')\overline{\psi}^3_{a_3'}(x_3')|\Omega\rangle. \quad (1.1)$$

This quantity is called six-point Green's function or correlation function. $\psi^i_{a_i}(x_i)$ are fermion field operators given in the Heisenberg picture, a_i are multi-indices in Dirac-space and any internal space the particle may have, *e.g.* color- and flavor-space in case of quarks. T is the time ordering operator and $|\Omega\rangle$ denotes the physical *i.e.* interacting vacuum. Time-ordered perturbation theory yields a power series of the correlation

function, which we will use in section 1.4 to derive the current matrix element:

$$G_{a_1a_2a_3;a_1'a_2'a_3'}(x_1,x_2,x_3;x_1',x_2',x_3')$$

$$= \frac{-1}{\langle 0|\mathrm{T}\exp\left(-\mathrm{i}\int \mathrm{d}t H_I(t)\right)|0\rangle}\sum_{k=0}^{\infty}\frac{(-\mathrm{i})^k}{k!}\int \mathrm{d}^4y_1\ldots\mathrm{d}^4y_k$$

$$\times\langle 0|\mathrm{T}\psi^1_{a_1}(x_1)\psi^2_{a_2}(x_2)\psi^3_{a_3}(x_3)\overline{\psi}^1_{a_1'}(x_1')\overline{\psi}^2_{a_2'}(x_2')\overline{\psi}^3_{a_3'}(x_3')\mathcal{H}_I(y_1)\ldots\mathcal{H}_I(y_k)|0\rangle, \quad (1.2)$$

where H_I is the Hamilton operator and $\mathcal{H}_I$ its density. $|0\rangle$ denotes the unperturbed vacuum now. The fermion field operators are now given in the interaction picture. In every order of the coupling constant one thus obtains by Wick's theorem a set of Feynman diagrams which have to be evaluated. In high energy scattering processes it may be sufficient to cut the expansion at some finite order. Since we are however interested in bound states, which lead to poles in the six-point Green's function, we need a way to go beyond perturbation theory, because a pole will never show up by considering only a finite number of Feynman diagrams.

1.2.2 An integral equation for the six-point function

A possible solution to this problem is to write down an integral equation whose iterative solution leads to a summation of an infinite number of Feynman diagrams. The basic idea can be found in refs. [8, 17, 18]. For the three-particle correlator, the integral equation looks as follows:

$$G_{a_1a_2a_3;a_1'a_2'a_3'}(x_1,x_2,x_3;x_1',x_2',x_3') = S^1_{F\,a_1a_2}(x_1,x_1')\,S^2_{F\,a_2a_2}(x_2,x_2')\,S^3_{F\,a_3a_2}(x_3,x_3')$$

$$-\mathrm{i}\int \mathrm{d}^4y_1\,\mathrm{d}^4y_2\,\mathrm{d}^4y_3\,S^1_{F\,a_1b_2}(x_1,y_1)\,S^2_{F\,a_2b_2}(x_2,y_2)\,S^3_{F\,a_3b_2}(x_3,y_3)$$

$$\times\int \mathrm{d}^4y_1'\,\mathrm{d}^4y_2'\,\mathrm{d}^4y_3'\,K^{(3)}_{b_1,b_2,b_3;b_1',b_2',b_3'}(y_1,y_2,y_3;y_1',y_2',y_3')G_{b_1',b_2',b_3';a_1',a_2',a_3'}(y_1',y_2',y_3';x_1',x_2',x_3')$$

$$-\mathrm{i}\sum_{\text{cycl. perm.}}\int \mathrm{d}^4y_1\,\mathrm{d}^4y_2\,S^1_{F\,a_1b_1}(x_1,y_1)\,S^2_{F\,a_2b_2}(x_2,y_2)$$

$$\times\int \mathrm{d}^4y_1'\,\mathrm{d}^4y_2'\,K^{(2)}_{b_1,b_2;b_1',b_2'}(y_1,y_2;y_1',y_2')G_{b_1',b_2',a_3;a_1',a_2',a_3'}(y_1',y_2',x_3;x_1',x_2',x_3'). \quad (1.3)$$

A summation over repeated indices b_i and b_i' is implicitly understood. The full fermion Feynman propagator is defined as:

$$S^i_{F\,a_ia_i'}(x_i,x_i') = \langle 0|T\psi^i_{a_i}(x_i)\overline{\psi}^i_{a_i'}(x_i')|0\rangle. \quad (1.4)$$

$K^{(3)}$ and $K^{(2)}$ are irreducible two- and three-particle kernels containing the sum of all diagrams, which cannot be separated in simpler diagrams by cutting only three or two fermion lines respectively. By introducing the inverse Feynman propagator through

$$\int \mathrm{d}^4y_i\,S^i_{F\,a_ib}(x_i,y_i)\,S^{i\,-1}_{F\,ba_i'}(y_i,x_i') = \delta_{a_ia_i'}\,\delta(x_i-x_i'), \quad (1.5)$$

one may write the irreducible two-particle kernel in a compact form:

$$\overline{K}^{(2)}_{a_1,a_2,a_3;a_1',a_2',a_3'}(x_1,x_2,x_3;x_1',x_2',x_3') := \sum_{\text{cycl. Perm.}} K^{(2)}_{a_i,a_j;a_i',a_j'}(x_i,x_j;x_i',x_j') S^i_{F\,a_i a_i'}(x_i,x_i'). \tag{1.6}$$

Let us denote the sum of the irreducible two- and three-particle kernels $K := K^{(3)} + \overline{K}^{(2)}$. The triple product of fermion propagators appearing in the integral equation (1.3) shall be denoted by:

$$G_{0a_1,a_2,a_3;a_1',a_2',a_3'}(x_1,x_2,x_3;x_1',x_2',x_3') := S^1_{F\,a_1a_1'}(x_1,x_1')\, S^2_{F\,a_2a_2'}(x_2,x_2')\, S^3_{F\,a_3a_3'}(x_3,x_3'). \tag{1.7}$$

In this and further sections we make use of a compact operator product notation which we want to introduce here:

$$[AB]_{a_1,a_2,a_3;a_1',a_2',a_3'}(x_1,x_2,x_3;x_1',x_2',x_3') := \int \mathrm{d}^4y_1\,\mathrm{d}^4y_2\,\mathrm{d}^4y_3$$

$$\times A_{a_1,a_2,a_3;b_1,b_2,b_3}(x_1,x_2,x_3;y_1,y_2,y_3)\, B_{b_1,b_2,b_3;a_1',a_2',a_3'}(y_1,y_2,y_3;x_1',x_2',x_3') \tag{1.8}$$

This notation finally allows us to write the integral equation in a compact form by omitting multi indices and arguments:

$$G = G_0 - \mathrm{i}\, G_0\, K\, G. \tag{1.9}$$

Because of translational invariance it is convenient to introduce a center-of-mass coordinate X and so-called Jacobi coordinates ξ and η:

$$\begin{aligned} X &:= \tfrac{1}{3}(x_1+x_2+x_3) & x_1 &= X + \tfrac{1}{2}\xi + \tfrac{1}{3}\eta \\ \xi &:= x_1 - x_2 & x_2 &= X - \tfrac{1}{2}\xi + \tfrac{1}{3}\eta \\ \eta &:= \tfrac{1}{2}(x_1+x_2-2x_3) & x_3 &= X - \tfrac{2}{3}\eta. \end{aligned} \tag{1.10}$$

The corresponding conjugate momenta are then given by the total four momentum P and the two relative momenta p_ξ and p_η:

$$\begin{aligned} P &:= p_1+p_2+p_3 & p_1 &= \tfrac{1}{3}P + p_\xi + \tfrac{1}{2}p_\eta \\ p_\xi &:= \tfrac{1}{2}(p_1-p_2) & p_2 &= \tfrac{1}{3}P - p_\xi + \tfrac{1}{2}p_\eta \\ p_\eta &:= \tfrac{1}{3}(p_1+p_2-2p_3) & p_3 &= \tfrac{1}{3}P - p_\eta. \end{aligned} \tag{1.11}$$

Due to energy-momentum conservation the integral equation in momentum space is only an eight-dimensional integral equation depending only parametrically on the total four momentum P. We thus define the Fourier transform of the objects appearing in the integral equation as follows:

$$[\mathcal{F}A](p_1,p_2,p_3;p_1',p_2',p_3') := \int \mathrm{d}^4x_1\,\mathrm{d}^4x_2\,\mathrm{d}^4x_3,\, e^{\mathrm{i}\left(\langle p_1,x_1\rangle+\langle p_2,x_2\rangle+\langle p_3,x_3\rangle\right)}$$

$$\times \int \mathrm{d}^4x_1'\,\mathrm{d}^4x_2'\,\mathrm{d}^4x_3'\, e^{-\mathrm{i}\left(\langle p_1',x_1'\rangle+\langle p_2',x_2'\rangle+\langle p_3',x_3'\rangle\right)} A(x_1,x_2,x_3;x_1',x_2',x_3')$$

$$= (2\pi)^4\delta^{(4)}(P-P')A_P(p_\xi,p_\eta;p_\xi',p_\eta'), \tag{1.12}$$

where $\langle \cdot\,, \cdot \rangle$ is the usual Minkowski scalar product. Parametrical dependence on the total four-momentum is now indicated by an index "P". We may define the Fourier transform of $\overline{K}^{(2)}$ in a similar way by introducing two-particle relative coordinates:

$$\overline{K}^{(2)}_{P\,a_1a_2a_3;a_1',a_2',a_3'}(p_\xi,p_\eta;p_\xi',p_\eta') = \sum_{(i,j,k)} K^{(2)}_{(\frac{2}{3}P+p_{\eta_k})\,a_ia_j;\,a_i'a_j'}(p_{\xi_k}-p'_{\eta_k}) \times S^k_{F\,a_ka_k'}{}^{-1}(\tfrac{1}{3}P-p_{\eta_k})(2\pi)^4\,\delta^{(4)}(p_{\eta_k}-p'_{\eta_k}), \quad (1.13)$$

where $p_{\xi_3} = p_\xi$ and $p_{\eta_3} = p_\eta$. The two other sets of two-particle coordinates are obtained by cyclic permutation of this set. The integral equation (1.3) in momentum space now takes the following form:

$$\begin{aligned} G_P(p_\xi,p_\eta;p_\xi',p_\eta') &= S_F^1(\tfrac{1}{3}P+p_\xi+\tfrac{1}{2}p_\eta)\otimes S_F^2(\tfrac{1}{3}P-p_\xi+\tfrac{1}{2}p_\eta)\otimes S_F^3(\tfrac{1}{3}P-p_\eta) \\ &\quad\times(2\pi)^4\delta^{(4)}(p_\xi-p_\xi')(2\pi)^4\delta^{(4)}(p_\eta-p_\eta') \\ &\quad-\mathrm{i}\,S_F^1(\tfrac{1}{3}P+p_\xi+\tfrac{1}{2}p_\eta)\otimes S_F^2(\tfrac{1}{3}P-p_\xi+\tfrac{1}{2}p_\eta)\otimes S_F^2(\tfrac{1}{3}P-p_\eta) \\ &\quad\times\int\frac{\mathrm{d}^4p_\xi''}{(2\pi)^4}\frac{\mathrm{d}^4p_\eta''}{(2\pi)^4}K_P(p_\xi,p_\eta;p_\xi'',p_\eta'')G_P(p_\xi'',p_\eta'';p_\xi',p_\eta'). \end{aligned} \quad (1.14)$$

The analog of the compact operator product notation (1.8) in momentum space is defined by:

$$[A_PB_P] := \int\frac{\mathrm{d}^4p_\xi''}{(2\pi)^4}\frac{\mathrm{d}^4p_\eta''}{(2\pi)^4}A_P(p_\xi,p_\eta;p_\xi'',p_\eta'')B_P(p_\xi'',p_\eta'';p_\xi',p_\eta'), \quad (1.15)$$

which allows us to write the momentum space integral equation in a compact form:

$$G_P = G_{0\,P} - \mathrm{i}\,G_{0\,P}\,K_P\,G_P. \quad (1.16)$$

The six-point Green's function contains in general the propagation of anti-fermions as well as scattering and bound states. To isolate the contributions of three-fermion bound states, we fix the time ordering $(x_1^0,x_2^0,x_3^0 > {x_1'}^0,{x_2'}^0,{x_3'}^0)$:

$$\begin{aligned} &G_{a_1a_2a_3;a_1'a_2'a_3'}(x_1,x_2,x_3;x_1',x_2',x_3') \\ &\quad= -\langle\Omega|T\{\psi^1_{a_1}(x_1)\psi^2_{a_2}(x_2)\psi^3_{a_3}(x_3)\}T\{\overline{\psi}^1_{a_1'}(x_1')\overline{\psi}^2_{a_2'}(x_2')\overline{\psi}^3_{a_3'}(x_3')\}|\Omega\rangle \\ &\quad\times\theta\Big(\min(x_1^0,x_2^0,x_3^0)-\max({x_1'}^0,{x_2'}^0,{x_3'}^0)\Big)+\text{different time orderings}. \end{aligned} \quad (1.17)$$

To separate the contributions of states with mass M and energy $\omega_{\vec{P}} = \sqrt{|\vec{P}|^2+M^2}$, one inserts a complete set of intermediate states $|\bar{P}\rangle$ with total four-momentum $\bar{P} = (\omega_{\vec{P}},\vec{P})$ and mass $\bar{P}^2 = M^2$ in between the time ordered products. The states $|\bar{P}\rangle$ are eigenstates of the total four-momentum operator $\hat{P} = \hat{p}_1+\hat{p}_2+\hat{p}_3$:

$$\hat{P}|\bar{P}\rangle = \bar{P}|\bar{P}\rangle, \quad (1.18)$$

and normalized in a Lorentz-invariant fashion:

$$\langle \bar{P}|\bar{P}'\rangle = 2\omega_{\vec{P}}\,(2\pi)^3\,\delta^{(3)}(\vec{P}-\vec{P}'). \tag{1.19}$$

After inserting these states we have:

$$\begin{aligned} &G_{a_1a_2a_3;a_1'a_2'a_3'}(x_1,x_2,x_3;x_1',x_2',x_3') \\ &= -\int \frac{\mathrm{d}^3P}{(2\pi)^3 2\omega_{\vec{P}}} \langle\Omega|T\{\psi^1_{a_1}(x_1)\psi^2_{a_2}(x_2)\psi^3_{a_3}(x_3)\}|\bar{P}\rangle\langle\bar{P}|T\{\overline{\psi}^1_{a_1'}(x_1')\overline{\psi}^2_{a_2'}(x_2')\overline{\psi}^3_{a_3'}(x_3')\}|\Omega\rangle \\ &\qquad\times\,\theta\Big(\min(x_1^0,x_2^0,x_3^0)-\max({x_1'}^0,{x_2'}^0,{x_3'}^0)\Big) + \text{different terms.} \end{aligned} \tag{1.20}$$

"Different terms" now contain contributions of different time-orderings as well as different intermediate states. The Bethe-Salpeter amplitude and its adjoint is defined as follows:

$$\chi_{\bar{P}\,a_1a_2a_3}(x_1,x_2,x_3) := \langle\Omega|T\{\psi^1_{a_1}(x_1)\psi^2_{a_2}(x_2)\psi^3_{a_3}(x_3)\}|\bar{P}\rangle \tag{1.21}$$

$$\overline{\chi}_{\bar{P}\,a_1'a_2'a_3'}(x_1',x_2',x_3') := \langle\bar{P}|T\{\overline{\psi}^1_{a_1'}(x_1')\overline{\psi}^2_{a_2'}(x_2')\overline{\psi}^3_{a_3'}(x_3')\}|\Omega\rangle. \tag{1.22}$$

Because of space-time translation invariance, the dependence on the total four-momentum factorizes:

$$\begin{aligned} \chi_{\bar{P}a_1a_2a_3}(x_1,x_2,x_3) &= e^{-\mathrm{i}\langle\bar{P},X\rangle}\chi_{\bar{P}a_1a_2a_3}(\xi,\eta) \\ &=: e^{-\mathrm{i}\langle\bar{P},X\rangle}\int\frac{\mathrm{d}^4p_\xi}{(2\pi)^4}\frac{\mathrm{d}^4p_\eta}{(2\pi)^4}e^{-\mathrm{i}\langle p_\xi,\xi\rangle}e^{-\mathrm{i}\langle p_\eta,\eta\rangle}\chi_{\bar{P}a_1a_2a_3}(p_\xi,p_\eta). \end{aligned} \tag{1.23}$$

By the Θ-function in eq. (1.20) a pole in the total energy variable is generated when Fourier transforming G into momentum space:

$$G_P(p_\xi,p_\eta;p_\xi',p_\eta') = \frac{-\mathrm{i}}{2\omega_{\vec{P}}}\frac{\chi_{\bar{P}}(p_\xi,p_\eta)\overline{\chi}_{\bar{P}}(p_\xi',p_\eta')}{P^0-\omega_{\vec{P}}+\mathrm{i}\,\epsilon} + \text{regular terms for } P^0\to\omega_{\vec{P}}. \tag{1.24}$$

1.2.3 The three-fermion Bethe-Salpeter equation

One obtains the Bethe-Salpeter equation simultaneously with a normalization condition for the Bethe-Salpeter amplitudes by a Laurent expansion of the integral equation (1.16) in the vicinity of a bound state pole (see ref. [5]). The Bethe-Salpeter equation for the Bethe-Salpeter amplitude in momentum space then reads as follows:

$$\begin{aligned} \chi_{\bar{P}a_1a_2a_3}(p_\xi,p_\eta) &= S^1_{Fa_1a_1'}(\tfrac{1}{3}\bar{P}+p_\xi+\tfrac{1}{2}p_\eta)S^2_{Fa_2a_2'}(\tfrac{1}{3}\bar{P}-p_\xi+\tfrac{1}{2}p_\eta)S^3_{Fa_3a_3'}(\tfrac{1}{3}\bar{P}-p_\eta) \\ &\quad\times(-\mathrm{i})\int\frac{\mathrm{d}^4p_\xi'}{(2\pi)^4}\frac{\mathrm{d}^4p_\eta'}{(2\pi)^4}K^{(3)}_{a_1'a_2'a_3';a_1''a_2''a_3''}(\bar{P},p_\xi,p_\eta,p_\xi',p_\eta')\chi_{\bar{P}a_1''a_2''a_3''}(p_\xi',p_\eta') \\ &\quad+\sum_{\text{cycl. perm.}} S^1_{Fa_1a_1'}(\tfrac{1}{3}\bar{P}+p_\xi+\tfrac{1}{2}p_\eta)S^2_{Fa_2a_2'}(\tfrac{1}{3}\bar{P}-p_\xi+\tfrac{1}{2}p_\eta) \\ &\qquad\times(-\mathrm{i})\int\frac{\mathrm{d}^4p_\xi'}{(2\pi)^4}K^{(2)}_{12\;a_1'a_2';a_1''a_2''}(\tfrac{2}{3}\bar{P}+p_\eta,p_\xi,p_\xi')\chi_{\bar{P}a_1''a_2''a_3}(p_\xi',p_\eta), \end{aligned} \tag{1.25}$$

where summation over repeated multi indices is tacitly understood. In compact operator product notation, the Bethe-Salpeter equation simply reads:

$$\chi_{\bar{P}} = -\mathrm{i}G_0 \left(K^{(3)} + \bar{K}^{(2)}\right) \chi_{\bar{P}}, \tag{1.26}$$

where a summation over multi-indices and momentum integrations is again tacitly understood. The normalization condition, that emerged from the Laurent expansion reads in a covariant form:

$$-\mathrm{i}\overline{\chi}_{\bar{P}} \left[P^\mu \frac{\partial}{\partial P^\mu} \left(G_0^{-1} + \mathrm{i}K^{(3)} + \mathrm{i}K^{(2)}\right)\right]_{P=\bar{P}} \chi_{\bar{P}} = 2M^2, \tag{1.27}$$

where we introduced the inverse three-particle propagator:

$$\begin{aligned} {G_0^{-1}}_{a_1a_2a_3;a_1'a_2'a_3'}(P, p_\xi, p_\eta, p_\xi', p_\eta') &:= (2\pi)^2\delta^{(4)}(p_\xi - p_\xi')(2\pi)^4\delta^{(4)}(p_\eta - p_\eta') \\ &\times {S_F^{1}}^{-1}_{a_1a_1'}(\tfrac{1}{3}\bar{P} + p_\xi + \tfrac{1}{2}p_\eta){S_F^{2}}^{-1}_{a_2a_2'}(\tfrac{1}{3}\bar{P} - p_\xi + \tfrac{1}{2}p_\eta){S_F^{3}}^{-1}_{a_3a_3'}(\tfrac{1}{3}\bar{P} - p_\eta). \end{aligned} \tag{1.28}$$

As already mentioned, the Bethe-Salpeter equation at the current status is phenomenologically applicable only within the framework of certain approximations which will be the content of the next section.

1.3 Approximations and the Salpeter equation

1.3.1 Approximations

The Bethe-Salpeter equation as presented in the previous section is exact. Its normalized solutions would result in the excitation spectra of baryons for example. However the two- and three-particle kernels are only defined within perturbation theory and the quark propagators are not known for physically interesting theories like QCD. Moreover the dependence on the relative energies cannot be handled at present. To overcome those obstacles, approximations have to be made, the first of which is the replacement of the full quark propagators by the free ones:

$$S_F^i(p_i) = \frac{\mathrm{i}}{\not{p}_i - m_i + \mathrm{i}\epsilon} \tag{1.29}$$

This approximation accounts for self-energy contributions merely by the introduction of effective fermion masses m_i. In case of QCD, this replacement corresponds to the point of view, that hadrons consist of quarks acquiring an effective constituent mass m_i, which is however treated as a free parameter in the framework described in refs. [5, 6, 7].

Neglecting retardation effects in the interaction kernels leads to the instantaneous approximation. This assumes that there is no dependence on the relative energies in

the rest frame of the baryon:

$$K^{(3)}(P, p_\xi, p_\eta, p'_\xi, p'_\eta)\Big|_{P=(M,\mathbf{0})} = V^{(3)}(\boldsymbol{p_\xi}, \boldsymbol{p_\eta}, \boldsymbol{p'_\xi}, \boldsymbol{p'_\eta}) \tag{1.30}$$

$$K^{(2)}(\tfrac{2}{3}P + p_\eta, p_\xi, p'_\xi)\Big|_{P=(M,\mathbf{0})} = V^{(2)}(\boldsymbol{p_\xi}, \boldsymbol{p'_\xi}) \tag{1.31}$$

These conditions can be formulated in any reference frame, if all momenta are replaced by:

$$p_\perp := p - \frac{\langle p, P\rangle}{P^2} P. \tag{1.32}$$

This space-like vector is perpendicular to the total four momentum and in the rest frame of the baryon has the desired form $p_\perp = (0, \boldsymbol{p})$. Thus formal covariance of the Bethe Salpeter equation is maintained.

1.3.2 Reduction to the Salpeter equation

Having outlined the approximations, we now demonstrate how the Bethe-Salpeter equation — which is an eight-dimensional integral equation — can be reduced to a six-dimensional integral equation, the so called Salpeter equation. The basic idea is to integrate out the dependence on the relative energies. This procedure is straightforward if there are only three particle kernels, which is the case for example in the Δ-baryon spectrum in the specific model considered here. However if there remains a residual two-body interaction, the unconnected peace of $K^{(2)}$ introduces a dependence on the relative energies, which spoils this reduction scheme. Nevertheless it is possible to formulate the reduction by introducing an effective three-body kernel accounting for the two-body interactions.

Let us begin with the case $K^{(2)} = 0$ to sketch the general procedure. In this case the Bethe-Salpeter equation is given by

$$\chi_{\bar{P}} = -\mathrm{i} G_0 V^{(3)} \chi_{\bar{P}}. \tag{1.33}$$

Since $V^{(3)}$ depends only on the spatial components of the relative momenta we may perform the integration over the relative energies in the operator product $V^{(3)}\chi_{\bar{P}}$ leading to the definition of the Salpeter amplitude:

$$\Phi_M(\boldsymbol{p_\xi}, \boldsymbol{p_\eta}) := \int \frac{\mathrm{d}p^0_\xi}{2\pi} \frac{\mathrm{d}p^0_\xi}{2\pi} \chi_M(p_\xi, p_\eta). \tag{1.34}$$

The Bethe-Salpeter equation then takes the form

$$\chi_M = -\mathrm{i} G_0 V^{(3)} \Phi_M := -\mathrm{i} G_0 \Gamma_M, \tag{1.35}$$

where we defined the so called vertex functions Γ, which in the rest frame of the baryon do not depend on the relative energies. Note that this equation can also be used to reconstruct the full Bethe-Salpeter amplitude once the Salpeter amplitude is known. We may once again integrate over p^0_ξ and p^0_η on both sides. To isolate the poles in the

relative energy variables in G_0, the fermion propagators are replaced by their partial fraction decomposition

$$S_F^i(p_i) = \mathrm{i}\left(\frac{\Lambda_i^+(\boldsymbol{p_i})}{p_i^0 - \omega_i(\boldsymbol{p_i}) + \mathrm{i}\epsilon} + \frac{\Lambda_i^-(\boldsymbol{p_i})}{p_i^0 + \omega_i(\boldsymbol{p_i}) - \mathrm{i}\epsilon}\right)\gamma^0, \tag{1.36}$$

where the single-particle relativistic energies ω_i are defined as usual:

$$\omega_i(\boldsymbol{p_i}) = \sqrt{|\boldsymbol{p_i}|^2 + m_i^2}. \tag{1.37}$$

The operators $\Lambda_i^\pm(\boldsymbol{p_i})$ project onto positive and negative energy solutions of the Dirac equation and are given explicitly by

$$\Lambda_i^\pm(\boldsymbol{p_i}) = \frac{\omega_i(\boldsymbol{p_i}) \pm H_i(\boldsymbol{p_i})}{2\omega_i(\boldsymbol{p_i})} \tag{1.38}$$

with the Dirac Hamiltonian

$$H_i(\boldsymbol{p_i}) = \boldsymbol{\alpha}\cdot\boldsymbol{p_i} + m_i\beta. \tag{1.39}$$

Now the integration can be performed. Using Cauchy's theorem we obtain at first:

$$\begin{aligned}
&\int \frac{\mathrm{d}p_\xi^0}{2\pi}\frac{\mathrm{d}p_\xi^0}{2\pi} G_0(P, p_\xi, p_\eta, p'_\xi, p'_\eta) \\
&= \mathrm{i}\left[\frac{\Lambda_1^+(\boldsymbol{p_1})\otimes\Lambda_2^+(\boldsymbol{p_2})\otimes\Lambda_3^+(\boldsymbol{p_3})}{M - \omega_1(\boldsymbol{p_1}) - \omega_2(\boldsymbol{p_2}) - \omega_3(\boldsymbol{p_3}) + \mathrm{i}\epsilon} + \frac{\Lambda_1^-(\boldsymbol{p_1})\otimes\Lambda_2^-(\boldsymbol{p_2})\otimes\Lambda_3^-(\boldsymbol{p_3})}{M + \omega_1(\boldsymbol{p_1}) + \omega_2(\boldsymbol{p_2}) + \omega_3(\boldsymbol{p_3}) - \mathrm{i}\epsilon}\right] \\
&\qquad \times \gamma^0\otimes\gamma^0\otimes\gamma^0 (2\pi)^3\delta^{(3)}(\boldsymbol{p_\xi} - \boldsymbol{p'_\xi})(2\pi)^3\delta^{(3)}(\boldsymbol{p_\eta} - \boldsymbol{p'_\eta}).
\end{aligned} \tag{1.40}$$

Finally we end up with the Salpeter equation by integrating over p_ξ^0 and p_η^0 in (1.35):

$$\begin{aligned}
\Phi_M(\boldsymbol{p_\xi}, \boldsymbol{p_\eta}) = &\left[\frac{\Lambda^{+++}}{(M - \Omega + \mathrm{i}\epsilon)} + \frac{\Lambda^{---}}{(M + \Omega - \mathrm{i}\epsilon)}\right]\gamma^0\otimes\gamma^0\otimes\gamma^0 \\
&\times \int \frac{\mathrm{d}^3p'_\xi}{(2\pi)^3}\frac{\mathrm{d}^3p'_\eta}{(2\pi)^3} V^{(3)}(\boldsymbol{p_\xi}, \boldsymbol{p_\eta}, \boldsymbol{p'_\xi}, \boldsymbol{p'_\eta})\Phi_M(\boldsymbol{p'_\xi}, \boldsymbol{p'_\xi}),
\end{aligned} \tag{1.41}$$

where we introduced the shorthand notations

$$\Lambda^{\pm\pm\pm} := \Lambda_1^\pm(\boldsymbol{p_1})\otimes\Lambda_2^\pm(\boldsymbol{p_2})\otimes\Lambda_3^\pm(\boldsymbol{p_3}) \tag{1.42a}$$

$$\Omega := \omega_1(\boldsymbol{p_1}) + \omega_2(\boldsymbol{p_2}) + \omega_3(\boldsymbol{p_3}). \tag{1.42b}$$

Because of the special projector structure in (1.40), the solutions to the Salpeter equation (1.41) are eigenstates of the Salpeter projector

$$\Lambda(\boldsymbol{p_\xi}, \boldsymbol{p_\eta}) := \Lambda^{+++} + \Lambda^{---}. \tag{1.43}$$

Consequently the Salpeter amplitudes involve only purely positive and negative energy components:

$$\Phi_M = \Lambda\Phi_M = \Phi_M^{+++} + \Phi_M^{---} := \Phi_M^\Lambda. \tag{1.44}$$

From this it is clear, that only the projected part $V_\Lambda^{(3)} := \bar{\Lambda} V^{(3)} \Lambda$ is of importance in the Salpeter equation (1.41). Here we defined $\bar{\Lambda} := \gamma^0 \otimes \gamma^0 \otimes \gamma^0 \Lambda \gamma^0 \otimes \gamma^0 \otimes \gamma^0$.

The situation changes, if we also include two-body interactions. Then the residual part

$$V_R^{(3)} := V^{(3)} - V_\Lambda^{(3)} \tag{1.45}$$

becomes important. Because $V_R^{(3)}$ appears only in conjunction with $\overline{K}_M^{(2)}$ (see ref. [5]), one defines the following resolvent:

$$\mathcal{G}_M \left[G_{0\,M}^{-1} + \mathrm{i}\, V_R^{(3)} + \mathrm{i}\, \overline{K}_M^{(2)} \right] = \mathbb{1}, \tag{1.46}$$

which allows us to recast the Bethe-Salpeter equation in the following form:

$$\chi_M = -\mathrm{i}\, \mathcal{G}_M\, V_\Lambda^{(3)}\, \chi_M. \tag{1.47}$$

All problematic contributions are now contained within the resolvent $\mathcal{G}_M$, which fulfills the following integral equation:

$$\mathcal{G}_M = G_{0\,M} - \mathrm{i}\, G_{0\,M} \left[V_R^{(3)} + \overline{K}_M^{(2)} \right] \mathcal{G}_M. \tag{1.48}$$

The reduction can now be performed because $V_\Lambda^{(3)}$ does not depend on the relative energies and we first obtain from the Bethe-Salpeter equation (1.47):

$$\chi_M = -\mathrm{i}\, \mathcal{G}_M V_\Lambda^{(3)}\, \Phi_M^\Lambda. \tag{1.49}$$

Integrating over p_ξ^0 and p_η^0 on both sides of eq. (1.49) and multiplying from the left with the Salpeter projector Λ then yields:

$$\Phi_M^\Lambda = -\mathrm{i}\, \langle \mathcal{G}_M \rangle_\Lambda\, V^{(3)}\, \Phi_M^\Lambda. \tag{1.50}$$

Here we defined the reduction of $\mathcal{G}_M$:

$$\langle \mathcal{G}_M \rangle_\Lambda(\boldsymbol{p_\xi}, \boldsymbol{p_\eta}, \boldsymbol{p'_\xi}, \boldsymbol{p'_\eta}) := \Lambda(\boldsymbol{p_\xi}, \boldsymbol{p_\eta}) \int \frac{\mathrm{d}p_\xi^0}{2\pi} \frac{\mathrm{d}p_\eta^0}{2\pi} \frac{\mathrm{d}p'^0_\xi}{2\pi} \frac{\mathrm{d}p'^0_\eta}{2\pi} \mathcal{G}_M(p_\xi, p_\eta, p'_\xi, p'_\eta)\, \overline{\Lambda}(\boldsymbol{p'_\xi}, \boldsymbol{p'_\eta}). \tag{1.51}$$

With the Neumann series of $\mathcal{G}_M$ from (1.48) one can represent $\langle \mathcal{G}_M \rangle_\Lambda$ as a power series with respect to $V_R^{(3)} + \overline{K}_M^{(2)}$:

$$\langle \mathcal{G}_M \rangle_\Lambda = \langle G_{0\,M} \rangle + \Lambda \Big\langle G_{0\,M} (-\mathrm{i}) \left[V_R^{(3)} + \overline{K}_M^{(2)} \right] G_{0\,M} \Big\rangle \overline{\Lambda} + \dots . \tag{1.52}$$

This expansion allows to identify the reducible and irreducible diagrams, where reducibility is now defined with respect to the reduced Salpeter propagator $\langle G_{0\,M} \rangle$. Thus we are looking for an effective irreducible kernel V_M^{eff} such that $\langle \mathcal{G}_M \rangle_\Lambda$ is the solution of the following integral equation:

$$\langle \mathcal{G}_M \rangle_\Lambda \stackrel{!}{=} \langle G_{0\,M} \rangle - \mathrm{i}\, \langle G_{0\,M} \rangle\, V_M^{\mathrm{eff}}\, \langle \mathcal{G}_M \rangle_\Lambda. \tag{1.53}$$

From (1.53) we see, that only the projected part of V_M^{eff} onto the subspace of purely positive and negative components appears. To determine V_M^{eff} uniquely it is therefore reasonable to demand:

$$\overline{\Lambda}\, V_M^{\mathrm{eff}} = V_M^{\mathrm{eff}}\, \Lambda = V_M^{\mathrm{eff}}. \tag{1.54}$$

Finally we get the Salpeter equation from (1.50) and (1.53):

$$\Phi_M^\Lambda = -\mathrm{i}\,\langle G_{0\,M}\rangle\,\left[V^{(3)} + V_M^{\mathrm{eff}}\right]\Phi_M^\Lambda. \tag{1.55}$$

To determine V_M^{eff} we insert the integral equation for $\langle\mathcal{G}_M\rangle_\Lambda$ (1.53) and $\mathcal{G}_M$ (1.48) into (1.51). Together with the restriction (1.54) we find a unique power series expansion of V_M^{eff} in orders i of the integral kernel $V_R^{(3)} + \overline{K}_M^{(2)}$ (see ref. [5]):

$$V_M^{\mathrm{eff}} = \sum_{i=1}^{\infty} V_M^{\mathrm{eff}(i)}. \tag{1.56}$$

If the power series is cut at some finite $k < \infty$, one obtains through the solution of

$$\Phi_M^{\Lambda\,(k)} = -\mathrm{i}\,\langle G_{0\,M}\rangle\,\left[V_\Lambda^{(3)} + \sum_{i=1}^{k} V_M^{\mathrm{eff}(i)}\right]\Phi_M^{\Lambda\,(k)} \tag{1.57}$$

an approximation of the Salpeter amplitude.

1.3.3 Born approximation

In first order of V_M^{eff} in (1.56) (Born approximation) the Salpeter equation may be written as an eigenvalue problem:

$$\mathcal{H}\,\Phi_M^\Lambda = M\,\Phi_M^\Lambda \tag{1.58}$$

(see refs. [5]), where the so called Salpeter Hamiltonian $\mathcal{H}$ in Born approximation is independent of the Mass M of the bound system:

$$\begin{aligned}
\left[\mathcal{H}\Phi_M^\Lambda\right](\boldsymbol{p_\xi},\boldsymbol{p_\eta}) &= \left[H_1(\boldsymbol{p_1})\otimes\mathbb{1}\otimes\mathbb{1} + \mathbb{1}\otimes H_2(\boldsymbol{p_2})\otimes\mathbb{1} + \mathbb{1}\otimes\mathbb{1}\otimes H_3(\boldsymbol{p_3})\right]\,\Phi_M^\Lambda(\boldsymbol{p_\xi},\boldsymbol{p_\eta}) \\
&+ \left[\Lambda_1^+(\boldsymbol{p_1})\otimes\Lambda_2^+(\boldsymbol{p_2})\otimes\Lambda_3^+(\boldsymbol{p_3}) + \Lambda_1^-(\boldsymbol{p_1})\otimes\Lambda_2^-(\boldsymbol{p_2})\otimes\Lambda_3^-(\boldsymbol{p_3})\right]\gamma^0\otimes\gamma^0\otimes\gamma^0 \\
&\quad\times\int\frac{\mathrm{d}^3p'_\xi}{(2\pi)^3}\frac{\mathrm{d}^3p'_\eta}{(2\pi)^3}\,V^{(3)}(\boldsymbol{p_\xi},\boldsymbol{p_\eta};\boldsymbol{p'_\xi},\boldsymbol{p'_\eta}) \\
&+ \left[\Lambda_1^+(\boldsymbol{p_1})\otimes\Lambda_2^+(\boldsymbol{p_2})\otimes\Lambda_3^+(\boldsymbol{p_3}) - \Lambda_1^-(\boldsymbol{p_1})\otimes\Lambda_2^-(\boldsymbol{p_2})\otimes\Lambda_3^-(\boldsymbol{p_3})\right]\gamma^0\otimes\gamma^0\otimes\mathbb{1} \\
&\quad\times\int\frac{\mathrm{d}^3p'_\xi}{(2\pi)^3}\,V^{(2)}(\boldsymbol{p'_\xi},\boldsymbol{p_\eta}) + \text{terms with interactions between fermions (23) and (31).}
\end{aligned} \tag{1.59}$$

From the normalization condition (1.27) a corresponding normalization for the Salpeter amplitudes can be deduced, which looks as follows in Born approximation:

$$\langle\Phi_M^\Lambda|\Phi_M^\Lambda\rangle = \int\frac{\mathrm{d}^3p_\xi}{(2\pi)^3}\frac{\mathrm{d}^3p_\eta}{(2\pi)^3}\sum_{a_1,a_2,a_3}\Phi_{M\,a_1a_2a_3}^{\Lambda\,*}(\boldsymbol{p_\xi},\boldsymbol{p_\eta})\Phi_{M\,a_1a_2a_3}^{\Lambda}(\boldsymbol{p_\xi},\boldsymbol{p_\eta}) = 2M. \tag{1.60}$$

This normalization conditions resembles the usual $\mathcal{L}^2$-norm of Schrödinger wavefunctions and induces a positive definite scalar product, which is given by:

$$\langle \Phi_1 | \Phi_2 \rangle := \int \frac{\mathrm{d}^3 p_\xi}{(2\pi)^3} \frac{\mathrm{d}^3 p_\eta}{(2\pi)^3} \sum_{a_1,a_2,a_3} \Phi^*_{1 a_1 a_2 a_3}(\boldsymbol{p_\xi}, \boldsymbol{p_\eta}) \Phi_{2 a_1 a_2 a_3}(\boldsymbol{p_\xi}, \boldsymbol{p_\eta}). \tag{1.61}$$

The existence of such a scalar product is of utmost importance since it is the aim of the present work to formulate static observables as expectation values with respect to this scalar product. The Salpeter Hamiltonian is hermitian with respect to this scalar product if one also puts the following condition on the two- and three-body interaction kernels:

$$\begin{aligned} V^{(3)}(\boldsymbol{p_\xi}, \boldsymbol{p_\eta}; \boldsymbol{p'_\xi}, \boldsymbol{p'_\eta}) &\stackrel{!}{=} \gamma^0 \otimes \gamma^0 \otimes \gamma^0 \; V^{(3)\dagger}(\boldsymbol{p_\xi}, \boldsymbol{p_\eta}; \boldsymbol{p'_\xi}, \boldsymbol{p'_\eta}) \; \gamma^0 \otimes \gamma^0 \otimes \gamma^0 \\ V^{(2)}(\boldsymbol{p'_\xi}, \boldsymbol{p_\xi}) &\stackrel{!}{=} \gamma^0 \otimes \gamma^0 \; V^{(2)\dagger}(\boldsymbol{p'_\xi}, \boldsymbol{p_\xi}) \; \gamma^0 \otimes \gamma^0. \end{aligned} \tag{1.62}$$

Because of the hermiticity of the Salpeter Hamiltonian its eigenvalues are real and its eigenstates are orthogonal.

1.4 Current matrix elements

The description of three interacting fermions propagating in an external electromagnetic field differs from that of three fermions interacting only among themselves. The external interaction is accounted for by an additional term in the Hamiltonian of the system. The electromagnetic bvtor current of a propagating fermion is given by the operator

$$j^\mu(x) = e : \bar{\psi}(x) \hat{q} \gamma^\mu \psi(x) :, \tag{1.63}$$

where e is the unit charge and $\hat{q}$ denotes the charge operator. In case of QCD the charge operator is related to the third isospin component T_3 and the hyper-charge Y, which is the sum of baryon number and strangeness, by the Gell-Mann/ Nishijima formula

$$\hat{q} = T_3 + Y/2 = T_3 + \tfrac{1}{3}\lambda_8/2 = \frac{1}{3} \begin{pmatrix} 2 & 0 & 0 \\ 0 & -1 & 0 \\ 0 & 0 & -1 \end{pmatrix}. \tag{1.64}$$

The symbol ": :" means normal ordering of the field operators. Thus the Hamiltonian density operator in the presence of an external electromagnetic field, represented by the four potential $A^\mu(x)$ is given by the addition of $j^\mu A_\mu$ to tho Hamiltonian density:

$$\mathcal{H}^A_I(x) := \mathcal{H}_I(x) + e : \bar{\psi}_I(x) \hat{q} \gamma^\mu \psi_I(x) : A_\mu(x). \tag{1.65}$$

All operators are written in the interaction picture here. Note that $\mathcal{H}_I(x)$ is the Hamiltonian density that appears in the six-point Green's function and thus contains those interactions that eventually lead to bound states whereas the term $e : \bar{\psi}_I \hat{q} \gamma^\mu \psi_I : A_\mu$ represents the coupling to the external field. Using time ordered perturbation theory

the six-point Green's function in the presence of $A_\mu(x)$ (which we denote by G^A) may be expressed as follows:

$$\begin{aligned} G^A(x_1, x_2, x_3; x_1', x_2', x_3') \\ &= -\langle \Omega^A | \mathrm{T} \psi^1(x_1)\psi^2(x_2)\psi^3(x_3)\bar{\psi}^1(x_1')\bar{\psi}^2(x_2')\bar{\psi}^3(x_3')|\Omega^A\rangle \\ &= \frac{-1}{\langle 0|\mathrm{T}\exp\left(-\mathrm{i}\int \mathrm{d}t H_I^A(t)\right)|0\rangle} \sum_{k=0}^{\infty} \frac{(-\mathrm{i})^k}{k!} \int \mathrm{d}^4y_1 \ldots \mathrm{d}^4y_k \\ &\quad \times \langle 0|\mathrm{T}\psi_I^1(x_1)\psi_I^2(x_2)\psi_I^3(x_3)\bar{\psi}_I^1(x_1')\bar{\psi}_I^2(x_2')\bar{\psi}_I^3(x_3')\mathcal{H}_I^A(y_1)\ldots\mathcal{H}_I^A(y_1)|0\rangle. \end{aligned} \tag{1.66}$$

Here $|\Omega^A\rangle$ denotes the physical vacuum (including interactions among the quarks and the coupling to the external field) *i.e.* the ground state of the Hamilton density operator given by (1.65) which in general differs from $|\Omega\rangle$. The unperturbed vacuum of the free theory is denoted by $|0\rangle$.

Suppose we were to use Wick's theorem to contract the field operators in the last line of equation (1.66) in every order of the coupling constants. As is well known all unconnected pieces of Feynman diagrams factor out and exponentiate to cancel against the factor $1/\langle 0|\mathrm{T}\exp\left(-\mathrm{i}\int \mathrm{d}t\mathcal{H}_I^A(t)\right)|0\rangle$. So the perturbation series contains diagrams with no pieces unconnected from external lines. The external electromagnetic field in this context corresponds not to an external line, because it couples to the current j^μ which appears in the interaction Hamiltonian $\mathcal{H}_I^A$. Therefore there are no diagrams in the perturbation series of G^A that contain couplings of the external electromagnetic field to fermions from the vacuum, for which an example is shown in figure 1.1. These types of diagrams should by no means be confused with diagrams in which the fermion loop ("sea quarks") couples to the propagating fermions ("valence quarks") through gauge bosons — a process, which is still contained in G^A. The foregoing result is physically reasonable since vacuum polarization diagrams should be considered as corrections to the external field itself, whereas the remaining diagrams include the response of the system to the applied field (see for example [22]). This fact allows us to rewrite the six-point Green's function in the presence of an external field:

$$\begin{aligned} G^A(x_1, x_2, x_3; x_1', x_2', x_3') = \frac{-1}{\langle 0|\mathrm{T}\exp\left(-\mathrm{i}\int \mathrm{d}t H_I(t)\right)|0\rangle} \sum_{k=0}^{\infty} \frac{(-\mathrm{i})^k}{k!} \int \mathrm{d}^4y_1 \ldots \mathrm{d}^4y_k \\ \times \langle 0|\mathrm{T}\psi_I^1(x_1)\psi_I^2(x_2)\psi_I^3(x_3)\bar{\psi}_I^1(x_1')\bar{\psi}_I^2(x_2')\bar{\psi}_I^3(x_3') \\ \times \left[\mathcal{H}_I(y_1) + e : \bar{\psi}_I(y_1)\hat{q}\gamma^\mu\psi_I(y_1)A_\mu(y_1) :\right] \ldots \\ \times \cdots \left[\mathcal{H}_I(y_k) + e : \bar{\psi}_I(y_k)\hat{q}\gamma^\mu\psi_I(y_k)A_\mu(y_k) :\right]|0\rangle \end{aligned} \tag{1.67}$$

When we write G^A in this form it is tacitly understood, because of the foregoing discussion, that A_μ is not contracted with vacuum bubbles.

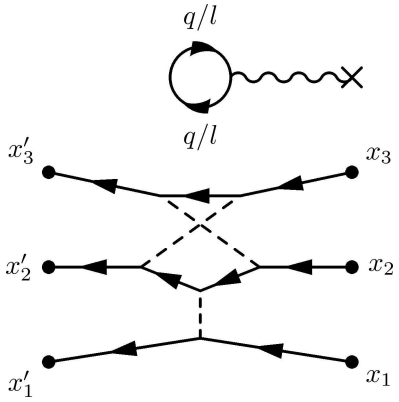

Figure 1.1: A diagram with the external field coupling to an unconnected piece (a quark or lepton loop in this case). The perturbation series of G^A does not contain such diagrams.

Finally we are ready to expand (1.67) up to first order in the external electromagnetic coupling. Since at the same time we want to retain the infinite sum in all other couplings, it is not sufficient to simply sum up to $k = 1$. Let us set $k > 0$ and inspect the k-fold product of interaction Hamilton density operators in (1.67):

$$\mathrm{T}\prod_{i=1}^{k}\left[\mathcal{H}_I(y_i) + e : \bar{\psi}_I(y_k)\hat{q}\gamma^\mu\psi_I(y_k)A_\mu(y_k) :\right] =$$

$$\mathrm{T}\prod_{i=1}^{k}\mathcal{H}_I(y_i) + \mathrm{T}\sum_{i=1}^{k}\left[e : \bar{\psi}_I(y_i)\hat{q}\gamma^\mu\psi_I(y_i)A_\mu(y_i) : \prod_{j\neq i}^{k}\mathcal{H}_I(y_j)\right] + \mathcal{O}(A_\mu^2) \quad (1.68)$$

The factorization of $: \bar{\psi}_I(y_i)\gamma^\mu\psi_I(y_i)A_\mu(y_i) :$ is allowed because of the time ordering operator. When we insert this expansion back into (1.67) we may rename a couple of integration variables in the second term of (1.68). In each summand rename y_i as y and rename the $(k-1)$ y_j's such that $j = 1, \ldots, (k-1)$. But doing so results in k equal summands and we obtain:

$$\begin{aligned}
G^A(x_1, x_2, x_3; x_1', x_2', x_3') = {} & \frac{-1}{\langle 0|\mathrm{T}\exp\left(-\mathrm{i}\int \mathrm{d}t\mathcal{H}_I(t)\right)|0\rangle}\sum_{k=0}^{\infty}\frac{(-\mathrm{i})^k}{k!}\int \mathrm{d}^4y_1\ldots\mathrm{d}^4y_k \\
& \times\langle 0|\mathrm{T}\psi_I^1(x_1)\psi_I^2(x_2)\psi_I^3(x_3)\bar{\psi}_I^1(x_1')\bar{\psi}_I^2(x_2')\bar{\psi}_I^3(x_3')\mathcal{H}_I(y_1)\ldots\mathcal{H}_I(y_k)|0\rangle \\
+ {} & \frac{-1}{\langle 0|\mathrm{T}\exp\left(-\mathrm{i}\int \mathrm{d}t\mathcal{H}_I(t)\right)|0\rangle}\sum_{k=1}^{\infty}\frac{(-\mathrm{i})^k}{(k-1)!}\int \mathrm{d}^4y_1\ldots\mathrm{d}^4y_{k-1} \\
& \times\langle 0|\mathrm{T}\psi_I^1(x_1)\psi_I^2(x_2)\psi_I^3(x_3)\bar{\psi}_I^1(x_1')\bar{\psi}_I^2(x_2')\bar{\psi}_I^3(x_3') \\
& \times\int \mathrm{d}^4y\, e : \bar{\psi}_I(y)\hat{q}\gamma^\mu\psi_I(y)A_\mu(y) : \mathcal{H}_I(y_1)\ldots\mathcal{H}_I(y_{k-1})|0\rangle + \mathcal{O}(A_\mu^2)
\end{aligned} \quad (1.69)$$

Note that the sum in the second term (the one containing A_μ) starts with $k = 1$ because the zeroth order ($k = 0$) is contained in the first term. Obviously the first term is the six-point Green's function G (1.2), describing the propagation of three fermions in the absence of any external field. The second term is the correction to it in first order of the external coupling. We may make a final modification to it by setting $(k-1) \to k$ and let the sum start with $k = 0$ to finally arrive at

$$G^A(x_1, x_2, x_3; x_1', x_2', x_3') = G(x_1, x_2, x_3; x_1', x_2', x_3') - \mathrm{i}\langle\Omega|\mathrm{T}\psi^1(x_1)\psi^2(x_2)\psi^3(x_3)\int j^\mu(y)A_\mu(y)\,\mathrm{d}y^4\,\bar\psi^1(x_1')\bar\psi^2(x_2')\bar\psi^3(x_3')|\Omega\rangle + \mathcal{O}(A_\mu^2) \tag{1.70}$$

Let us concentrate on the first order term in (1.70). We fix the following time-ordering which corresponds to three fermions coupling to the external field, while propagating forward in time

$$\min\{{x_1'}^0, {x_2'}^0, {x_3'}^0\} > y^0 > \max\{x_1^0, x_2^0, x_3^0\} \tag{1.71}$$

The time ordered product then factorizes into three parts and the insertion of two complete sets of intermediate states is possible:

$$\begin{aligned} G^A_{(1)}(x_1, x_2, x_3; x_1', x_2', x_3') = \mathrm{i}\int\frac{\mathrm{d}^3P'}{(2\pi)^3 2\omega_{\bar P'}}\int\frac{\mathrm{d}^3P}{(2\pi)^3 2\omega_{\bar P}}\int\mathrm{d}^4y A_\mu(y) \\ \times\langle\Omega|\mathrm{T}\psi^1(x_1)\psi^2(x_2)\psi^3(x_3)|P'\rangle\langle P'|j^\mu(y)|P\rangle\langle P|\bar\psi^1(x_1')\bar\psi^2(x_2')\bar\psi^3(x_3')|\Omega\rangle \\ \times\Theta(\min\{{x_1'}^0, {x_2'}^0, {x_3'}^0\} - y^0)\,\Theta(y^0 - \max\{x_1^0, x_2^0, x_3^0\}) + \text{other terms} \end{aligned} \tag{1.72}$$

"Other terms" contains different time orderings and different bound states. Transforming to momentum space then yields a pole in each of the two total energy variables, because of the Θ-functions:

$$G^A_{(1)P',P}(p_\xi, p_\eta, p_\xi', p_\eta') = \frac{\mathrm{i}A_\mu(P'-P)\chi_{P'}(p_\xi', p_\eta')\langle P'|j^\mu(0)|P\rangle\chi_P(p_\xi, p_\eta)}{4\omega_{\boldsymbol{P'}}\omega_{\boldsymbol{P}}(P^{0\prime} - \omega_{P'} + \mathrm{i}\epsilon)(P^0 - \omega_P + \mathrm{i}\epsilon)} \tag{1.73}$$

To find an expression for the current matrix element $\langle P'|j^\mu(0)|P\rangle$ appearing in (1.73) we transform G^A (1.70) into an integral equation. This can however only be done approximately. We take only those diagrams of the perturbation series of G^A that have the property that by cutting only fermion lines it is possible to isolate the vertex of the external field. This procedure is referred to as the impulse approximation. All diagrams of this type sum up as indicated in figure 1.2 and lead to a modification of the full dressed quark propagators:

$$S_F^A(x, x') = S_F(x - x') - \mathrm{i}e\int\mathrm{d}^4y S_F(x-y)\hat q A_\mu(y)\gamma^\mu S_F(y - x') \tag{1.74}$$

Replacing in the integral equation for the six-point Green's function (1.9) S_F with S_F^A then leads to an integral equation for G^A:

$$G^A = G_0^A - \mathrm{i}G_0^A K^A G^A, \tag{1.75}$$

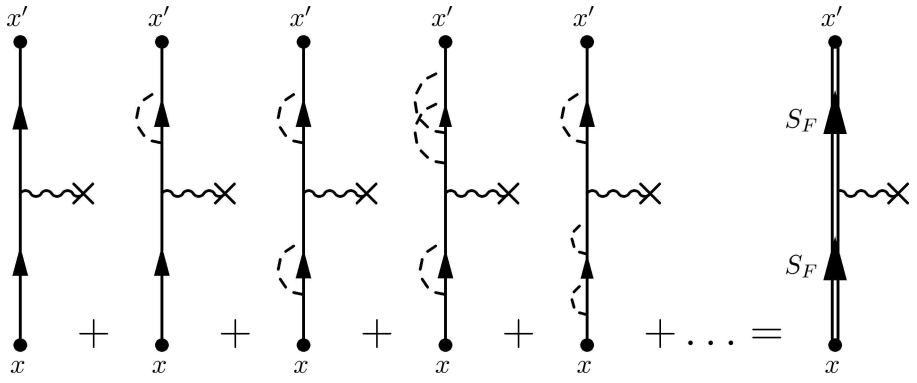

Figure 1.2: Perturbation series of the full dressed quark propagator in first order of the external coupling in impulse approximation.

where G_0^A and K^A follow from G_0 and K resp. by replacing S_F with S_F^A. From (1.75) it follows the first order in the external coupling:

$$G^A_{(1)} = G^A_{0\,(1)} - \mathrm{i}G^A_{0\,(1)}KG - \mathrm{i}G_0K^A_{(1)}G - \mathrm{i}G_0KG^A_{(1)}\,. \tag{1.76}$$

This equation may be put in the form

$$G^A_{(1)} = G(G_0^{-1}G^A_{0\,(1)}G_0^{-1} - \mathrm{i}K^A_{(1)})G\,. \tag{1.77}$$

Let us define the so called current kernel by

$$K^j := G_0^{-1}G^A_{0\,(1)}G_0^{-1} - \mathrm{i}K^A_{(1)}\,. \tag{1.78}$$

As was shown in section 1.2, a bound state gives rise to a pole in the total energy variable P^0 (see eq. 1.24). It then follows from (1.77) by explicitly writing out the operator product:

$$\begin{aligned} G^A_{(1)P,P'}(p_\xi,p_\eta,p'_\xi,p'_\eta) = \\ \frac{-1}{4\omega_{\boldsymbol{P}}\omega_{\boldsymbol{P'}}}\frac{\chi_P(p_\xi,p_\eta)}{(P^0-\omega_{\boldsymbol{P}}+\mathrm{i}\epsilon)}\Big[\int\frac{\mathrm{d}^4p''_\xi}{(2\pi)^4}\int\frac{\mathrm{d}^4p''_\eta}{(2\pi)^4}\int\frac{\mathrm{d}^4p'''_\xi}{(2\pi)^4}\int\frac{\mathrm{d}^4p'''_\eta}{(2\pi)^4} \\ \times\,\bar\chi_P(p''_\xi,p''_\eta)\;K^j_{P,P'}(p''_\xi,p''_\eta,p''_\xi,p''_\eta)\;\chi_{P'}(p'''_\xi,p'''_\eta)\Big]\frac{\bar\chi_{P'}(p'_\xi,p'_\eta)}{(P'^0-\omega'_{\boldsymbol{P'}}+\mathrm{i}\epsilon)} \\ +\text{ regular terms for } P^0\to\omega_{\boldsymbol{P}} \text{ and } P'^0\to\omega'_{\boldsymbol{P'}} \end{aligned} \tag{1.79}$$

Comparing this result with (1.73) then yields

$$\begin{aligned} A_\mu(P'-P)\langle P'|j^\mu(0)|P\rangle &= -\bar\chi_P\;K^j_{P,P'}\;\chi_{P'} \\ &= -\int\frac{\mathrm{d}^4p_\xi}{(2\pi)^4}\int\frac{\mathrm{d}^4p_\eta}{(2\pi)^4}\int\frac{\mathrm{d}^4p'_\xi}{(2\pi)^4}\int\frac{\mathrm{d}^4p'_\eta}{(2\pi)^4}\bar\chi_P(p_\xi,p_\eta)\;K^j_{P,P'}(p_\xi,p_\eta,p'_\xi,p'_\eta)\;\chi_P(p'_\xi,p'_\eta). \end{aligned} \tag{1.80}$$

We have to determine the current kernel now. From its definition (1.78) we see that it consists of two terms. Let us write out the first term explicitly:

$$G_0^{-1}G^A_{0\,(1)}G_0^{-1} = {S_F^1}^{-1}(\tfrac{1}{3}P+p_\xi+\tfrac{1}{2}p_\eta)\otimes {S_F^2}^{-1}(\tfrac{1}{3}P-p_\xi+\tfrac{1}{2}p_\eta)\otimes\hat{q}A_\mu(\tfrac{1}{3}P-p_\eta-\tfrac{1}{3}P'+p'_\eta)\gamma^\mu$$
$$\times\,(2\pi)^4\delta^{(4)}(p_\xi-p'_\xi)\;(2\pi)^4\delta^{(4)}\left(\tfrac{2}{3}(P-P')+p_\eta-p'_\eta\right)\,.$$
$$+\,\text{corresponding photon couplings to first two fermions.}\quad(1.81)$$

The second term of the current kernel contains the two body interaction kernel:

$$-\mathrm{i}K^A_{(1)} = K^{(2)}_{\left(\frac{2}{3}P+p_\eta\right)}(p_\xi,p'_\xi)\otimes\hat{q}A_\mu(\tfrac{1}{3}P-p_\eta-\tfrac{1}{3}P'-p'_\eta)\;(2\pi)^4\delta^{(4)}\left(\tfrac{2}{3}(P-P')+p_\eta-p'_\eta\right)$$
$$+\,\text{corresponding photon couplings to first two fermions.}\quad(1.82)$$

As is obvious from (1.80) we need a prescription of how to reconstruct the Bethe-Salpeter amplitude from the Salpeter amplitude. If there are no two-body interactions then such a prescription can be obtained from the Bethe-Salpeter equation itself:

$$\chi_M = -\mathrm{i}G_0V^{(3)}\phi^\Lambda_M = -\mathrm{i}G_0\Gamma. \tag{1.83}$$

Accordingly for the adjoint Bethe-Salpeter amplitude it follows:

$$\bar{\chi}_M = -\mathrm{i}\bar{\phi}^\Lambda_M V^{(3)}G_0 = -\mathrm{i}\bar{\Gamma}G_0. \tag{1.84}$$

The quantity Γ and its adjoint $\bar{\Gamma}$ which has been defined in these equations is called amputated Bethe-Salpeter amplitude or vertex function. Inserting both equation together with (1.81) then gives the current matrix element in case of vanishing two-body interactions:

$$\langle P'|j^\mu(0)|P\rangle = -3\int\frac{\mathrm{d}^4p_\xi}{(2\pi)^4}\int\frac{\mathrm{d}^4p_\eta}{(2\pi)^4}\overline{\Gamma}_{P'}(p_\xi,p_\eta)S_F^1(p_\xi+\tfrac{1}{2}p_\eta)\otimes S_F^2(-p_\xi+\tfrac{1}{2}p_\eta)$$
$$\otimes\,S_F^3(P'-p_\eta)\gamma^\mu\hat{q}S_F^3(P-p_\eta)\Gamma_P(p_\xi,p_\eta). \tag{1.85}$$

In this expression the external field couples to the third quark only. The factor 3 now accounts for the couplings to the remaining two quarks. This is legitimate since the vertex functions are totally antisymmetric under permutations of the three fermions.

If there is a two-body interaction then the reconstruction procedure becomes more involved. In principle there is a reconstruction formula (1.49), which could be used, if V_{eff} and ϕ^Λ where known. As we pointed out in section 1.3 however the Salpeter equation is truncated and so the Bethe-Salpeter amplitude reconstructed from the truncated Salpeter amplitude ${\phi^\Lambda_M}^{(k)}$ via (1.49) is not a solution of the Bethe-Salpeter equation anymore. A consistent reduction scheme is required. Consistent in the sense, that the reduction of the k-th order approximated Bethe-Salpeter amplitude via (1.34) leads to the k-th order approximated Salpeter amplitude ${\phi^\Lambda_M}^{(k)}$. This reconstruction scheme is discussed in appendix A. As is shown there, the k-th order approximation

$\chi_M^{(k)}$ of the Bethe-Salpeter amplitude can be reconstructed from the k-th order Salpeter amplitude $\Phi_M^{\Lambda\,(k)}$ via the following relation:

$$\chi_M^{(k)} = -\mathrm{i}\sum_{i=0}^{k} \mathcal{G}_M^{R,k} \left(V_\Lambda^{(3)} + \sum_{i=1}^{k} V_M^{\mathrm{eff}\,(i)} \right) \Phi_M^{\Lambda\,(k)}. \tag{1.86}$$

By introducing the vertex function and its adjoint in the presence of two-particle interactions

$$\Gamma_M^{\Lambda\,(k)} := -\mathrm{i} \left(V_\Lambda^{(3)} + \sum_{i=1}^{k} V_M^{\mathrm{eff}\,(i)} \right) \Phi_M^{\Lambda\,(k)} \tag{1.87}$$

$$\overline{\Gamma}_M^{\Lambda\,(k)} := -\mathrm{i}\overline{\Phi}_M^{\Lambda\,(k)} \left(V_\Lambda^{(3)} + \sum_{i=1}^{3} V_M^{\mathrm{eff}\,(i)} \right), \tag{1.88}$$

we may write (1.80) in a compact notation as:

$$A_\mu(P'-P)\langle P'|j^\mu(0)|P\rangle = -\overline{\Gamma}_P^{\Lambda\,(k)} \mathcal{K}_{P,P'} \Gamma_M^{\Lambda\,(k)}, \tag{1.89}$$

thus defining the so called effective current kernel $\mathcal{K}_{P,P'}$:

$$\mathcal{K}_{P,P'} := \left(\sum_{i=0}^{k} \mathcal{G}_P^{R,k\,(i)} \right) K_{P,P'}^{j} \left(\sum_{j=0}^{k} \mathcal{G}_{P'}^{R,k\,(j)} \right) \tag{1.90}$$

Consistently $\mathcal{K}_{P,P'}^{j}$ is expanded up to the same order in the residual kernel as is $\Gamma_{P'}^{(k)}$. In our calculations we considered so far the lowest order i. e. $V_{\mathrm{eff}} \approx V_{\mathrm{eff}}^{(1)}$ and $\phi_M^\Lambda \approx \phi_M^{\Lambda\,(1)}$. The zeroth order contribution to the effective current kernel is then given by

$$\begin{aligned} \mathcal{K}_{P,P'}^{j\,(0)} &= G_0 \; K_{P,P'}^{j\,(0)} G_0 \\ &= S_F^1(p_\xi + \tfrac{1}{2}p_\eta) \otimes S_F^2(-p_\xi + \tfrac{1}{2}p_\eta) \otimes S_F^3(P'-p_\eta) A_\mu(P'-P)\gamma^\mu \hat{q} S_F^3(P-p_\eta) \\ &\quad \times (2\pi)^4 \delta^{(4)}(p_\xi - p'_\xi) \; (2\pi)^4 \delta^{(4)}\left(p_\eta - p'_\eta\right). \end{aligned} \tag{1.91}$$

The first order contribution reads

$$\begin{aligned} \mathcal{K}_{P,P'}^{j\,(1)} = G_0 \; K_{P,P'}^{j\,(1)} G_0 - \mathrm{i}\, G_0 \; K_{P,P'}^{j\,(0)} G_0 \left(V_R^{(3)} + \overline{K}_{P'}^{(2)} - V_{P'}^{\mathrm{eff}\,(1)} \right) G_0 \\ - \mathrm{i}\, G_0 \; \left(V_R^{(3)} + \overline{K}_{P'}^{(2)} - V_{P'}^{\mathrm{eff}\,(1)} \right) G_0 K_{P,P'}^{j\,(0)} G_0 \end{aligned} \tag{1.92}$$

Due to its complexity this contribution has not been considered so far in our calculations. Thus we find with the zeroth order contribution (1.91) by inserting (1.90) into (1.80) that the current matrix element in case of two-body interactions is given by

$$\begin{aligned} \langle P'|j^\mu(0)|P\rangle = -3 \int \frac{\mathrm{d}^4 p_\xi}{(2\pi)^4} \int \frac{\mathrm{d}^4 p_\eta}{(2\pi)^4} \overline{\Gamma}_{P'}^{\Lambda}(p_\xi, p_\eta) S_F^1(p_\xi + \tfrac{1}{2}p_\eta) \otimes S_F^2(-p_\xi + \tfrac{1}{2}p_\eta) \\ \otimes S_F^3(P'-p_\eta)\gamma^\mu \hat{q} S_F^3(P-p_\eta) \Gamma_P^\Lambda(p_\xi, p_\eta). \end{aligned} \tag{1.93}$$

Note that it differs from the case of vanishing two-body interactions (1.85) only by the appearance of the projected vertex functions Γ^{Λ}_{M}. We therefore write $\Gamma^{(\Lambda)}_{M}$ in the following derivations to cover both cases at once.

We want to bring the current matrix element in a form that is more adapted for subsequent calculations. From now on we work in the Breit frame. Since in this reference frame there is only one independent three-momentum variable (the incoming and outgoing bound states are on-shell and their three-momenta are back-to-back) we express all kinematic quantities through the spatial components of the four-momentum transfer $q := P' - P$. Then the four momentum of the incoming baryon is given by

$$P = \begin{pmatrix} \sqrt{M^2 + |\boldsymbol{q}/2|^2} \\ \boldsymbol{q}/2 \end{pmatrix}. \tag{1.94}$$

Consequently the four momentum of the outgoing baryon is given by space reflection:

$$P' = \mathcal{P}P = \begin{pmatrix} \sqrt{M^2 + |\boldsymbol{q}/2|^2} \\ -\boldsymbol{q}/2 \end{pmatrix}. \tag{1.95}$$

The three-momentum transfer $\boldsymbol{q}$ enters the current matrix element at four places, twice through the vertex functions and twice through the propagator of the quark which couples to the photon. We would like to reduce this number of appearances to simplify the following calculations. To this end the current matrix element undergoes a series of transformations now. First with the definition of the adjoint vertex function and its boost prescription it follows:

$$\begin{aligned}
\overline{\Gamma}_{\mathcal{P}P}(p_\xi, p_\eta) &= \Gamma^{\dagger}_{\mathcal{P}P}(p_\xi, p_\eta)\gamma^0 \otimes \gamma^0 \otimes \gamma^0 \\
&= \left[S_{\Lambda_{\mathcal{P}P}} \otimes S_{\Lambda_{\mathcal{P}P}} \otimes S_{\Lambda_{\mathcal{P}P}} \Gamma_M(\overrightarrow{\Lambda^{-1}_{\mathcal{P}P} p_\xi}, \overrightarrow{\Lambda^{-1}_{\mathcal{P}P} p_\eta}) \right]^{\dagger} \gamma^0 \otimes \gamma^0 \otimes \gamma^0 \\
&= \Gamma^{\dagger}_{M}(\overrightarrow{\Lambda_P p_\xi}, \overrightarrow{\Lambda_P p_\eta}) \left[S_{\Lambda_{\mathcal{P}P}} \otimes S_{\Lambda_{\mathcal{P}P}} \otimes S_{\Lambda_{\mathcal{P}P}} \right] \left[\gamma^0 \otimes \gamma^0 \otimes \gamma^0 \right] \\
&= \Gamma^{\dagger}_{M}(\overrightarrow{\Lambda_P p_\xi}, \overrightarrow{\Lambda_P p_\eta}) \left[\gamma^0 \otimes \gamma^0 \otimes \gamma^0 \right] \left[S_{\Lambda_P} \otimes S_{\Lambda_P} \otimes S_{\Lambda_P} \right] \\
&= \overline{\Gamma}_{M}(\overrightarrow{\Lambda_P p_\xi}, \overrightarrow{\Lambda_P p_\eta}) \left[S_{\Lambda_P} \otimes S_{\Lambda_P} \otimes S_{\Lambda_P} \right],
\end{aligned} \tag{1.96}$$

where the identities $S^{\dagger}_{\Lambda_P} = S_{\Lambda_P}$, $S_{\Lambda_P}\gamma^0 = \gamma^0 S_{\Lambda_{\mathcal{P}P}}$ and $\Lambda^{-1}_{\mathcal{P}P} = \Lambda_P$ have been used. Note, that the vertex function in the rest frame of the baryon just depends on the spatial components of the boosted momenta, which have been indicated by arrows instead of bold symbols for a better readability. We insert this result (1.96) together with the boost prescription of the vertex function into the current matrix element (1.93):

$$\begin{aligned}
\langle \mathcal{P}P | j^\mu(0) | P \rangle = -3 \int \frac{d^4 p_\xi}{(2\pi)^4} \int \frac{d^4 p_\eta}{(2\pi)^4} \overline{\Gamma}^{(\Lambda)}_{M}(\overrightarrow{\Lambda_P p_\xi}, \overrightarrow{\Lambda_P p_\eta}) \left[S_{\Lambda_P} \otimes S_{\Lambda_P} \otimes S_{\Lambda_P} \right] \times \\
S^1_F(p_\xi + \tfrac{1}{2} p_\eta) \otimes S^2_F(-p_\xi + \tfrac{1}{2} p_\eta) \otimes S^3_F(\mathcal{P}P - p_\eta) \gamma^\mu \hat{q} S^3_F(P - p_\eta) \times \\
\left[S_{\Lambda_P} \otimes S_{\Lambda_P} \otimes S_{\Lambda_P} \right] \Gamma^{(\Lambda)}_{M}(\overrightarrow{\Lambda^{-1}_P p_\xi}, \overrightarrow{\Lambda^{-1}_P p_\eta})
\end{aligned} \tag{1.97}$$

Since we want to move the triple boost next to the adjoint vertex function to the right, but the action of γ^0 on S_{Λ_P} is different from that of γ^i $(i = 1, 2, 3)$, we have to make a distinction between both cases. Let us start with $\gamma^\mu = \gamma^0$ by using the identities

$$S_{\Lambda_{P_B}} S_F(q) = S_F(\Lambda_{P_B} q) S_{\Lambda_{P_B}} \tag{1.98}$$

and $S_{\Lambda_P}\gamma^0 = \gamma^0 S_{\Lambda_{\mathcal{P}P}}$ again:

$$\begin{aligned}\langle \mathcal{P}P|j^0(0)|P\rangle = -3 \int \frac{d^4p_\xi}{(2\pi)^4} \int \frac{d^4p_\eta}{(2\pi)^4} \bar{\Gamma}_M(\overrightarrow{\Lambda_P p_\xi}, \overrightarrow{\Lambda_P p_\eta}) \\ \times \left[S_F^1(\Lambda_P p_\xi + \tfrac{1}{2}\Lambda_P p_\eta) \otimes S_F^2(-\Lambda_P p_\xi + \tfrac{1}{2}\Lambda_P p_\eta) \otimes S_F^3(M - \Lambda_P p_\eta)\right] \left[S^2_{\Lambda_P} \otimes S^2_{\Lambda_P} \otimes \mathbb{1}\right] \\ \times \left[\mathbb{1} \otimes \mathbb{1} \otimes \gamma^0 \hat{q} S_F^3(M - \Lambda_P^{-1} p_\eta)\right] \Gamma_M(\overrightarrow{\Lambda_P^{-1} p_\xi}, \overrightarrow{\Lambda_P^{-1} p_\eta})\end{aligned} \tag{1.99}$$

Finally using the formula for integral transformations and the fact that a proper orthochronous Lorentz transformation has unit determinant, we arrive at:

$$\begin{aligned}\langle \mathcal{P}P|j^0(0)|P\rangle = -3 \int \frac{d^4p_\xi}{(2\pi)^4} \int \frac{d^4p_\eta}{(2\pi)^4} \bar{\Gamma}^{(\Lambda)}_M(\boldsymbol{p_\xi}, \boldsymbol{p_\eta}) \\ \times \left[S_F^1(p_\xi + \tfrac{1}{2}p_\eta) \otimes S_F^2(-p_\xi + p_\eta) \otimes S_F^3(M - p_\eta)\right] \left[S^2_{\Lambda_P} \otimes S^2_{\Lambda_P} \otimes \mathbb{1}\right] \\ \times \left[\mathbb{1} \otimes \mathbb{1} \otimes \gamma^0 \hat{q} S_F^3(M - \Lambda_P^{-1^2} p_\eta)\right] \Gamma^{(\Lambda)}_M(\overrightarrow{\Lambda_P^{-1^2} p_\xi}, \overrightarrow{\Lambda_P^{-1^2} p_\eta})\end{aligned} \tag{1.100}$$

For the case $\gamma^\mu = \gamma^i$, $i = 1, 2, 3$ and subsequent calculations it is advisable to have a clever way to deal with boosts. As can be shown, a boost from the rest-frame of a particle with mass M into a frame where it has three-momentum $\boldsymbol{P}$ is given by the operation:

$$\Lambda_P\, x = \mathcal{T} x + 2\langle \mathcal{P}x, \hat{P}\rangle \hat{P}, \tag{1.101}$$

where $\mathcal{T}$ means time inversion, i. e. $\mathcal{T}(x^0, \boldsymbol{x}) = (-x^0, \boldsymbol{x})$ and $\hat{P}$ is a unit bvtor that depends on $\boldsymbol{P}$ and the rest mass M of the particle and is defined as follows:

$$\hat{P} := \begin{pmatrix} \sqrt{\frac{1+\omega_M(\boldsymbol{P})/M}{2}} \\ \frac{1}{\sqrt{2(1+\omega_M(\boldsymbol{P})/M)}} \frac{\boldsymbol{P}}{M} \end{pmatrix}. \tag{1.102}$$

Accordingly the inverse boost is given by:

$$\Lambda_P^{-1} x = \mathcal{T} x + 2\langle x, \hat{P}\rangle \mathcal{P}\hat{P}, \tag{1.103}$$

and the representation of the boost and its inverse on a Dirac spinor is accomplished by the matrices:

$$S_{\Lambda_P} = \gamma(\hat{P})\gamma^0 \tag{1.104}$$

$$S^{-1}_{\Lambda_P} = \gamma^0\gamma(\hat{P}), \tag{1.105}$$

where $\gamma(\hat{P}) := P^\mu \gamma_\mu$. Using the explicit representation for S_{Λ_P} as given by eq. (1.104), it is easy to show that:

$$\gamma^i S_{\Lambda_P} = S_{\Lambda_P} \left(\gamma^i + 2\hat{P}^i \gamma(\hat{P}) \right). \tag{1.106}$$

With this, the spatial components of the current matrix element can be written as:

$$\begin{aligned} \langle \mathcal{P}P|j^i(0)|P\rangle = -3 \int \frac{d^4p_\xi}{(2\pi)^4} \int \frac{d^4p_\eta}{(2\pi)^4} \bar{\Gamma}_M^{(\Lambda)}(\boldsymbol{p_\xi}, \boldsymbol{p_\eta}) \\ \times \left[S_F^1(p_\xi + \tfrac{1}{2}p_\eta) \otimes S_F^2(-p_\xi + p_\eta) \otimes S_F^3(M - p_\eta) \right] \left[S_{\Lambda_P}^2 \otimes S_{\Lambda_P}^2 \otimes S_{\Lambda_P}^2 \right] \\ \times \left[\mathbb{1} \otimes \mathbb{1} \otimes \hat{q} \left(\gamma^i + 2\hat{P}^i \gamma(\hat{P}) \right) S_F^3(M - \Lambda_P^{-1^2} p_\eta) \right] \Gamma_M^{(\Lambda)}(\overrightarrow{\Lambda_P^{-1^2} p_\xi}, \overrightarrow{\Lambda_P^{-1^2} p_\eta}) \end{aligned} \tag{1.107}$$

Note the difference to (1.100). In addition to the extra term $2\hat{P}^i\gamma(\hat{P})$, a triple tensor product of $S^2_{\Lambda_P}$ now appears instead of a double one.

Since in both, the time component, eq. (1.100), as well as in the spatial components, eq. (1.107), of the current matrix element two successive boost operations appear, it is helpful to study this operation in more detail. To evaluate $S^2_{\Lambda_P}$, we use the explicit representation given by eq. (1.104):

$$\begin{aligned} S^2_{\Lambda_P} &= \gamma(\hat{P})\gamma^0\gamma(\hat{P})\gamma^0 \\ &= \gamma(\hat{P})\gamma(\mathcal{P}\hat{P}) \\ &= \left(\gamma^0\hat{P}^0 - \boldsymbol{\gamma}\cdot\hat{\boldsymbol{P}}\right)\left(\gamma^0\hat{P}^0 + \boldsymbol{\gamma}\cdot\hat{\boldsymbol{P}}\right) \\ &= (\hat{P}^0)^2 + |\hat{\boldsymbol{P}}|^2 - 2\hat{P}^0(\hat{\boldsymbol{P}}\cdot\boldsymbol{\gamma})\gamma^0 \\ &= \gamma(\tilde{P})\gamma^0, \end{aligned} \tag{1.108}$$

where $(\boldsymbol{x}\cdot\boldsymbol{\gamma})(\boldsymbol{x}\cdot\boldsymbol{\gamma}) = -|\boldsymbol{x}|^2$ has been used. We defined a new unit vector along the way:

$$\tilde{P} := \begin{pmatrix} (\hat{P}^0)^2 + |\hat{\boldsymbol{P}}|^2 \\ 2\hat{P}^0\hat{\boldsymbol{P}} \end{pmatrix} = \frac{1}{M}\begin{pmatrix} \sqrt{M^2 + |\boldsymbol{P}/2|^2} \\ \boldsymbol{P}/2 \end{pmatrix} = \frac{\bar{P}}{M}. \tag{1.109}$$

To compute $(\Lambda_P)^2$ and $(\Lambda_P^{-1})^2$ we make use of eqns. (1.101) and (1.103) and the previous result on $S^2_{\Lambda_P}$ to obtain:

$$(\Lambda_P)^2 x = \mathcal{T}x - 2\langle x, \mathcal{T}\tilde{P}\rangle\tilde{P} \tag{1.110}$$

$$(\Lambda_P^{-1})^2 x = \mathcal{T}x - 2\langle x, \tilde{P}\rangle\mathcal{T}\tilde{P}. \tag{1.111}$$

Note, that due to the double boost of the incoming vertex function, the $\boldsymbol{P}$-dependence becomes rather simple. An asymmetric definition of the current matrix element — *i.e.* when the external electromagnetic field is given in the rest-frame of the incoming or outgoing baryon — would have led to a more complicated $\boldsymbol{P}$-dependence because of the appearance of $\hat{P}$ in the boost instead of $\tilde{P}$.

1.5 A Quark model based on the Salpeter equation

As has already been mentioned in the introduction, the analytic results to be derived in the following chapters will be tested in a concrete physical application. The most interesting phenomena are observed with strongly interacting particles and so we are looking for a quark model that is based on the Bethe-Salpeter formalism described in section 1.2 and its approximation via the Salpeter equation described in section 1.3. Recall that the approximations that led to the Salpeter equation where free propagators, which corresponded to the introduction of effective fermion masses, and instantaneous interaction kernels. Both, effective quark masses and the interaction among the quarks are however not derivable from QCD at present and so one is forced to apply phenomenologically motivated assumptions about their very nature. A model, that is based on the field theoretic foundations of the Bethe-Salpeter formalism and at the same time very successful in describing the observed baryon mass spectra is described in refs. [5, 6, 7]. We briefly want to touch upon its prominent features in this section. It assumes a linearly rising confinement potential which accounts for the fact, that free quarks are never seen in nature. Moreover this form of the potential together with an appropriate Dirac structure is able to describe the linear Regge trajectory, *i.e.* the linear dependence of the excitation masses squared on the total spin, very well. The fine structure of the spectra is accounted for by a residual interaction motivated by an effective instanton Lagrangian, sometimes called 't Hooft's force. It is this residual interaction that leads to the octet-decuplet mass splitting but also to a lowering of the nucleons first radial excitation, the so-called Roper resonance. The explicit form of both interactions is discussed in the following two subsections.

1.5.1 Confinement potential

The gross structure of the baryon and meson spectra suggests a linear and flavor-independent confinement potential. In the model of refs. [6, 7] a local three-body potential has been chosen which has the following form:

$$V^{(3)}(x_1,x_2,x_3;x_1',x_2',x_3') = V^{(3)}_{\text{conf}}(\boldsymbol{x}_1,\boldsymbol{x}_2,\boldsymbol{x}_3) \\ \times \delta^{(1)}(x_1^0-x_2^0)\,\delta^{(1)}(x_2^0-x_3^0)\,\delta^{(4)}(x_1-x_1')\,\delta^{(4)}(x_2-x_2')\,\delta^{(4)}(x_3-x_3'). \quad (1.112)$$

This potential also carries a spinorial structure. The radial dependence of $V^{(3)}_{\text{conf}}$ should be linearly rising with the common distance of the quarks and in addition exhibit an offset. For the spinorial structure one demands covariance, parity- ($\mathcal{P}$), time-reversal- ($\mathcal{T}$) and $\mathcal{CPT}$-invariance and in addition hermiticity (1.62). From phenomenological observations there are a number of potentials which fulfill these properties. In ref. [19] different approaches have been studied. It turned out, that the following confinement potential together with the residual interaction to be discussed in the next subsection

leads to a satisfactory description of the baryon spectra:

$$V^{(3)}_{\text{conf}}(\boldsymbol{x}_1,\boldsymbol{x}_2,\boldsymbol{x}_3) = \tfrac{3}{4}a\left[\mathbb{1}\otimes\mathbb{1}\otimes\mathbb{1}+\gamma^0\otimes\gamma^0\otimes\mathbb{1}+\text{cycl. perm.}\right] + \tfrac{1}{2}b\sum_{i<j}|\boldsymbol{x}_i-\boldsymbol{x}_j|\left[-\mathbb{1}\otimes\mathbb{1}\otimes\mathbb{1}+\gamma^0\otimes\gamma^0\otimes\mathbb{1}+\text{cycl. perm.}\right]. \quad (1.113)$$

The constant offset a and the slope b enter the model as free parameters and have to be fitted to the experimentally observed baryon spectra.

1.5.2 't Hooft's instanton induced interaction

The confinement potential alone cannot account for all patterns in the baryon spectra like *e.g.* the octet-decuplet splitting of the ground state baryons. Therefore a residual interaction has to be used. In the quark model we describe, 't Hooft's instanton induced interaction takes this part. The instantaneous two-body interaction looks as follows:

$$V^{(2)}(x_1,x_2;x_1',x_2') = V^{(2)}_{\text{'t Hooft}}(\boldsymbol{x}_1-\boldsymbol{x}_2)\,\delta^{(1)}(x^0)\,\delta^{(4)}(x_1-x_1')\,\delta^{(4)}(x_2-x_2'). \quad (1.114)$$

Instantons induce an effective interaction among the quarks as has been shown in refs. [20, 21]. From the effective instanton Lagrangian density an effective two-body potential can be deduced which looks as follows (see ref. [5]):

$$V^{(2)}_{\text{'t Hooft}} = -4v_{\text{reg}}(\boldsymbol{x}_1-\boldsymbol{x}_2)\left[\mathbb{1}\otimes\mathbb{1}+\gamma^5\otimes\gamma^5\right] \times\mathcal{P}^{\mathcal{D}}_{S_{12}=0}\otimes\left(g_{nn}\mathcal{P}^{\mathcal{F}}_{\mathcal{A}}(nn)+g_{ns}\mathcal{P}^{\mathcal{F}}_{\mathcal{A}}(ns)\right)\otimes\mathcal{P}^{\mathcal{C}}_{\bar{3}}. \quad (1.115)$$

$\mathcal{P}^{\mathcal{D}}_{S_{12}=0}$ projects onto antisymmetric spin singlet configurations of both interacting quarks, $\mathcal{P}^{\mathcal{F}}_{\mathcal{A}}(f_1f_2)$ onto antisymmetric flavor states and $\mathcal{P}^{\mathcal{C}}_{\bar{3}}$ onto color-anti-triplet states. The effective coupling strengths g_{nn} and g_{ns} enter the model as free parameters. The effective instanton kernel contains δ-distributions $\delta^{(3)}(\boldsymbol{x}_1-\boldsymbol{x}_2)$, which lead to divergences when iterated in the Salpeter equation. Therefore the δ-distribution is regularized by replacing it with a Gaussian:

$$\delta^{(3)}(\boldsymbol{x}_1-\boldsymbol{x}_2) \;\to\; v_{\text{reg}}(\boldsymbol{x}_1-\boldsymbol{x}_2) \;=\; \frac{1}{\lambda^3\pi^{\frac{3}{2}}}\exp\left(-\frac{|\boldsymbol{x}_1-\boldsymbol{x}_2|^2}{\lambda^2}\right). \quad (1.116)$$

The constant λ which appears in the regularization also enters the model as a free parameter and is an effective instanton cutoff size or range parameter.

1.5.3 Light baryon spectra

Because isospin symmetry is assumed between the lightest quarks u and d, there is only one non-strange quark mass parameter. In total there are seven parameters that enter the model, two quark masses, two confinement parameters and three instanton parameters. We have listed those in table 1.1 together with their actual values from ref. [6, 7]. To fix these values the following procedure is adopted. Since the instanton

constituent quark masses	non-strange	m_n	330	MeV
	strange	m_s	670	MeV
confinement force	offset	a	-744	MeV
	slope	b	470	MeV fm^{-1}
residual instanton interaction	non-strange/non-strange coupling	g_{nn}	136	MeV fm^3
	non-strange/strange coupling	g_{ns}	94	MeV fm^3
	cutoff	λ	0.4	fm

Table 1.1: The seven parameters (two quark masses, two confinement force parameters and three instanton interaction parameters) entering the model.

force only acts on antisymmetric flavor states the Δ-spectrum is determined by the confinement force alone. Therefore the two confinement parameters a, b and the non-strange quark mass m_n are fitted to the well-known Δ-resonances. Likewise the strange quark mass m_s is fitted to the masses of the strange decuplet baryons (Σ^*, Ξ^*, Ω) where the instanton force also has no effect. The coupling strengths g_{nn}, g_{ns} and range λ of the 't Hooft's force are finally fitted to the octet-decuplet mass splitting like $\Delta - N$ and $\Sigma^* - \Lambda$. The resulting nucleon spectrum is shown in fig. 1.3 compared to the experimentally known resonances from ref. [15]. The model is able to describe the nucleon spectrum quite well. In particular the linear Regge trajectory is reproduced, but also the position of the Roper resonance $\mathrm{P}_{11}(1440)$ is almost hit. The latter observation is not self-evident, since almost all nonrelativistic quark models fail to describe this resonance. In ref. [6] it could be verified, that it is the effect of 't Hooft's force which is responsible for a lowering of the Roper resonance down to almost its empirical value. Besides the octet-decuplet splitting this is however not the only influence of this force. In addition it has been shown, that also the appearance of "parity doublets" are due to the instanton interaction. These doublet can be found in the nucleon spectrum as a degeneracy between *e.g.* the states $\mathrm{N}\frac{5}{2}^+(1680)$, $\mathrm{N}\frac{5}{2}^-(1675)$ and $\mathrm{N}\frac{9}{2}^+(2220)$, $\mathrm{N}\frac{9}{2}^-(2250)$. The instanton force lowers selected resonances to produce almost degenerate states. It must be noted that the appearance of these parity doublets is more or less accidental and strongly depends on the value of the instanton coupling strength.

To complete the brief discussion of this quark model, we show the ground states of the baryon octet and decuplet in fig. 1.4 since most of the static observables that are to be calculated in the present work are those of these states.

1.6 Summary

In this chapter we laid the foundations for the following studies on static properties of relativistic three-fermion systems in general and especially on static observables of baryons. Since we are looking for a field theoretic description of those observables, we needed an appropriate approach, which we found in the Bethe-Salpeter formalism. Since the Bethe-Salpeter equation is solvable only in special but physically unimportant cases, approximations had to be adopted, which consisted in the introduction of

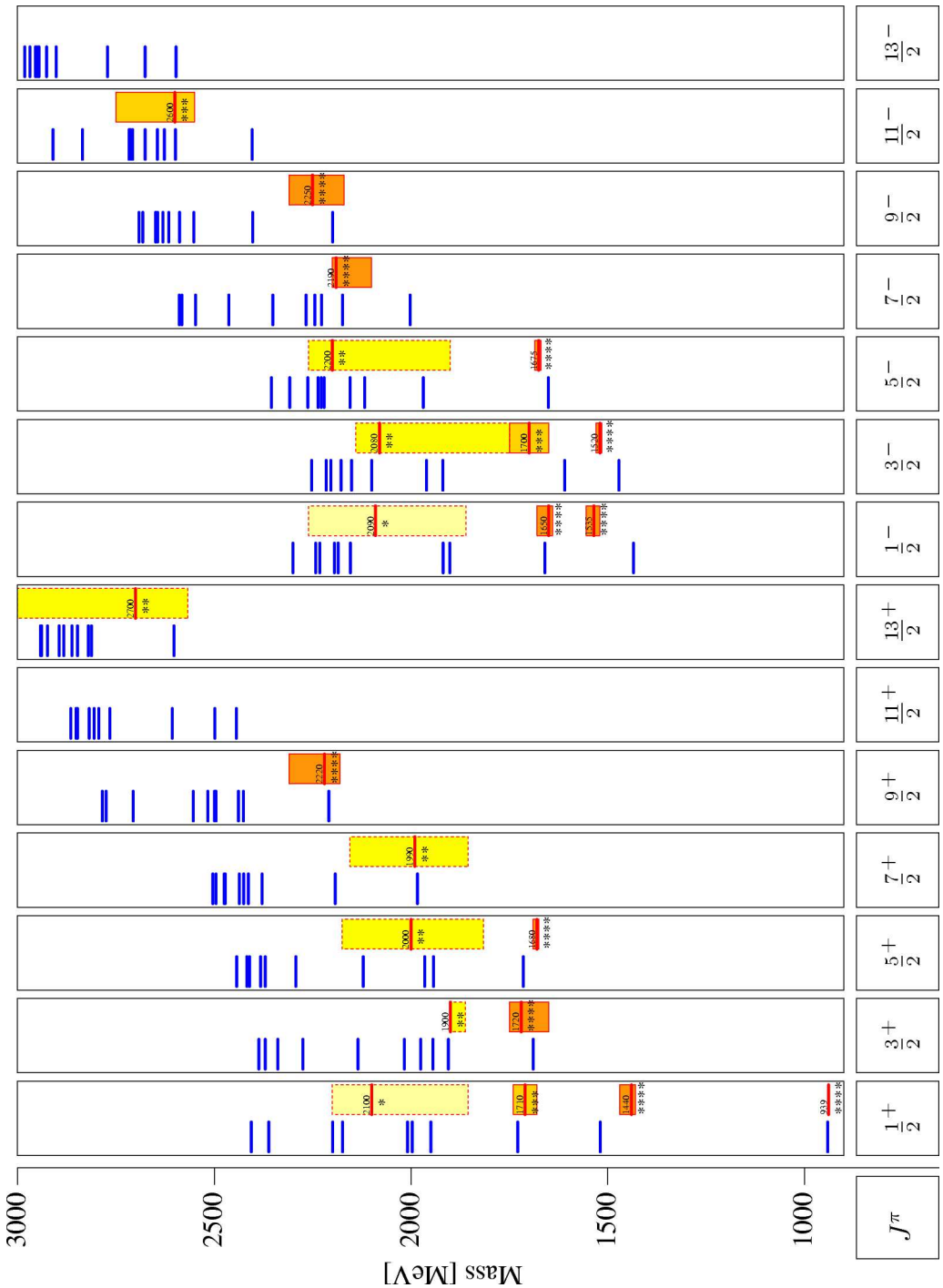

Figure 1.3: The nucleon-spectrum calculated in the quark model of refs. [6, 7]. In each column the left bars correspond to the theoretical predictions whereas the right ones denote the measured masses, whose reliability is depicted by stars (see ref. [15] for a definition). The shaded boxes, which are darker for better established resonances, indicate the experimental uncertainties.

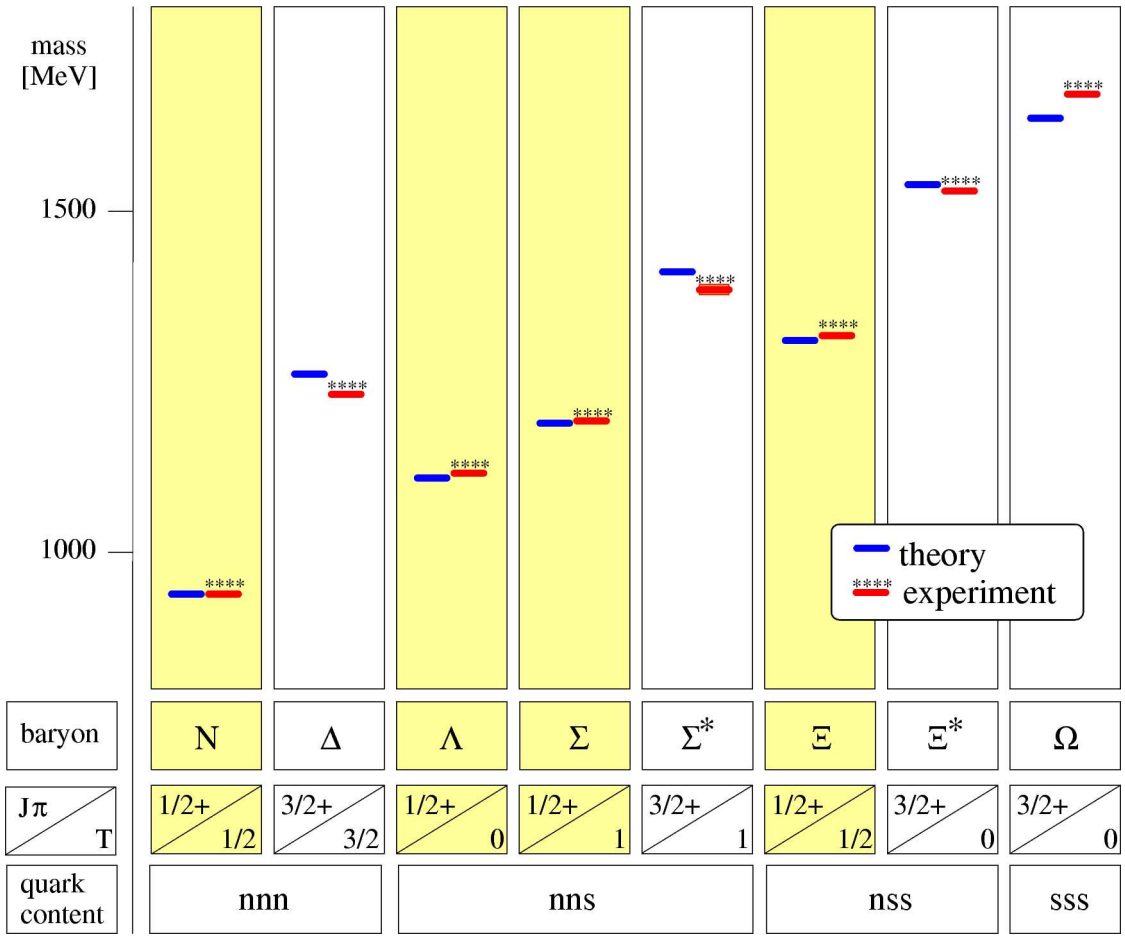

Figure 1.4: Comparison between the theoretical (left) and experimental (right) ground state masses of the baryon octet (shaded columns) and decuplet. J is the total spin of the baryon, π its parity and T the total isospin.

free-form fermion propagators with effective fermion masses and the assumption of instantaneous interaction kernels, thus leading to the Salpeter equation. The solutions of this equation where found to obey a norm inducing a positive definite scalar product, which makes a formulation of static observables as expectation values with respect to Salpeter amplitudes in principle possible. To find such a static approach, the derivation of a current matrix element involving Salpeter amplitudes is indispensable. We demonstrated how this matrix element can be found starting from the modification of the interaction Hamiltonian to account for the coupling of the system to an applied external electromagnetic field. The current matrix element was prepared to ease subsequent calculations. Since the analytic results of the next chapters will be applied to static properties of baryons, we introduced a quark model, which is successful in reproducing the observed baryon mass spectra, having its field theoretical foundations in the Bethe-Salpeter formalism. We are thus well prepared with both a current matrix element based on quantum field theory under certain assumptions on the interactions among the fermions and a phenomenological description of baryon mass spectra, delivering Salpeter amplitudes as input to test our results but also the quark model as such.

Chapter 2

Charge radii

Our first goal is to find an expression for the charge radius of a relativistic three-fermion system, that is described according to the Bethe-Salpeter formalism presented in the preceding chapter. Once the expression is found, we will apply it to the computation of baryon charge radii within the quark model of the preceding chapter based on the Bethe-Salpeter approach.

2.1 Introduction and overview

The charge radius is the first moment of a charge distribution and therefore provides crucial information about the extension of the charge in space. The nonrelativistic charge radius of a composite system of N particles is given by:

$$\langle r^2 \rangle = \frac{\langle \psi | \sum_{i=1}^{N} q_i (\boldsymbol{x_i} - \boldsymbol{R})^2 | \psi \rangle}{q \langle \psi | \psi \rangle}, \tag{2.1}$$

where q_i is the charge of particle i, $\boldsymbol{x_i}$ its position, $\boldsymbol{R}$ the center of mass coordinate and q the net charge of the system. The normalization to the net charge is of course dropped in case of uncharged systems. A direct relativistic generalization of this expression is unknown. Equation 2.1 is therefore not a suitable starting point for us, since we are interested in systems that behave relativistically like quarks bound in hadrons. On the other hand in field theoretic descriptions of bound states the charge radius is usually extracted from the electric form factor in the limit of vanishing squared four-momentum transfer of the probing photon. This method however has the shortcoming that the form factor has to be known at several momentum transfers, since the charge radius is defined as the slope at the photon point. This means that at least the incoming or outgoing particle has a finite three-momentum due to energy-momentum conservation. One is thus obliged to boost the wavefunction, which makes the numerical computation more involved. But moreover one obscures the internal structure of the composite system with this method. Although eq. (2.1) is discarded for the computation of relativistic systems, it has a simple physical interpretation. In this chapter we therefore show a way to synthesize both approaches. The field theoretic input has been described in the foregoing chapter on the Bethe-Salpeter formalism. We believe that it constitutes

a suitable starting point, because its foundation on quantum field theory allows for a relativistic and formally covariant description of bound states. Moreover it has been successfully applied to both the description of baryon mass spectra (see refs. [6, 7]) as well as electromagnetic observables (see refs. [11, 16]).

There are at least two approaches at hand to start the computation of charge radii. Classical electrodynamics tells us that the radius of a charge distribution $\rho(\boldsymbol{x})$ is given by the weighted mean $\int \mathrm{d}^3x|\boldsymbol{x}|^2\rho(\boldsymbol{x})/q$, where the total charge q is the integral $q = \int \mathrm{d}^3x\rho(\boldsymbol{x})$. By replacing ρ with the time component of the four-vector current of a quantum system we bridge the gap to quantum field theory and by Fourier transformation $|\boldsymbol{x}|^2$ becomes the Laplace operator with respect to the momentum transfer of the probing photon. The second approach is motivated by the definition of the charge radius as the slope of the electric form factor taken as a function of the four-momentum transfer squared Q^2.

In section 2.2 we will follow the first approach. The connection to the Bethe-Salpeter formalism of chapter 1 is made via the time component of the current matrix element (1.100). We first evaluate the Laplacian of that matrix element with respect to the momentum transfer and then take the static limit $\boldsymbol{P} \to 0$ analytically. Subsequently the integration over the relative energies may be performed and the vertex functions be replaced by Salpeter amplitudes. The resulting equation expresses the charge radius as an expectation value of a relativistic version of the simple operator of eq. 2.1. The nonrelativistic Schrödinger wavefunctions are replaced by Salpeter amplitudes.

Before we interpret the result of this section in detail, we give an alternative derivation starting from the second approach mentioned above in section 2.3. We briefly review the introduction of the form factors from a Lorentz-invariant decomposition of the electromagnetic vector current. We then show that the definition of the charge radius as the slope of the electric form factor at vanishing momentum transfer squared is in fact equivalent to its definition from charge distributions. This proof is generic, *i.e.* model independent. Becoming specific, we utilize the results of the preceding chapter and study the Q^2-dependence of the current matrix elements time component (1.100). Therefore we expand the boost acting on the incoming Salpeter amplitude in an exponential, which is possible since the Lorentz transformations form a Lie group. The elements of the Lie algebra are given by infinitesimal boosts whose action on wavefunctions is well known. The parameter that appears in the exponential depends on the momentum transfer which allows us to separate the Q^2-dependence from the matrix element and to compute the first derivative with respect to Q^2. After integrating over the relative energy variables we indeed recover the same result as in section 2.3.

In the following section 2.4 we assign a physical interpretation to the results of the two preceding sections. As already mentioned our method has the advantage that the underlying structure of the static observable is not obscured although the formalism has a relativistic and field theoretical background. The resulting expression for the charge radius is then indeed a relativistic generalization of eq. (2.1). The Schrödinger wavefunctions are replaced by Salpeter amplitudes, for which it is essential to have a scalar product given by eq. (1.61). The fermion masses are replaced by the relativistic single-particle energies and the nonrelativistic center of mass by its canonical relativistic counterpart. In addition the operator is multiplied by a relativistic weight factor.

Such a result calls for a numerical application, which we realize with the model described briefly in chapter 1 and in detail in refs. [6, 7]. We study first the charge radii of proton and neutron. While the proton mean square charge radius can nicely be reproduced the magnitude of the neutron charge radius is too large by a factor of almost two. To examine this situation, we analyze the dependence of these results on the choice of the model parameter set. It is well known, that the size of the instanton cutoff parameter may be varied, altering the nucleon mass spectrum only slightly after appropriately adjusting the instanton coupling strength. We might expect however that the effect on the charge radius is somewhat more visible. Indeed we find a small dependence of the proton charge radius but a drastic dependence of the neutron charge radius on the choice of these two parameters. The nucleon charge radii have also been extracted from form factor calculations which have been performed within the same model in ref. [11]. We find a strong deviation between both calculations in the neutron charge radius. A reanalysis of the form factor calculation will however show, that the extraction of the radius was erroneous. Although the experimental data are rather sparse, we have also added our results for the hyperon charge radii, which we also compare against form factor calculations. Finally, to demonstrate the importance of a relativistic treatment of baryon charge radii, we have taken the nonrelativistic limit of our analytic result, which basically coincides with eq. 2.1 and calculated the charge radii with respect to Salpeter amplitudes. The charge radii drop by about a factor of two as compared to the fully relativistic calculation.

2.2 From charge distributions to charge radii

We start our derivation in this section with a very simple definition of the charge radius borrowed from classical electrodynamics. Given some charge distribution $\rho(\boldsymbol{x})$ one defines its mean square radius by:

$$\langle r^2 \rangle = \frac{1}{q} \int \mathrm{d}^3x |\boldsymbol{x}|^2 \rho(\boldsymbol{x}). \tag{2.2}$$

The radius is normalized by the net charge q, which is simply the integral of $\rho(\boldsymbol{x})$ over space:

$$q = \int \mathrm{d}^3x \, \rho(\boldsymbol{x}). \tag{2.3}$$

However if the charge distribution has no net charge — as is the case for example with the neutron — the normalization $1/q$ is of course dropped. If we turn to quantum mechanical systems, the charge distribution is given by the time component $j^0(x)$ of the four vector current of a state vector $|\psi\rangle$:

$$\rho(\boldsymbol{x}) = \frac{\langle \psi | j^0(\boldsymbol{x}) | \psi \rangle}{\langle \psi | \psi \rangle}. \tag{2.4}$$

Such a state $|\psi\rangle$ can be represented as a superposition of momentum eigenstates

$$|\psi\rangle = \int \frac{\mathrm{d}^3P}{\omega_{\boldsymbol{P}}} \psi(\boldsymbol{P}) |P\rangle. \tag{2.5}$$

$\psi(\boldsymbol{P})$ is the wavefunction in momentum space and the states $|P\rangle$ are normalized according to:

$$\langle P|P'\rangle = 2\omega_{\boldsymbol{P}}(2\pi)^3\delta^{(3)}(\boldsymbol{P}-\boldsymbol{P'}). \tag{2.6}$$

This immediately fixes the normalization of the states $|\psi\rangle$:

$$\langle\psi|\psi\rangle = 2(2\pi)^3\int\frac{\mathrm{d}^3P}{\omega_{\boldsymbol{P}}}\psi^*(\boldsymbol{P})\psi(\boldsymbol{P}). \tag{2.7}$$

Let us further investigate the charge distribution by inserting (2.5) into (2.4):

$$\begin{aligned}\rho(\boldsymbol{x}) =&\frac{1}{\langle\psi|\psi\rangle}\int\frac{\mathrm{d}^3P}{\omega_{\boldsymbol{P}}}\int\frac{\mathrm{d}^3P'}{\omega_{\boldsymbol{P'}}}\psi^*(\boldsymbol{P})\psi(\boldsymbol{P'})\langle P|j^0(\boldsymbol{x})|P'\rangle\\ =&\frac{1}{\langle\psi|\psi\rangle}\int\frac{\mathrm{d}^3P}{\omega_{\boldsymbol{P}}}\int\frac{\mathrm{d}^3P'}{\omega_{\boldsymbol{P'}}}\exp\left(\mathrm{i}(\boldsymbol{P}-\boldsymbol{P'})\cdot x\right)\psi^*(\boldsymbol{P})\psi(\boldsymbol{P'})\langle P|j^0(0)|P'\rangle.\end{aligned} \tag{2.8}$$

In the last line we used space translational invariance to separate the spatial dependence. As is well known the integral $\int\mathrm{d}^3x\exp(\mathrm{i}\boldsymbol{p}\cdot\boldsymbol{x})$ is a representation of the delta distribution. So it follows

$$\begin{aligned}\int\mathrm{d}^3x|\boldsymbol{x}|^2\exp\left(\mathrm{i}(\boldsymbol{P}-\boldsymbol{P'})\cdot\boldsymbol{x}\right) =& -\tfrac{1}{4}(\boldsymbol{\nabla_P}-\boldsymbol{\nabla_{P'}})^2\int\mathrm{d}^3x\exp\left(\mathrm{i}(\boldsymbol{P}-\boldsymbol{P'})\cdot\boldsymbol{x}\right)\\ =&-\frac{(2\pi)^3}{4}(\boldsymbol{\nabla_P}-\boldsymbol{\nabla_{P'}})^2\,\delta^{(3)}(\boldsymbol{P}-\boldsymbol{P'}).\end{aligned} \tag{2.9}$$

To write the derivative as $\frac{1}{4}(\boldsymbol{\nabla_P}-\boldsymbol{\nabla_{P'}})^2$ instead of simply $\Delta_{\boldsymbol{P}}$ or $\Delta_{\boldsymbol{P'}}$ will be justified in the end of the calculation. It will turn out there that this highly symmetric derivative will guarantee that the end result depends on a current matrix given in the Breit frame. Using (2.5), (2.8) and (2.9) we obtain:

$$\begin{aligned}\int\mathrm{d}^3x|\boldsymbol{x}|^2\langle\psi|j^0(\boldsymbol{x})|\psi\rangle = -\frac{(2\pi)^3}{4}\int\frac{\mathrm{d}^3P}{\omega_{\boldsymbol{P}}}\int\frac{\mathrm{d}^3P'}{\omega_{\boldsymbol{P'}}}\psi^*(\boldsymbol{P})\psi(\boldsymbol{P'})\\ \times\langle P|j^0(0)|P'\rangle(\boldsymbol{\nabla_P}-\boldsymbol{\nabla_{P'}})^2\delta^{(3)}(\boldsymbol{P}-\boldsymbol{P'}).\end{aligned} \tag{2.10}$$

On the right hand side of this equation we may now integrate by parts twice and subsequently do one of the two momentum integrations:

$$\begin{aligned}&\int\mathrm{d}^3x|\boldsymbol{x}|^2\langle\psi|j^0(\boldsymbol{x})|\psi\rangle\\ &=-\frac{(2\pi)^3}{4}\int\mathrm{d}^3P\frac{|\psi(\boldsymbol{P})|^2}{\omega_{\boldsymbol{P}}^2}\left[(\boldsymbol{\nabla_P}-\boldsymbol{\nabla_{P'}})^2\langle P|j^0(0)|P'\rangle\right]_{\boldsymbol{P'}=\boldsymbol{P}}\\ &\quad-\frac{(2\pi)^3}{4}\int\mathrm{d}^3P\left[(\boldsymbol{\nabla_P}-\boldsymbol{\nabla_{P'}})^2\exp(\mathrm{i}(\omega_{\boldsymbol{P}}-\omega_{\boldsymbol{P'}})x^0)\frac{\psi^*(\boldsymbol{P})}{\omega_{\boldsymbol{P}}}\frac{\psi(\boldsymbol{P'})}{\omega_{\boldsymbol{P'}}}\right]_{\boldsymbol{P'}=\boldsymbol{P}}\langle P|j^0(0)|P\rangle\\ &\quad-\frac{(2\pi)^3}{2}\int\mathrm{d}^3P\left[(\boldsymbol{\nabla_P}-\boldsymbol{\nabla_{P'}})\exp(\mathrm{i}(\omega_{\boldsymbol{P}}-\omega_{\boldsymbol{P'}})x^0)\frac{\psi^*(\boldsymbol{P})}{\omega_{\boldsymbol{P}}}\frac{\psi(\boldsymbol{P'})}{\omega_{\boldsymbol{P'}}}\right]_{\boldsymbol{P'}=\boldsymbol{P}}\\ &\qquad\times\left[(\boldsymbol{\nabla_P}-\boldsymbol{\nabla_{P'}})\langle P|j^0(0)|P'\rangle\right]_{\boldsymbol{P'}=\boldsymbol{P}}\end{aligned} \tag{2.11}$$

The last of this three terms vanishes because $\boldsymbol{\nabla}_{\boldsymbol{P}}$ and $\boldsymbol{\nabla}_{\boldsymbol{P'}}$ change sign under space reflection in other words are of odd parity. So if the states $|P\rangle$ have definite parity (which we assume, since ultimately we want to describe for example baryonic states) then $\langle P|j^0(0)\boldsymbol{\nabla}_{\boldsymbol{P}}|P\rangle = 0$.

So far we have considered wave packets that consist of a superposition of states with different momenta. To obtain states with definite *i.e.* sharp momenta consider first a Gaussian wave packet with a width proportional to some parameter ϵ:

$$\psi(\boldsymbol{P}) = \exp(-|\boldsymbol{P}|^2/(2\epsilon^2)) \tag{2.12}$$

Before we let ϵ go to zero to define a definite momentum state let us inspect the second term in (2.11). Because for the Gaussian wave packet from (2.12) the wavefunction is real *i.e.* $\psi^*(\boldsymbol{P}) = \psi(\boldsymbol{P})$ we have:

$$\left[(\boldsymbol{\nabla}_{\boldsymbol{P}} - \boldsymbol{\nabla}_{\boldsymbol{P'}})\frac{\psi(\boldsymbol{P})}{\omega_{\boldsymbol{P}}}\frac{\psi(\boldsymbol{P'})}{\omega_{\boldsymbol{P'}}}\right]_{\boldsymbol{P'}=\boldsymbol{P}} = \left[(\boldsymbol{\nabla}_{\boldsymbol{P}} - \boldsymbol{\nabla}_{\boldsymbol{P'}})^2\frac{\psi(\boldsymbol{P})}{\omega_{\boldsymbol{P}}}\frac{\psi(\boldsymbol{P'})}{\omega_{\boldsymbol{P'}}}\right]_{\boldsymbol{P'}=\boldsymbol{P}} = 0. \tag{2.13}$$

Thus also this term does not contribute to the charge radius and we are left with the first term in (2.11) only. It should be noted however that the disappearance of this term is due to the special symmetric setup that we used in (2.9). However as this term is proportional to the net charge $\langle P|j^0(0)|P\rangle$ of the system, it represents the contribution of the net charge to the mean square radius. So in other setups or reference frames this term is removed by hand because one is interested in the intrinsic charge radius of the system originating from the internal dynamics. But as will be shown below, the final result for the charge radius in this calculation turns out to be an expectation value with respect to wavefunctions given in the rest frame of the baryon. It is obvious, that in this system of reference the contribution from the net charge vanishes.

Let us now turn to the limit $\epsilon \to 0$ again. Since in this limit $\exp(-|\boldsymbol{P}|^2/\epsilon^2)$ is another representation of the delta distribution we find

$$\lim_{\epsilon\to 0}\frac{|\psi(\boldsymbol{P})|^2}{\omega_{\boldsymbol{P}}\langle\psi(\boldsymbol{P})|\psi(\boldsymbol{P})\rangle} = \frac{\delta^{(3)}(\boldsymbol{P})}{2\omega_{\boldsymbol{P}}(2\pi)^3\int \mathrm{d}^3P\delta^{(3)}(\boldsymbol{P})/\omega_{\boldsymbol{P}}} = \frac{\delta^{(3)}(\boldsymbol{P})}{2(2\pi)^3}. \tag{2.14}$$

Inserting this together with the first term of (2.11) into the basic definition of the charge radius (2.2) yields

$$\begin{aligned}\langle r^2\rangle &= -\frac{1}{8q}\int\frac{\mathrm{d}^3P}{\omega_{\boldsymbol{P}}}\delta^{(3)}(\boldsymbol{P})\left[(\boldsymbol{\nabla}_{\boldsymbol{P}} - \boldsymbol{\nabla}_{\boldsymbol{P'}})^2\langle P|j^0(0)|P'\rangle\right]_{\boldsymbol{P'}=\boldsymbol{P}}\\ &= -\frac{1}{8Mq}(\boldsymbol{\nabla}_{\boldsymbol{P}} - \boldsymbol{\nabla}_{\boldsymbol{P'}})^2\langle P|j^0(0)|P'\rangle\Big|_{\boldsymbol{P'}=\boldsymbol{P}=0},\end{aligned} \tag{2.15}$$

where M is the rest mass of the system. As promised the current matrix element is given in the Breit frame if we make the following transformations:

$$\begin{aligned}(\boldsymbol{\nabla}_{\boldsymbol{P}} - \boldsymbol{\nabla}_{\boldsymbol{P'}})^2\langle P|j^0(0)|P'\rangle\Big|_{\boldsymbol{P'}=\boldsymbol{P}=0} &= (-\boldsymbol{\nabla}_{\boldsymbol{P}} + \boldsymbol{\nabla}_{\boldsymbol{P'}})^2\langle P|j^0(0)|P'\rangle\Big|_{\boldsymbol{P'}=\boldsymbol{P}=0}\\ &= (\boldsymbol{\nabla}_{\boldsymbol{P}} + \boldsymbol{\nabla}_{\boldsymbol{P'}})^2\langle \mathcal{P}P|j^0(0)|P'\rangle\Big|_{\boldsymbol{P'}=\boldsymbol{P}=0}\\ &= \Delta_{\boldsymbol{P}}\langle \mathcal{P}P|j^0(0)|P\rangle\Big|_{\boldsymbol{P}=0}.\end{aligned} \tag{2.16}$$

We then finally end up with an expression for the charge radius that will be — together with the current matrix element from the previous chapter — the starting point for subsequent calculations:

$$\langle r^2\rangle = -\frac{1}{8Mq}\Delta_{\boldsymbol{P}}\langle \mathcal{P}P|j^0(0)|P\rangle\Big|_{\boldsymbol{P}=0}. \tag{2.17}$$

The further procedure seems obvious. After inserting the current matrix element that we derived in the previous chapter (1.100) one has to calculate the Laplacian with respect to $\boldsymbol{P}$ and then take the static limit $\boldsymbol{P}\to 0$. However the calculation then becomes rather lengthy and complex, so we present a different approach here.

We observe, that the $\boldsymbol{P}$-dependence in the current matrix element (1.100) is given by the following part:

$$\left[S^2_{\Lambda_P}\otimes S^2_{\Lambda_P}\otimes S^3_F(M-\Lambda_P^{-1^2}p_\eta)\right]\Gamma^\Lambda_M(\overrightarrow{\Lambda_P^{-1^2}p_\xi},\overrightarrow{\Lambda_P^{-1^2}p_\eta}) := B_S(P)f(\Lambda_P^{-1^2}p_\xi,\Lambda_P^{-1^2}p_\eta). \tag{2.18}$$

We made the definitions:

$$B_S(P) := S^2_{\Lambda_P}\otimes S^2_{\Lambda_P}\otimes \mathbb{1} \tag{2.19}$$

$$f(\Lambda_P^{-1^2}p_\xi,\Lambda_P^{-1^2}p_\eta) := \left[\mathbb{1}\otimes\mathbb{1}\otimes S^3_F(M-\Lambda_P^{-1^2}p_\eta)\right]\Gamma^\Lambda_M(\overrightarrow{\Lambda_P^{-1^2}p_\xi},\overrightarrow{\Lambda_P^{-1^2}p_\eta}) \tag{2.20}$$

The idea is now to define an operator carrying the $\boldsymbol{P}$-dependence in the following way:

$$B(P)f(p_\xi,p_\eta) := B_S(P)f(\Lambda_P^{-1^2}p_\xi,\Lambda_P^{-1^2}p_\eta). \tag{2.21}$$

Sometimes this operation is referred to as the "pullback". Before we proceed let us define

$$\frac{\partial}{\partial \boldsymbol{P}^i}f(P) := f(P)_{,i} \tag{2.22}$$

just to have a shorter notation. Evaluating $B(P)_{,i}$ now seems to be the next step, but let us compute $B^{-1}(P)B(P)_{,i}$ instead. In the limit $\boldsymbol{P}\to 0$ both expressions coincide but as we will see using the second one will ease the calculation of the Laplacian $\Delta_P B(P)$. From the definition of $B(P)$ we readily get

$$B^{-1}(P)B(P)_{,i}f(p_\xi,p_\eta) =$$

$$\left[B_S^{-1}(P)B_S(P)_{,i} + \left((\Lambda_P^{-1})^2_{,i}\,\Lambda_P^2\,p_\xi\right)^\mu\frac{\partial}{\partial p_\xi^\mu} + \left((\Lambda_P^{-1})^2_{,i}\,\Lambda_P^2\,p_\eta\right)^\mu\frac{\partial}{\partial p_\eta^\mu}\right]f(p_\xi,p_\eta) \tag{2.23}$$

Let us turn to the first term involving $B_S(P)_{,i}$. From the definition (2.19) we have

$$B_S^{-1}(P)B_S(P)_{,i} = S^{-1^2}_{\Lambda_P}S^2_{\Lambda_P,i}\otimes\mathbb{1}\otimes\mathbb{1} + \mathbb{1}\otimes S^{-1^2}_{\Lambda_P}S^2_{\Lambda_P,i}\otimes\mathbb{1} \tag{2.24}$$

With the explicit form of $S^2_{\Lambda_P}$ (1.108) the evaluation of the derivative becomes rather easy:

$$S^2_{\Lambda_P,i} = \gamma(\tilde{P}_{,i})\gamma^0 = -\gamma^0\gamma(\mathcal{T}\tilde{P}_{,i}) = -\gamma^0\gamma(K_{,i}). \tag{2.25}$$

For later convenience we defined $K := \mathcal{T}\tilde{P}$. Although we might calculate $K_{,i}$ at this stage let us postpone this to keep the notation simple. With the preceding equation we then find

$$\begin{aligned} S_{\Lambda_P}^{-1\,2} S^2_{\Lambda_P,i} &= -\gamma^0\gamma(\tilde{P})\gamma^0\gamma(K_{,i}) = \gamma(K)\gamma(K_{,i}) = K^\mu K^\nu_{,i}\gamma_\mu\gamma_\nu \\ &= \tfrac{1}{2}(K^\mu K^\nu_{,i} - K^\nu K^\mu_{,i})\gamma_\mu\gamma_\nu \end{aligned} \tag{2.26}$$

In the last step we used the fact that K is a unit vector and so $(K^\mu K^\nu g_{\mu\nu})_{,i} = 0$. We thus finally have

$$B_S^{-1}(P)B_S(P)_{,i} = \tfrac{1}{2}(K^\mu K^\nu_{,i} - K^\nu K^\mu_{,i})(\gamma_\mu\gamma_\nu \otimes \mathbb{1} \otimes \mathbb{1} + \mathbb{1} \otimes \gamma_\mu\gamma_\nu \otimes \mathbb{1}). \tag{2.27}$$

For the evaluation of $(\Lambda_P^{-1})^2_{,i}\,\Lambda_P^2$ we use the representation (1.110) from where we first have

$$(\Lambda_P^{-1})^2_{,i}\,x = (\mathcal{T}x - 2\langle x, \tilde{P}\rangle\mathcal{T}\tilde{P})_{,i} = -2(\langle x, \tilde{P}_{,i}\rangle K + \langle x, \tilde{P}\rangle K_{,i}). \tag{2.28}$$

Using this result we obtain

$$\begin{aligned} (\Lambda_P^{-1})^2_{,i}\,\Lambda_P^2\,x &= -2(\langle \Lambda_P^2\,x, \tilde{P}_{,i}\rangle K + \langle \Lambda_P^2\,x, \tilde{P}\rangle K_{,i}) \\ &= -2(\langle x, K_{,i}\rangle K - 2\langle x, K\rangle\langle \tilde{P}, \tilde{P}_{,i}\rangle K + \langle x, K\rangle K_{,i} - 2\langle x, K\rangle\langle \tilde{P}, \tilde{P}\rangle K_{,i}) \\ &= 2(K_{,i}\langle x, K\rangle - K\langle x, K_{,i}\rangle) \\ &= 2(K_{,i}K^\nu - KK^\nu_{,i})x_\nu, \end{aligned} \tag{2.29}$$

where $\langle \tilde{P}, \tilde{P}\rangle = 1$ and the consequential relation $\langle \tilde{P}, \tilde{P}\rangle_{,i} = 0$ has been used in the third line. Putting together (2.23), (2.27) and (2.29) we get

$$\begin{aligned} B^{-1}(P)B(P)_{,i} = -2(K^\mu_{,i}K^\nu - K^\mu K^\nu_{,i}) \\ \times \left(p_{\xi\,\mu}\frac{\partial}{\partial p^\nu_\xi} + p_{\eta\,\mu}\frac{\partial}{\partial p^\nu_\eta} + \tfrac{1}{4}\gamma_\mu\gamma_\nu \otimes \mathbb{1} \otimes \mathbb{1} + \mathbb{1} \otimes \tfrac{1}{4}\gamma_\mu\gamma_\nu \otimes \mathbb{1} \right). \end{aligned} \tag{2.30}$$

Let us call this operator $A_i(P) := B^{-1}(P)B(P)_{,i}$. We are now ready to calculate the Laplacian in the limit $\boldsymbol{P} \to 0$:

$$\begin{aligned} B^{-1}(P)\Delta_P B(P)\Big|_{\boldsymbol{P}=0} &= \sum_{i=1}^3 B^{-1}(P)\tfrac{\partial}{\partial P^i}B(P)B^{-1}(P)\tfrac{\partial}{\partial P^i}B(P)\Big|_{\boldsymbol{P}=0} \\ &= \sum_{i=1}^3 B^{-1}(P)\tfrac{\partial}{\partial P^i}B(P)A_i(P)\Big|_{\boldsymbol{P}=0} \\ &= \sum_{i=1}^3 \left(A_i(P)A_i(P) + \tfrac{\partial}{\partial P^i}A_i(P)\right)\Big|_{\boldsymbol{P}=0}. \end{aligned} \tag{2.31}$$

From its definition we instantly see that $K|_{\boldsymbol{P}=0} = (-1,0,0,0)$ and furthermore that $K^0_{,i}|_{\boldsymbol{P}=0} = 0$ and $K^i_{,j}|_{\boldsymbol{P}=0} = \delta_{ij}/M$, so it follows:

$$(K^\mu_{,i}K^\nu - K^\mu K^\nu_{,i})\Big|_{\boldsymbol{P}=0} = -\tfrac{1}{M}(\delta^\mu_i\delta^\nu_0 - \delta^\mu_0\delta^\nu_i). \tag{2.32}$$

This result when plugged into (2.30) then yields:

$$\begin{aligned} A_i(\bar{M}) = -\tfrac{2}{M}\big(&- p_{\xi i}\tfrac{\partial}{\partial p^0_\xi} + p_{\xi 0}\tfrac{\partial}{\partial p^i_\xi} - p_{\eta i}\tfrac{\partial}{\partial p^0_\eta} + p_{\eta 0}\tfrac{\partial}{\partial p^i_\eta} \\ &+ \tfrac{1}{4}[\gamma_i,\gamma_0]\otimes\mathbb{1}\otimes\mathbb{1} + \mathbb{1}\otimes\tfrac{1}{4}[\gamma_i,\gamma_0]\otimes\mathbb{1}\big) \\ = -\tfrac{2}{M}\Big[&p^i_\xi\tfrac{\partial}{\partial p^0_\xi} + p^0_\xi\tfrac{\partial}{\partial p^i_\xi} + p^i_\eta\tfrac{\partial}{\partial p^0_\eta} + p^0_\eta\tfrac{\partial}{\partial p^i_\eta} - \tfrac{1}{2}(\alpha^i\otimes\mathbb{1}\otimes\mathbb{1} - \mathbb{1}\otimes\alpha^i\otimes\mathbb{1})\Big], \end{aligned} \tag{2.33}$$

where $\bar{M} := (M,\mathbf{0})$ is the total four-momentum in the rest-frame.

We still need to calculate $\sum_{i=1}^3 \frac{\partial}{\partial P^i}A_i(P)\big|_{\boldsymbol{P}=0}$ from (2.31). Because of the skewness we find

$$\sum_{i=1}^3 \tfrac{\partial}{\partial P^i}(K^\mu_{,i}K^\nu - K^\mu K^\nu_{,i}) = (\Delta_P K^\mu)K^\nu - K^\mu(\Delta_P K^\nu). \tag{2.34}$$

From the definition of K it follows $\Delta_P K^0\big|_{\boldsymbol{P}=0} = -\boldsymbol{\nabla}_{\boldsymbol{P}}\cdot(\boldsymbol{P}/M\omega_{\boldsymbol{P}})\big|_{\boldsymbol{P}=0} = -3/M^2$ and $\Delta_P K^i\big|_{\boldsymbol{P}=0} = 0$ and with that finally

$$\sum_{i=1}^3 \tfrac{\partial}{\partial P^i}(K^\mu_{,i}K^\nu - K^\mu K^\nu_{,i})\Big|_{\boldsymbol{P}=0} = -\tfrac{3}{M^2}(\delta^\mu_0\delta^\nu_0 - \delta^\mu_0\delta^\nu_0) = 0. \tag{2.35}$$

So we see that $\sum_{i=1}^3 \frac{\partial}{\partial P^i}A_i(P)\big|_{\boldsymbol{P}=0} = 0$. The vanishing of this term is not accidental, for one can show that $\frac{\partial}{\partial P^i}A_j(P)\big|_{\boldsymbol{P}=0} = -[A_i(\bar{M}),A_j(\bar{M})]_-$. Together with (2.31) we then deduce that $\frac{\partial}{\partial P^i}\frac{\partial}{\partial P^j}B(P)\big|_{\boldsymbol{P}=0} = \frac{1}{2}[A_i(\bar{M})A_j(\bar{M}) + A_j(\bar{M})A_i(\bar{M})]$. So the commutator reflects the symmetry under permutation of indices $(i \leftrightarrow j)$. In case of the charge radius this is obviously irrelevant and so the commutator vanishes.

We now have everything set up to embark upon the final part of the calculation of charge radii in which we will integrate out the dependence on the relative energies. Inserting the current matrix element (1.100) into (2.17) and using (2.31) then yields:

$$\begin{aligned} \langle r^2\rangle = \frac{3}{8Mq}\int\frac{d^4p_\xi}{(2\pi)^4}\int\frac{d^4p_\eta}{(2\pi)^4}&\bar{\Gamma}^\Lambda_M(\boldsymbol{p_\xi},\boldsymbol{p_\eta}) \\ &\times\big[S^1_F(p_\xi+\tfrac{1}{2}p_\eta)\otimes S^2_F(-p_\xi+p_\eta)\otimes S^3_F(M-p_\eta)\big]\sum_{i=1}^3 A_i(\bar{M})A_i(\bar{M}) \\ &\times\big[\mathbb{1}\otimes\mathbb{1}\otimes\gamma^0\hat{q}S^3_F(M-p_\eta)\big]\,\Gamma^\Lambda_M(\boldsymbol{p_\xi},\boldsymbol{p_\eta}). \end{aligned} \tag{2.36}$$

When we test our results with the quark model described in refs. [6, 7] we will restrict ourselves to the computation of the charge radii of the baryon octet, because it is experimentally much better covered than the decuplet. As already mentioned in this

case the vertex function contains only purely positive and negative energy components, *i.e.* in the current matrix element Γ^{Λ}_{M} appears. This is due to the fact, that the reconstruction procedure of the vertex function described in appendix A yields projected vertex functions because of the action of the two-body residual force which acts in the baryon octet but not in the decuplet. Using the partial fraction decomposition (1.36) of the propagators then yields:

$$\begin{aligned}\langle r^2\rangle = \frac{3}{8Mq}\int\frac{\mathrm{d}^4p_\xi}{(2\pi)^4}\int\frac{\mathrm{d}^4p_\eta}{(2\pi)^4}\bar{\Gamma}^{\Lambda}_{M}(\boldsymbol{p_\xi},\boldsymbol{p_\eta})\\ \left[\frac{\Lambda_1^+\otimes\Lambda_2^+\otimes\Lambda_3^+}{(p_\xi^0+\frac{1}{2}p_\eta^0-\omega_1+\mathrm{i}\epsilon)(-p_\xi^0+\frac{1}{2}p_\eta^0-\omega_2+\mathrm{i}\epsilon)(M-p_\eta^0-\omega_3+\mathrm{i}\epsilon)}\right.\\ \left.+\frac{\Lambda_1^-\otimes\Lambda_2^-\otimes\Lambda_3^-}{(p_\xi^0+\frac{1}{2}p_\eta^0+\omega_1-\mathrm{i}\epsilon)(-p_\xi^0+\frac{1}{2}p_\eta^0+\omega_2-\mathrm{i}\epsilon)(M-p_\eta^0+\omega_3-\mathrm{i}\epsilon)}\right]\\ [\gamma^0\otimes\gamma^0\otimes\mathbb{1}]\sum_{i=1}^{3}A_i(\bar{M})A_i(\bar{M})\hat{q}^3\\ \left[\frac{\mathbb{1}\otimes\mathbb{1}\otimes\Lambda_3^+}{(M-p_\eta^0-\omega_3+\mathrm{i}\epsilon)}+\frac{\mathbb{1}\otimes\mathbb{1}\otimes\Lambda_3^-}{(M-p_\eta^0+\omega_3-\mathrm{i}\epsilon)}\right][\mathbb{1}\otimes\mathbb{1}\otimes\gamma^0]\Gamma^{\Lambda}_{M}(\boldsymbol{p_\xi},\boldsymbol{p_\eta})\end{aligned}\tag{2.37}$$

Because of the special projector structure of the vertex functions, the integrand contains only pure energy components. The integration over the relative energies p_ξ^0 and p_η^0 is shown in appendix B in a generic way for a product of an arbitrary number of operators $A_i(\bar{M})$. In case of the charge radius we obtain from (B.7):

$$\begin{aligned}\langle r^2\rangle = -\frac{3}{8Mq}\int\frac{\mathrm{d}^3p_\xi}{(2\pi)^3}\int\frac{\mathrm{d}^3p_\eta}{(2\pi)^3}\bar{\Gamma}^{\Lambda}_{M}(\boldsymbol{p_\xi},\boldsymbol{p_\eta})\\ \left\{\frac{\Lambda^{+++}}{(M-\Omega)}[\gamma^0\otimes\gamma^0\otimes\mathbb{1}]\sum_{i=1}^{3}A_i^+A_i^+\hat{q}^3\frac{\mathbb{1}\otimes\mathbb{1}\otimes\Lambda_3^+}{(M-\Omega)}\right.\\ \left.+\frac{\Lambda^{---}}{(M+\Omega)}[\gamma^0\otimes\gamma^0\otimes\mathbb{1}]\sum_{i=1}^{3}A_i^-A_i^-\hat{q}^3\frac{\mathbb{1}\otimes\mathbb{1}\otimes\Lambda_3^-}{(M+\Omega)}\right\}\\ [\mathbb{1}\otimes\mathbb{1}\otimes\gamma^0]\Gamma^{\Lambda}_{M}(\boldsymbol{p_\xi},\boldsymbol{p_\eta}),\end{aligned}\tag{2.38}$$

where $A^i_\pm$ is defined according to eq. (B.12) as follows:

$$A^i_\pm := -\tfrac{2}{M}\left[\pm\tfrac{1}{2}(\omega_1-\omega_2)\tfrac{\partial}{\partial p^i_\xi}\pm(\omega_1+\omega_2)\tfrac{\partial}{\partial p^i_\eta}-\tfrac{1}{2}(\alpha^i\otimes\mathbb{1}\otimes\mathbb{1}+\mathbb{1}\otimes\alpha^i\otimes\mathbb{1})\right]\tag{2.39}$$

Remember that Ω is the sum of the relativistic single-particle energies and $\Lambda^{\pm\pm\pm}$ the triple tensor product of single-particle energy projection operators. Both shorthand notations have been defined in eq. (1.42). One may now use the commutator

$\{\gamma^0, \alpha^i\}_+ = 0$ to commute $\gamma^0 \otimes \gamma^0 \otimes \mathbb{1}$ with $\sum_{i=1}^3 A_i^\pm A_i^\pm$ and obtains:

$$\begin{aligned}\langle r^2\rangle = -\frac{3}{8Mq}\int\frac{\mathrm{d}^3p_\xi}{(2\pi)^3}\int\frac{\mathrm{d}^3p_\eta}{(2\pi)^3}\bar\Gamma_M^\Lambda(\boldsymbol{p_\xi},\boldsymbol{p_\eta})\\ \times\left[\frac{\Lambda^{+++}}{(M-\Omega)}\sum_{i=1}^3 A_i'^+A_i'^+\frac{\mathbb{1}\otimes\mathbb{1}\otimes\Lambda_3^+}{(M-\Omega)}+\frac{\Lambda^{---}}{(M+\Omega)}\sum_{i=1}^3 A_i'^-A_i'^-\frac{\mathbb{1}\otimes\mathbb{1}\otimes\Lambda_3^-}{(M+\Omega)}\right]\\ \times\hat q^3[\gamma^0\otimes\gamma^0\otimes\gamma^0]\Gamma_M^\Lambda(\boldsymbol{p_\xi},\boldsymbol{p_\eta}),\end{aligned}\tag{2.40}$$

with

$$A_i'^\pm := -\tfrac{2}{M}\left[\pm\tfrac12(\omega_1-\omega_2)\tfrac{\partial}{\partial p_\xi^i}\pm(\omega_1+\omega_2)\tfrac{\partial}{\partial p_\eta^i}+\tfrac12(\alpha^i\otimes\mathbb{1}\otimes\mathbb{1}+\mathbb{1}\otimes\alpha^i\otimes\mathbb{1})\right].\tag{2.41}$$

With the simple commutation rule

$$\Lambda_i^\pm(\boldsymbol{p_i})\alpha^j = \alpha^j\Lambda_i^\mp(\boldsymbol{p_i})\pm\frac{p_i^j}{\omega_i(\boldsymbol{p_i})}\mathbb{1}\tag{2.42}$$

one can derive the following relation:

$$\begin{aligned}&\Lambda_1^\pm\otimes\Lambda_2^\pm\otimes\mathbb{1}\left[\pm\tfrac12(\omega_1-\omega_2)\tfrac{\partial}{\partial p_\xi^i}\pm(\omega_1+\omega_2)\tfrac{\partial}{\partial p_\eta^i}+\tfrac12(\alpha^i\otimes\mathbb{1}\otimes\mathbb{1}+\mathbb{1}\otimes\alpha^i\otimes\mathbb{1})\right]\\ &=\pm\Lambda_1^\pm\otimes\Lambda_2^\pm\otimes\mathbb{1}\left[\tfrac12(\omega_1-\omega_2)\tfrac{\partial}{\partial p_\xi^i}+(\omega_1+\omega_2)\tfrac{\partial}{\partial p_\eta^i}+\tfrac{p_1^i}{2\omega_1}+\tfrac{p_2^i}{2\omega_2}\right]\Lambda_1^\pm\otimes\Lambda_2^\pm\otimes\mathbb{1},\end{aligned}\tag{2.43}$$

which allows us to rewrite (2.40):

$$\begin{aligned}\langle r^2\rangle = -\frac{3}{8Mq}\int\frac{\mathrm{d}^3p_\xi}{(2\pi)^3}\int\frac{\mathrm{d}^3p_\eta}{(2\pi)^3}\bar\Gamma_M^\Lambda(\boldsymbol{p_\xi},\boldsymbol{p_\eta})\\ \times\left[\frac{\Lambda^{+++}}{(M-\Omega)}+\frac{\Lambda^{---}}{(M+\Omega)}\right]\sum_{i=1}^3 A_i''A_i''\hat q^3\left[\frac{\Lambda^{+++}}{(M-\Omega)}+\frac{\Lambda^{---}}{(M+\Omega)}\right]\\ \times[\gamma^0\otimes\gamma^0\otimes\gamma^0]\Gamma_M^\Lambda(\boldsymbol{p_\xi},\boldsymbol{p_\eta}),\end{aligned}\tag{2.44}$$

where

$$A_i'' = -\tfrac{2}{M}\left[\tfrac12(\omega_1-\omega_2)\tfrac{\partial}{\partial p_\xi^i}+(\omega_1+\omega_2)\tfrac{\partial}{\partial p_\eta^i}+\tfrac{p_1^i}{2\omega_1}+\tfrac{p_2^i}{2\omega_2}\right].\tag{2.45}$$

Finally the replacement of the vertex functions by Salpeter amplitudes is possible. The relevant relations, namely (A.13) and (A.14) are derived in appendix A. Using these we finally end up with:

$$\begin{aligned}\langle r^2\rangle &= \frac{1}{2Mq}\int\frac{\mathrm{d}^3p_\xi}{(2\pi)^3}\int\frac{\mathrm{d}^3p_\eta}{(2\pi)^3}{\Phi_M^\Lambda}^\dagger(\boldsymbol{p_\xi},\boldsymbol{p_\eta})\hat r^2\Phi_M^\Lambda(\boldsymbol{p_\xi},\boldsymbol{p_\eta})\\ &= \frac{\langle\Phi_M^\Lambda|\hat r^2|\Phi_M^\Lambda\rangle}{2M}.\end{aligned}\tag{2.46}$$

The operator $\hat{r}^2$ is defined as follows:

$$\hat{r}^2 := -\frac{3}{4}\sum_{i=1}^{3} A_i'' A_i'' \hat{q}^3. \tag{2.47}$$

This operator may now be brought in a form, which makes it possible to give it a sensible physical interpretation. To this end, we first note, that it is hermitian with respect to the Salpeter scalar product induced by the normalization condition (1.60). This follows from the observation, that A_i'' is anti-hermitian:

$$\begin{aligned} A_i'' &= -\tfrac{2}{M}\left[\tfrac{1}{2}(\omega_1-\omega_2)\tfrac{\partial}{\partial p_\xi^i} + (\omega_1+\omega_2)\tfrac{\partial}{\partial p_\eta^i} + \tfrac{p_1^i}{2\omega_1} + \tfrac{p_2^i}{2\omega_2}\right] \\ &= -\tfrac{1}{M}\left[\tfrac{1}{2}(\omega_1-\omega_2)\tfrac{\partial}{\partial p_\xi^i} + (\omega_1+\omega_2)\tfrac{\partial}{\partial p_\eta^i} - \text{h.c.}\right] \end{aligned} \tag{2.48}$$

and therefore $A_i'' A_i''$ is hermitian. Although it is appropriate for the numerical implementation to work with relative coordinates, single-particle coordinates are better suited to find a physical interpretation. From the relations (1.11) between both coordinate sets we have for the spatial components the Jacobian:

$$J(\boldsymbol{P}, \boldsymbol{p_\xi}, \boldsymbol{p_\eta}) = \begin{pmatrix} \frac{1}{3} & 1 & \frac{1}{2} \\ \frac{1}{3} & -1 & \frac{1}{2} \\ \frac{1}{3} & 0 & -1 \end{pmatrix} \tag{2.49}$$

which leads to:

$$\frac{\partial}{\partial p_\xi^i} = \frac{\partial}{\partial p_1^i} - \frac{\partial}{\partial p_2^i} \tag{2.50}$$

$$\frac{\partial}{\partial p_\eta^i} = \frac{1}{2}\frac{\partial}{\partial p_1^i} + \frac{1}{2}\frac{\partial}{\partial p_2^i} - \frac{\partial}{\partial p_3^i}. \tag{2.51}$$

Then by re-expressing the derivatives in (2.48) in terms of one particle coordinates one finds:

$$\begin{aligned} &\tfrac{1}{2}(\omega_1-\omega_2)\tfrac{\partial}{\partial p_\xi^i} + (\omega_1+\omega_2)\tfrac{\partial}{\partial p_\eta^i} \\ &\quad= \tfrac{1}{2}(\omega_1-\omega_2)(\tfrac{\partial}{\partial p_1^i} - \tfrac{\partial}{\partial p_2^i}) + (\omega_1+\omega_2)(\tfrac{1}{2}\tfrac{\partial}{\partial p_1^i} + \tfrac{1}{2}\tfrac{\partial}{\partial p_2^i} - \tfrac{\partial}{\partial p_3^i}) \\ &\quad= \omega_1\tfrac{\partial}{\partial p_1^i} + \omega_2\tfrac{\partial}{\partial p_2^i} - (\omega_1+\omega_2)\tfrac{\partial}{\partial p_3^i} \\ &\quad= -\Omega\left(\tfrac{\partial}{\partial p_3^i} - \frac{1}{\Omega}\sum_{\alpha=1}^{3}\omega_\alpha\tfrac{\partial}{\partial p_\alpha^i}\right), \end{aligned} \tag{2.52}$$

where $\Omega := \omega_1+\omega_2+\omega_3$ is again the sum of the single-particle energies. It is useful to define:

$$\hat{R}^i := \frac{1}{\Omega}\sum_{\alpha=1}^{3}\omega_\alpha \mathrm{i}\tfrac{\partial}{\partial p_\alpha^i}, \tag{2.53}$$

which turns out to be the relativistic center of mass of a three-particle system as will be discussed in detail below. In one particle coordinates the charge radius operator (2.46) then takes the form:

$$\hat{r}^2 = 3\frac{\hat{q}^3}{2}\left[\frac{\Omega}{M}\left(\mathrm{i}\boldsymbol{\nabla}_{\boldsymbol{p_3}} - \hat{\boldsymbol{R}}\right) + \text{h. c.}\right]^2. \tag{2.54}$$

This expression is still not symmetric in all three particles. The third quark seems to play a special role. However this asymmetry is only due to the fact that in deriving the current matrix element in chapter 1 we exploited the total asymmetry of the vertex functions under particle interchange and coupled the photon to the third quark exclusively accounting for the other couplings by multiplying with a factor of 3. If we reverse this procedure, cancel the factor of 3 and symmetrize the expression over the three particles, we end up with:

$$\langle r^2\rangle = \frac{1}{2M}\langle\Phi^\Lambda_M|\sum_{\alpha=1}^{3}\left\{\frac{\hat{q}^\alpha}{2}\left[\frac{\Omega}{M}\left(\mathrm{i}\boldsymbol{\nabla}_{\boldsymbol{p_\alpha}} - \hat{\boldsymbol{R}}\right) + \text{h. c.}\right]^2\right\}|\Phi^\Lambda_M\rangle. \tag{2.55}$$

This expression calls for a physical interpretation. However we want postpone its discussion to study first the results that we obtained so far in the context of form factors.

2.3 From form factors to charge radii

In the last section the derivation of the charge radius operator started from defining the mean square radius of a charge distribution. As is well known there is another definition of the charge radius that involves the electric form factor. In this context the charge radius is defined as the slope of the electric form factor at the photon point. In this section we first investigate the interconnection between both definitions and show that they indeed coincide. We then give an alternative derivation of the charge radius in relativistic quark models with instantaneous interaction kernels, starting from the representation of boosts as exponentials of the boost generators of the Lorentz group.

Let us briefly recall some basic definitions in the context of form factors. From current conservation and Lorentz invariance the electromagnetic vector current of a spin-1/2 state can be parameterized as follows:

$$\langle P',\lambda'|j_\mu(0)|P,\lambda\rangle = e\bar{u}_{\lambda'}(P')\left[\gamma_\mu\left(F_1(Q^2)+F_2(Q^2)\right) - \frac{P'_\mu+P_\mu}{2M}F_2(Q^2)\right]u_\lambda(P). \tag{2.56}$$

F_1 and F_2 are the Dirac and Pauli form factors respectively. The Dirac form factor is normalized to the charge q whereas the Pauli form factor is normalized to the anomalous magnetic moment κ of the system. Both form factors are functions of the invariant momentum transfer squared $Q^2 := -q^2 = -(P'-P)^2$. The Dirac spinors are normalized in a Lorentz invariant fashion:

$$\bar{u}_{\lambda'}(P)u_\lambda(P) = \left(\xi^\dagger_{\lambda'}\sqrt{\sigma(P)}, \xi^\dagger_{\lambda'}\sqrt{\bar{\sigma}(P)}\right)\cdot\begin{pmatrix}\sqrt{\bar{\sigma}(P)}\xi_\lambda\\ \sqrt{\sigma(P)}\xi_\lambda\end{pmatrix} = 2M\,\delta_{\lambda'\lambda}. \tag{2.57}$$

Here we made use of the familiar definitions $\sigma(P) := \sigma^\mu P_\mu$, $\sigma^\mu := (\mathbb{1}, \boldsymbol{\sigma})$ and $\bar{\sigma}^\mu := (\mathbb{1}, -\boldsymbol{\sigma})$. Also the identity $\sigma(P)\bar{\sigma}(P) = P^2 = M^2$ has been used. Similarly one shows that

$$\bar{u}_{\lambda'}(\mathcal{P}P)u_\lambda(P) = \left(\xi^\dagger_{\lambda'}\sqrt{\bar{\sigma}(P)}, \xi^\dagger_{\lambda'}\sqrt{\sigma(P)}\right)\cdot\begin{pmatrix}\sqrt{\bar{\sigma}(P)}\xi_\lambda\\ \sqrt{\sigma(P)}\xi_\lambda\end{pmatrix} = 2\sqrt{M^2+Q^2/4}\delta_{\lambda'\lambda} \quad (2.58)$$

as well as

$$\bar{u}_{\lambda'}(\mathcal{P}P)\gamma_0 u_\lambda(P) = \left(\xi^\dagger_{\lambda'}\sqrt{\bar{\sigma}(P)}, \xi^\dagger_{\lambda'}\sqrt{\sigma(P)}\right)\cdot\begin{pmatrix}\sqrt{\sigma(P)}\xi_\lambda\\ \sqrt{\bar{\sigma}(P)}\xi_\lambda\end{pmatrix} = 2M\delta_{\lambda'\lambda}. \quad (2.59)$$

Using both expressions one can write the time component of the electromagnetic vector current (2.56) in the Breit frame as

$$\langle \mathcal{P}P, \lambda|j^0(0)|P,\lambda\rangle = 2eM\left[F_1(Q^2) - \frac{Q^2}{4M^2}F_2(Q^2)\right] = 2eMG_E(Q^2), \quad (2.60)$$

where $G_E(Q^2)$ is the electric Sachs form factor. It is defined together with the magnetic Sachs form factor as a combination of the Dirac and Pauli form factors:

$$G_E(Q^2) := F_1(Q^2) - \frac{Q^2}{4M^2}F_2(Q^2) \quad (2.61a)$$

$$G_M(Q^2) := F_1(Q^2) + F_2(Q^2). \quad (2.61b)$$

The charge radius is defined as the slope of the electric form factor at the photon point *i.e.* at $Q^2 = 0$:

$$\langle r^2\rangle = -\frac{6}{G_E(0)}\frac{\mathrm{d}G_E(Q^2)}{\mathrm{d}Q^2}\bigg|_{Q^2=0}. \quad (2.62)$$

Since $G_E(0) = F_1(0) = q$ the normalization $1/G_E(0)$ is dropped in case of uncharged particles. From this definition together with (2.60) we then find

$$\langle r^2\rangle = -\frac{3}{Mq}\frac{\mathrm{d}}{\mathrm{d}Q^2}\langle \mathcal{P}P,\lambda|j^0(0)|P,\lambda\rangle\bigg|_{Q^2=0}. \quad (2.63)$$

This result has to be compared to the one that we obtained in the previous section, namely equation (2.17). There we found the Laplace operator with respect to $\boldsymbol{P}$ instead of a single derivative with respect to Q^2 acting on the current matrix element. However both expressions turn out to be exactly equal: From the parameterization of the vector current (2.56) it is clear that the current matrix element $\langle \mathcal{P}P,\lambda|j^0(0)|P,\lambda\rangle$ depends on Q^2. In the Breit frame the dependence of Q^2 on the momenta of the incoming and outgoing bound state becomes rather simple. It reads $Q^2 = 4|\boldsymbol{P}|^2$. Then for any function f depending on $4|\boldsymbol{P}|^2$ the following identity holds:

$$\Delta_{\boldsymbol{P}} f(4|\boldsymbol{P}|^2) = 4\left(\Delta_{\boldsymbol{P}}|\boldsymbol{P}|^2\right)\frac{\mathrm{d}}{\mathrm{d}Q^2}f(Q^2) = 24\frac{\mathrm{d}}{\mathrm{d}Q^2}f(Q^2). \quad (2.64)$$

Inserting this into (2.63) we get:

$$\langle r^2\rangle = -\frac{1}{8Mq}\Delta_{\boldsymbol{P}}\langle \mathcal{P}P|j^0(0)|P\rangle\bigg|_{\boldsymbol{P}=0}, \quad (2.65)$$

which is exactly (2.17). Therefore the definition of the charge radius from form factors is equivalent to that from charge distributions. However it is worth studying the form factor approach in more detail. Expression (2.63) for the mean square charge radius is easier to evaluate than (2.17) because it contains only a first order derivative with respect to Q^2. It is thus essential to know the Q^2-dependence of the current matrix element $\langle \mathcal{P}P,\lambda|j^0(0)|P,\lambda\rangle$. So let us once again inspect the P-dependent part of the current matrix element (1.100):

$$\Big[S^2_{\Lambda_P}\otimes S^2_{\Lambda_P}\otimes S^3_F(M-\Lambda_P^{-1^2}p_\eta)\Big]\,\Gamma^\Lambda_M(\overrightarrow{\Lambda_P^{-1^2}p_\xi},\overrightarrow{\Lambda_P^{-1^2}p_\eta})$$
$$:=\big[S^2_{\Lambda_P}\otimes S^2_{\Lambda_P}\otimes \mathbb{1}\big]\,f(\Lambda_P^{-1^2}p_\xi,\Lambda_P^{-1^2}p_\eta). \quad (2.66)$$

We now exploit an important property of Lie groups, namely that every group element may be represented as an exponential mapping of the Lie algebra:

$$\begin{aligned}
[S_{\Lambda_P}\otimes S_{\Lambda_P}\otimes\mathbb{1}]\,f(\Lambda_P^{-1}p_\xi,\Lambda_P^{-1}p_\eta) &= \exp(-\mathrm{i}\,\boldsymbol{\eta}(P)\cdot\hat{\boldsymbol{K}})f(p_\xi,p_\eta)\\
\big[S^2_{\Lambda_P}\otimes S^2_{\Lambda_P}\otimes\mathbb{1}\big]\,f(\Lambda_P^{-1^2}p_\xi,\Lambda_P^{-1^2}p_\eta) &= \Big[\exp(-\mathrm{i}\,\boldsymbol{\eta}(P)\cdot\hat{\boldsymbol{K}})\Big]^2 f(p_\xi,p_\eta)\\
&= \exp(-2\mathrm{i}\,\boldsymbol{\eta}(P)\cdot\hat{\boldsymbol{K}})f(p_\xi,p_\eta) \qquad (2.67)
\end{aligned}$$

The parameter $\boldsymbol{\eta}$, commonly called rapidity, is defined as follows:

$$\boldsymbol{\eta}(P):=\frac{\boldsymbol{P}}{P^0}=\frac{-\boldsymbol{q}}{2\sqrt{M^2+Q^2/4}}, \qquad (2.68)$$

where the last equality follows from the Breit frame kinematics (1.94). The operator $\hat{\boldsymbol{K}}$ is an infinitesimal boost. The generators of the Lorentz group are given by the following skew symmetric tensors (see *e.g.* [22]):

$$J^{\mu\nu} = \mathrm{i}(x^\mu\partial^\nu - x^\nu\partial^\mu) \qquad (2.69)$$

$$S^{\mu\nu} = \tfrac{\mathrm{i}}{4}[\gamma^\mu,\gamma^\nu]_-, \qquad (2.70)$$

Because of skewness there are six independent quantities. J^{0i} are the three generators of boosts and the remaining three operators generate rotations (in fact they are the angular momentum operators). In momentum space we have $J^{\mu\nu}_p=\mathrm{i}(p^\mu\partial/\partial p_\nu - p^\nu\partial/\partial p_\mu)$. $S^{\mu\nu}$ are the corresponding generators in Dirac space. The infinitesimal boost $\hat{\boldsymbol{K}}$ then simply reads

$$\begin{aligned}
\hat{K}^i &= -J^{0i}_{p_\xi} - J^{0i}_{p_\eta} + S^{0i}\otimes\mathbb{1}\otimes\mathbb{1} + \mathbb{1}\otimes S^{0i}\otimes\mathbb{1}\\
&= \mathrm{i}\big(-p^0_\xi\tfrac{\partial}{\partial p^i_\xi} - p^i_\xi\tfrac{\partial}{\partial p^0_\xi} - p^0_\eta\tfrac{\partial}{\partial p^i_\eta} - p^i_\eta\tfrac{\partial}{\partial p^0_\eta} + \tfrac{1}{2}\alpha^i\otimes\mathbb{1}\otimes\mathbb{1} + \mathbb{1}\otimes\tfrac{1}{2}\alpha^i\otimes\mathbb{1}\big).
\end{aligned} \qquad (2.71)$$

Inserting (2.67) back into the current matrix element (1.100) we find

$$\begin{aligned}
\langle\mathcal{P}P|j^0(0)|P\rangle = -3\int\frac{d^4p_\xi}{(2\pi)^4}\int\frac{d^4p_\eta}{(2\pi)^4}\bar{\Gamma}^\Lambda_M(\boldsymbol{p_\xi},\boldsymbol{p_\eta})\\
\times\big[S^1_F(p_\xi+\tfrac{1}{2}p_\eta)\otimes S^2_F(-p_\xi+p_\eta)\otimes S^3_F(M-p_\eta)\big]\exp(-2\mathrm{i}\,\boldsymbol{\eta}(P)\cdot\hat{\boldsymbol{K}})\\
\times\big[\mathbb{1}\otimes\mathbb{1}\otimes\gamma^0\hat{q}S^3_F(M-p_\eta)\big]\,\Gamma^\Lambda_M(\boldsymbol{p_\xi},\boldsymbol{p_\eta}). \qquad (2.72)
\end{aligned}$$

By using parity arguments we will now show that only even powers of $\boldsymbol{\eta}(P)$ are contained in this matrix element. Since the vertex functions describe bound states with definite parity we have

$$\mathcal{P}\Gamma_M^\Lambda(p_\xi, p_\eta) = \pi\Gamma_M^\Lambda(p_\xi, p_\eta), \tag{2.73}$$

where $\pi = \pm 1$ depending on the bound state to be considered. The propagators are even under the action of the parity operator:

$$\mathcal{P}\frac{\mathrm{i}}{\not{p} - m + \mathrm{i}\epsilon}\mathcal{P} = \gamma^0\frac{\mathrm{i}}{(\mathcal{P}p)_\mu\gamma^\mu - m + \mathrm{i}\epsilon}\gamma^0 = \frac{\mathrm{i}}{\not{p} - m + \mathrm{i}\epsilon}. \tag{2.74}$$

And finally the boost generator $\hat{K}^i$ is odd under parity. So in the end when expanding the exponential in (2.72), terms containing odd powers of $\boldsymbol{K}$ and consequently odd powers of $\boldsymbol{\eta}(P)$ vanish due to parity.

Since the charge radius is proportional to the slope of the current matrix element (2.72) at $Q^2 = 0$, we are interested in the term of the expansion linear in Q^2 and thus — because $|\boldsymbol{\eta}(P)|^2$ is of order Q^2 — linear in $|\boldsymbol{\eta}(P)|^2$. Writing the expansion explicitly out up to this order we have:

$$\begin{aligned}\langle \mathcal{P}P|j^0(0)|P\rangle = 2Mq - 3\int\frac{d^4p_\xi}{(2\pi)^4}\int\frac{d^4p_\eta}{(2\pi)^4}\bar{\Gamma}_M^\Lambda(\boldsymbol{p_\xi}, \boldsymbol{p_\eta})\\ \times\left[S_F^1(p_\xi + \tfrac{1}{2}p_\eta)\otimes S_F^2(-p_\xi + p_\eta)\otimes S_F^3(M - p_\eta)\right]\left[-2\sum_{i,j=1}^{3}\eta^i(P)\eta^j(P)\hat{K}^i\hat{K}^j\right]\\ \times\left[\mathbb{1}\otimes\mathbb{1}\otimes\gamma^0\hat{q}S_F^3(M - p_\eta)\right]\Gamma_M^\Lambda(\boldsymbol{p_\xi}, \boldsymbol{p_\eta}) + \mathcal{O}(\boldsymbol{\eta}^4).\end{aligned} \tag{2.75}$$

By inserting this into (2.63), the charge radius then takes the form:

$$\begin{aligned}\langle r^2\rangle = -\frac{18}{Mq}\sum_{i,j=1}^{3}\left[\frac{\mathrm{d}}{\mathrm{d}Q^2}\eta^i(P)\eta^j(P)\right]_{Q^2=0}\int\frac{d^4p_\xi}{(2\pi)^4}\int\frac{d^4p_\eta}{(2\pi)^4}\bar{\Gamma}_M^\Lambda(\boldsymbol{p_\xi}, \boldsymbol{p_\eta})\\ \times\left[S_F^1(p_\xi + \tfrac{1}{2}p_\eta)\otimes S_F^2(-p_\xi + p_\eta)\otimes S_F^3(M - p_\eta)\right]\hat{K}^i\hat{K}^j\\ \times\left[\mathbb{1}\otimes\mathbb{1}\otimes\gamma^0\hat{q}S_F^3(M - p_\eta)\right]\Gamma_M^\Lambda(\boldsymbol{p_\xi}, \boldsymbol{p_\eta}).\end{aligned} \tag{2.76}$$

We want to integrate out the dependence on the relative energies now. Fortunately by inspection of (2.33) and (2.71) we find a simple relation between $A_i(M)$ and $\hat{K}^i$:

$$\hat{K}^i = \mathrm{i}\frac{M}{2}A_i(M). \tag{2.77}$$

This relation allows us to use appendix B where the integration is shown in detail. Furthermore we may use relation (2.43) and subsequently replace the vertex functions by Salpeter amplitudes to obtain:

$$\langle r^2\rangle = \frac{18}{Mq}\sum_{i,j=1}^{3}\left[\frac{\mathrm{d}}{\mathrm{d}Q^2}\eta^i(P)\eta^j(P)\right]_{Q^2=0}\langle\Phi_M^\Lambda|\hat{K}'^i\hat{K}'^j\hat{q}^3|\Phi_M^\Lambda\rangle, \tag{2.78}$$

where

$$\hat{K}'^i := \tfrac{1}{2}(\omega_1-\omega_2)\mathrm{i}\tfrac{\partial}{\partial p^i_\xi} + (\omega_1+\omega_2)\mathrm{i}\tfrac{\partial}{\partial p^i_\eta} + \tfrac{\mathrm{i}p^i_1}{2\omega_1} + \tfrac{\mathrm{i}p^i_2}{2\omega_2} \tag{2.79}$$

is a tensor operator of rank 1, that is a vector operator. Consequently $\hat{K}'^i\hat{K}'^j$ is a Cartesian tensor operator of rank 2. As is well known, every Cartesian tensor may be decomposed into irreducible representations of the rotation group $SO(3)$. The decomposition of a rank-2 tensor T_{ij} is given by:

$$\begin{aligned} T_{ij} &= \tfrac{1}{3}\mathrm{tr}(T)\delta_{ij} + \tfrac{1}{2}(T_{ij}-T_{ji}) + \tfrac{1}{2}(T_{ij}+T_{ji}-\tfrac{2}{3}\mathrm{tr}(T)\delta_{ij}) \\ &= T^{[0]}_{ij} + T^{[1]}_{ij} + T^{[2]}_{ij}. \end{aligned} \tag{2.80}$$

According to their transformation properties under rotations, the first term belongs to the one-dimensional scalar representation ($T^{[0]}_{ij}$), the second to the three-dimensional vector representation ($T^{[1]}_{ij}$) and the last to the five-dimensional representation ($T^{[2]}_{ij}$) of spin 2. Let us now address the question, which of these representations will vanish due to selection rules in the scalar product in (2.78). Let us start with the vector representation:

$$\sum_{i,j=1}^{3}\left[\frac{\mathrm{d}}{\mathrm{d}Q^2}\eta^i(P)\eta^j(P)\right]_{Q^2=0}\langle\Phi^\Lambda_M|\tfrac{1}{2}\left(\hat{K}'^i\hat{K}'^j-\hat{K}'^j\hat{K}'^i\right)\hat{q}^3|\Phi^\Lambda_M\rangle = 0. \tag{2.81}$$

This is so, because $\eta^i(P)\eta^j(P)$ is symmetric, whereas $\hat{K}'^i\hat{K}'^j-\hat{K}'^j\hat{K}'^i$ is antisymmetric under the exchange of indices. For the spin 2 representation we cite the Wigner-Eckart theorem and in particular the triangularity relation which states, that:

$$\langle j_1|T^{[k]}_q|j_2\rangle = 0 \quad \text{unless} \quad |j_1-j_2|\le k\le j_1+j_2. \tag{2.82}$$

In our case $j_1=j_2=\frac{1}{2}$ and $k=2$, so the spin 2 representation in (2.80) gives no contribution. Only the scalar representation contributes and we get from (2.80) and (2.78):

$$\langle r^2\rangle = \frac{6}{Mq}\left[\frac{\mathrm{d}}{\mathrm{d}Q^2}\boldsymbol{\eta}^2(P)\right]_{Q^2=0}\langle\Phi^\Lambda_M|\hat{\boldsymbol{K}}'^2\hat{q}^3|\Phi^\Lambda_M\rangle. \tag{2.83}$$

Recalling the definition of the rapidity (2.68) we find:

$$\left.\frac{\mathrm{d}}{\mathrm{d}Q^2}\boldsymbol{\eta}^2(P)\right|_{Q^2=0} = \left.\frac{\mathrm{d}}{\mathrm{d}Q^2}\frac{Q^2}{4(M^2+Q^2/4)}\right|_{Q^2=0} = \frac{1}{4M^2}, \tag{2.84}$$

which brings us to our final result:

$$\langle r^2\rangle = \frac{1}{2Mq}\langle\Phi^\Lambda_M|\frac{3\hat{\boldsymbol{K}}'^2}{M^2}\hat{q}^3|\Phi^\Lambda_M\rangle. \tag{2.85}$$

Comparison of $\hat{K}'^i$ (2.79) with A''_i (2.45) shows that

$$\frac{3\hat{\boldsymbol{K}}'^2}{M^2}\hat{q}^3 = \hat{r}^2, \tag{2.86}$$

where $\hat{r}^2$ is the operator defined in (2.47). Thus the result of this section (2.85) is exactly the same as that of the previous one (2.46). Specifically what has been said there about the symmetry under particle exchange also applies here and we may write (2.85) in the usual symmetric form:

$$\langle r^2\rangle = \frac{1}{2M}\langle\Phi_M^\Lambda|\sum_{\alpha=1}^{3}\frac{\hat{q}^\alpha}{2}\left[\frac{\Omega}{M}\left(\mathrm{i}\boldsymbol{\nabla}_{\boldsymbol{p}_\alpha}-\hat{\boldsymbol{R}}\right)+\text{h. c.}\right]^2|\Phi_M^\Lambda\rangle. \tag{2.87}$$

2.4 Interpretation

Having derived an analytic expression for the mean square charge radius of a relativistic three-fermion system with instantaneous interaction kernels, in two different ways, it is worthwhile to give the result a meaningful physical interpretation.

So let us start with the factor $1/(2M)$ in (2.87) which takes into account the normalization of the Salpeter amplitudes (1.60):

$$\langle\Phi_M^\Lambda|\Phi_M^\Lambda\rangle = \int\frac{\mathrm{d}^3p_\xi}{(2\pi)^3}\frac{\mathrm{d}^3p_\eta}{(2\pi)^3}\sum_{a_1a_2a_3}\Phi_{M\,a_1a_2a_3}^{\Lambda\,*}(\vec{p}_\xi,\vec{p}_\eta)\Phi_{M\,a_1a_2a_3}^{\Lambda}(\vec{p}_\xi,\vec{p}_\eta) = 2M. \tag{2.88}$$

Hence this factor must be there to guarantee that the expectation value is independent of the normalization of the Salpeter amplitudes. To interpret the operator between the Salpeter amplitudes it is useful to note that $\mathrm{i}\boldsymbol{\nabla}_{\boldsymbol{p}_\alpha}$ is the position operator in momentum space:

$$\mathrm{i}\boldsymbol{\nabla}_{\boldsymbol{p}_\alpha} \equiv \hat{\boldsymbol{x}}_{\boldsymbol{\alpha}}. \tag{2.89}$$

Consequently the quantity $\hat{\boldsymbol{R}}$ as defined in (2.53) is the canonical relativistic center of mass of a three-particle system:

$$\hat{\boldsymbol{R}} = \frac{1}{\Omega}\sum_{\alpha=1}^{3}\omega_\alpha\hat{\boldsymbol{x}}_{\boldsymbol{\alpha}}. \tag{2.90}$$

For fermion momenta small compared to the their masses, i. e. $|\boldsymbol{p}_{\boldsymbol{\alpha}}| \ll m_\alpha$, we have $\omega_\alpha \to m_\alpha$ and thus the expression reduces to the well known nonrelativistic center of mass:

$$\hat{\boldsymbol{R}}_{\mathrm{nr}} = \frac{1}{m_1+m_2+m_3}\sum_{\alpha=1}^{3}m_\alpha\hat{\boldsymbol{x}}_{\boldsymbol{p}_\alpha}. \tag{2.91}$$

The expression

$$\mathrm{i}\boldsymbol{\nabla}_{\boldsymbol{p}_\alpha}-\hat{\boldsymbol{R}} = \hat{\boldsymbol{x}}_{\boldsymbol{\alpha}}-\frac{1}{\Omega}\sum_{\beta=1}^{3}\omega_\beta\hat{\boldsymbol{x}}_{\boldsymbol{p}_\beta} \tag{2.92}$$

then corresponds to the position of particle α measured from the center of mass. Figure 2.1 illustrates the situation.

Another aspect of this structure is translational invariance. Consider a three-particle bound state $|\boldsymbol{P}\rangle$ such as the Salpeter amplitudes with total four-momentum P. Space-time translations of this state are generated by the four-vector operator $\hat{P} = \hat{p}_1+\hat{p}_2+\hat{p}_3$.

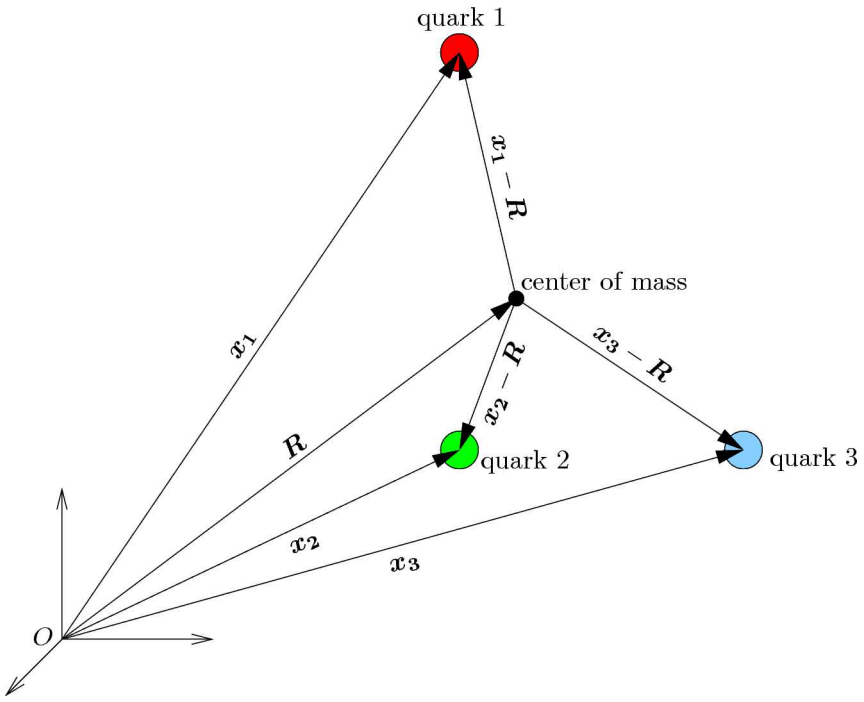

Figure 2.1: O denotes the origin of the reference frame, $\boldsymbol{R}$ the position vector of the relativistic center of mass and $\boldsymbol{x_1}$, $\boldsymbol{x_2}$, $\boldsymbol{x_3}$ the position vectors of the three fermions.

Now consider the translated state

$$\exp(-\mathrm{i}\boldsymbol{a}\cdot\hat{\boldsymbol{P}})|P\rangle = \exp(-\mathrm{i}\boldsymbol{a}\cdot\boldsymbol{P})|P\rangle = \exp(-\mathrm{i}\boldsymbol{a}\cdot(\boldsymbol{p_1}+\boldsymbol{p_2}+\boldsymbol{p_3}))|P\rangle. \tag{2.93}$$

If we let $(\mathrm{i}\boldsymbol{\nabla}_{\boldsymbol{p_\alpha}} - \hat{\boldsymbol{R}})$ act on the translated state, we find:

$$\begin{aligned}(\mathrm{i}\boldsymbol{\nabla}_{\boldsymbol{p_\alpha}} - \hat{\boldsymbol{R}})\exp(-\mathrm{i}\boldsymbol{a}\cdot\boldsymbol{P})|P\rangle &= \left(\mathrm{i}\boldsymbol{\nabla}_{\boldsymbol{p_\alpha}} - \frac{1}{\Omega}\sum_{\beta=1}^{3}\omega_\beta \mathrm{i}\boldsymbol{\nabla}_{\boldsymbol{p_\beta}}\right)\exp(-\mathrm{i}\boldsymbol{a}\cdot\boldsymbol{P})|P\rangle \\ &= \exp(-\mathrm{i}\boldsymbol{a}\cdot\boldsymbol{P})\left(\mathrm{i}\boldsymbol{\nabla}_{\boldsymbol{p_\alpha}} - \frac{1}{\Omega}\sum_{\beta=1}^{3}\omega_\beta \mathrm{i}\boldsymbol{\nabla}_{\boldsymbol{p_\beta}}\right)|P\rangle \\ &\quad + \left(\boldsymbol{a} - \frac{\sum_{\beta=1}^{3}\omega_\beta}{\Omega}\boldsymbol{a}\right)|P\rangle \\ &= \exp(-\mathrm{i}\boldsymbol{a}\cdot\boldsymbol{P})(\mathrm{i}\boldsymbol{\nabla}_{\boldsymbol{p_\alpha}} - \hat{\boldsymbol{R}})|P\rangle. \end{aligned} \tag{2.94}$$

In other words $(\mathrm{i}\boldsymbol{\nabla}_{\boldsymbol{p_\alpha}} - \hat{\boldsymbol{R}})$ commutes with spatial translations and hence the matrix element (2.87) is translationally invariant.

We also want to give a short comment about the hermiticity of the charge radius operator. First attempts to derive this operator not in the Breit frame but in a frame, where one particle is at rest showed that the final result would not be hermitian. There were in addition to the hermitian operator of (2.87) anti-hermitian terms which

originated from the asymmetric reference frame. Therefore the derivation was done in the Breit frame resulting in a hermitian operator. This in the end also justifies the choice of the derivatives in eq. (2.9), which might seem artificially complicated at first sight.

2.5 Results

In this section we present numerical results for the charge radii of the baryon octet obtained with our formula (2.87). We take the Salpeter amplitudes that were obtained by calculating the baryon spectrum as described in refs. [6, 7] and introduce no further parameters, *i.e.* the parameters are fixed by the spectrum. In this sense the numbers that we show here are predictions. We start with the radii of proton and neutron and compare them both to experiment as well as to form factor calculations which were carried out in the same model. The same will be done for the hyperon radii, which are however experimentally poorly covered.

2.5.1 Nucleon charge radii

For the proton we find a charge radius of

$$\sqrt{\langle r^2 \rangle_{\text{proton}}} = 0.86\,\text{fm} \tag{2.95}$$

in excellent agreement with the experimental value of $0.870 \pm 0.008\,\text{fm}$ from [15]. The mean square charge radius of the neutron however results in

$$\langle r^2 \rangle_{\text{neutron}} = -0.206\,\text{fm}^2 \tag{2.96}$$

and overestimates the empirical number of $-0.1161 \pm 0.0022\,\text{fm}^2$ from [15] by 77 %.

To shed some light on this discrepancy we analyze the dependence of these numbers on the range of the instanton force. The charge radii above where obtained by taking the parameter set as given in table 1.1. It is however known that the mass spectrum basically remains unchanged when one modifies the instanton cutoff parameter and simultaneously readjusts the instanton coupling strength. This assertion is demonstrated in fig. 2.2 where the nucleon spectrum is shown with the parameters from table 1.1, i. e. an instanton cutoff of 0.4 fm and a coupling strength of 136 MeV fm^3 compared to the spectrum at an instanton cutoff of 0.6 fm and a coupling strength of 263 MeV fm^3. The changes of the spectrum are marginal. Since the range of the instanton force influences the amount of diquark correlations in the nucleon wave functions we might however expect that the choice of the effective instanton range has a more pronounced influence on the charge radii which are a direct measure of these correlations. Therefore we have computed the charge radii of proton and neutron at different instanton cutoff parameters and accordingly adjusted coupling strengths. Figure 2.3 shows the resulting effect on the charge radii for effective instanton ranges between 0.2 fm and 0.8 fm. With increasing cutoff the absolute value of both mean square charge radii decrease by approximately the same amount. The shift is about 0.2 fm^2 between $\lambda = 0.2$ fm and

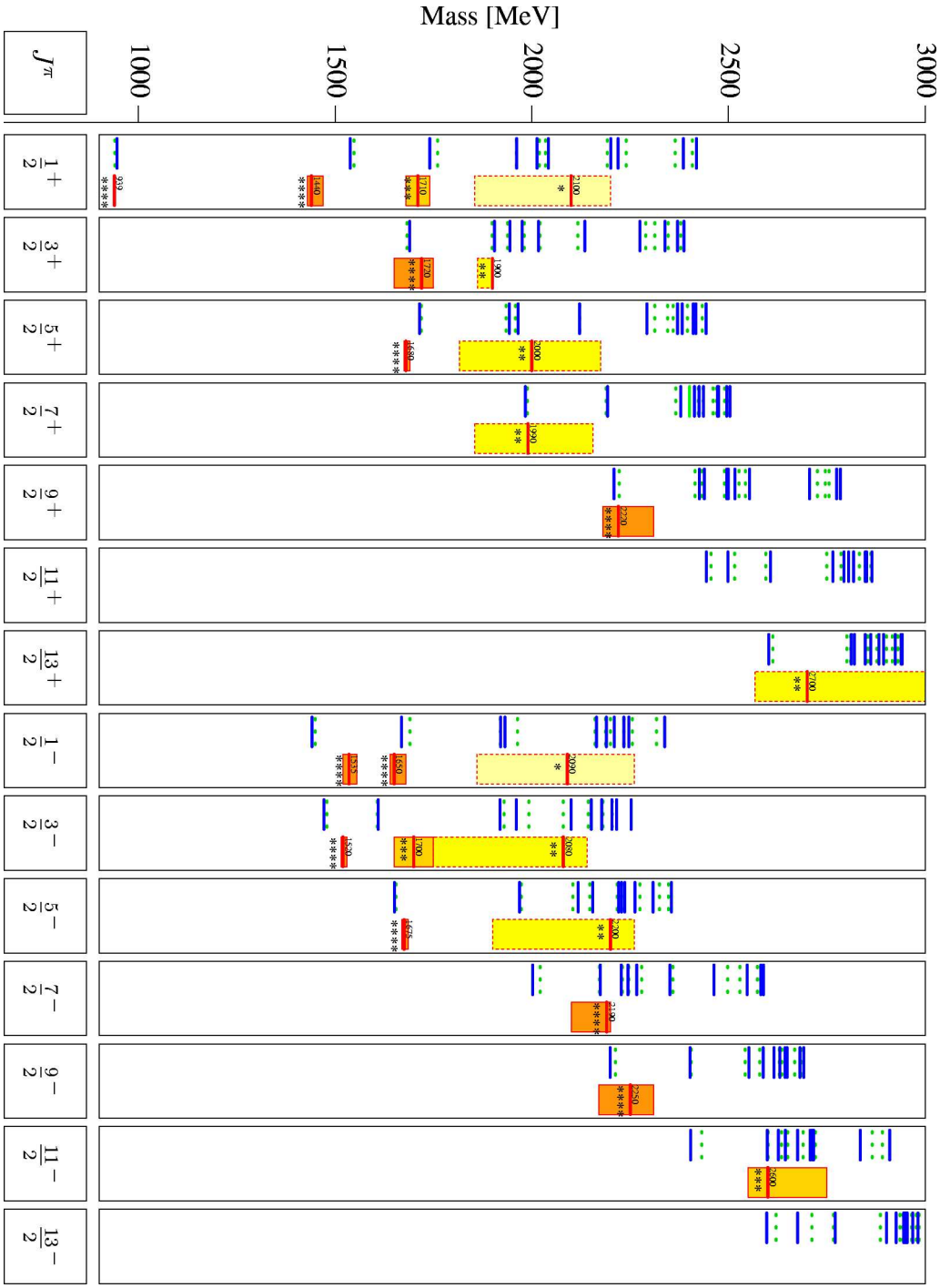

Figure 2.2: The nucleon spectrum with two different choices for the instanton parameters. Full bars correspond to the standard set ($\lambda = 0.4$ fm, $g_{nn} = 136$ MeV) and dashed bars to an instanton cutoff of 0.6 fm and a coupling strength of 263 MeV fm^3.

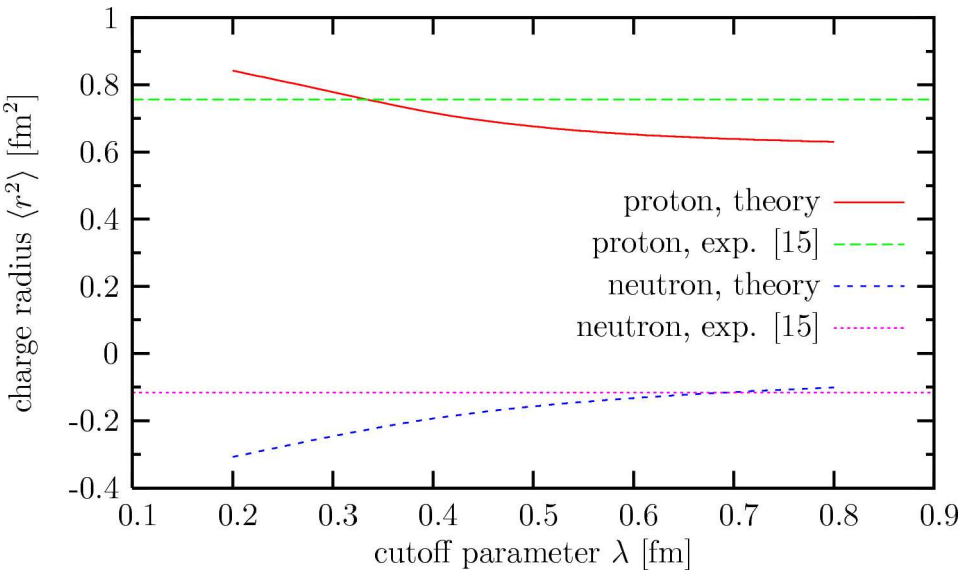

Figure 2.3: The mean square charge radii of proton and neutron as a function of the instanton cutoff parameter λ. Also shown are the experimental values as horizontal lines.

$\lambda = 0.8$ fm. We have also included the empirical values taken from [15] in the figure. Obviously, coincidence with the experimental proton charge radius is obtained at a cutoff between 0.3 fm and 0.4 fm, whereas the neutron charge radius hits experiment around a cutoff of 0.7 fm. So the choice of $\lambda = 0.4$ favors the proton charge radius to be in much better agreement with experiment as compared to the neutron radius whose smallness induces the large relative error of 77 % at that particular cutoff. It is obvious that there exists a choice of the cutoff parameter where the relative errors of both charge radii to their experimental values are of comparable size. Figure 2.4 shows the relative errors as a function of the cutoff. The plot impressively shows the large relative variation of the neutron radius due to its smallness, whereas the effect on the proton is moderate. We find that the errors of both radii with respect to the empirical values, namely 14 % are the same at $\lambda = 0.6$ fm and an instanton coupling strength of 263 MeV fm^3. With this particular choice the proton mean square charge radius amounts to 0.65 fm^2 which corresponds to 0.81 fm and the neutron charge radius becomes 0.132 fm^2.

We have thus found a compromise in the parameter set which minimizes the "collective" error of both proton and neutron charge radius. Whether this choice of parameters also has an effect on other electromagnetic observables of the nucleon such as magnetic moments and form factors will also be studied in subsequent chapters. The present status does not allow to draw the conclusion that the parameter set should be altered.

Comparison with form factor calculations

It worth to compare the proton (2.95) and neutron (2.96) charge radii with results that arise from electric form factor calculations within the same model and the same set of

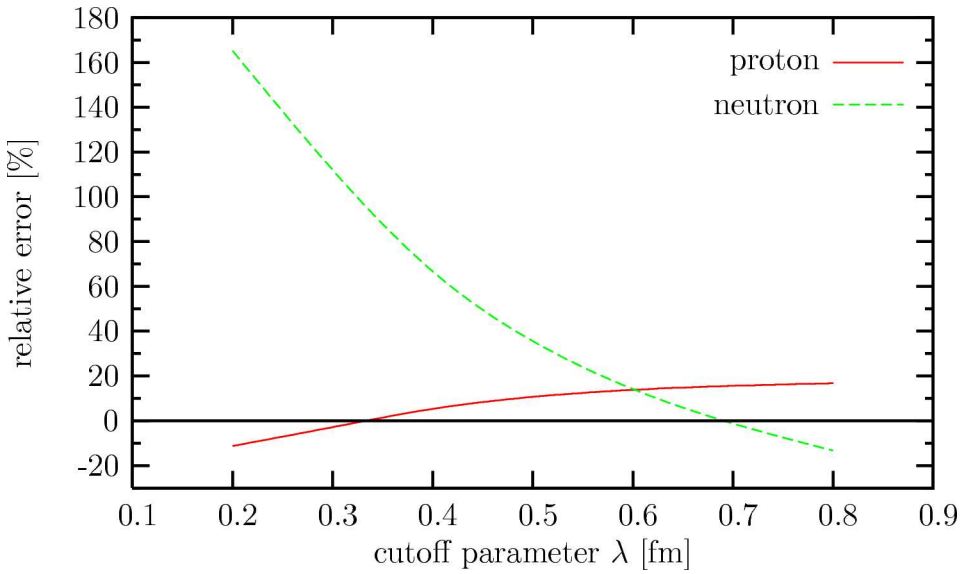

Figure 2.4: The relative errors of the charge radii of proton and neutron with respect to the experimental values as a function of the instanton cutoff parameter λ.

parameters as given by table 1.1. The authors of [11] quote 0.82 fm as the proton charge radius which compares nicely with our value. When comparing these values it must be noted however, that the Salpeter amplitudes and vertex functions are expanded in a oscillator basis as briefly described in appendix D. We worked in a basis with 16 oscillator shells whereas the authors of [11] only used 12. A clear advantage of the method presented in this work becomes apparent here. When extracting the charge radius from a form factor the latter has to be known at several finite momentum transfers to determine its slope. But at finite momentum transfer at least one of the wavefunctions that enter the current matrix element has to be boosted which makes the numerical computation more involved and consequently takes more time. With our method none of the wavefunctions has to be boosted and thus all of the angular integrations and all but one radial integration can be performed analytically which results in a noticeable reduction of computation time. Thus the difference in the dimensions of the oscillator basis of both approaches is explained. When we repeat our computation with 12 oscillator shells the resulting value of 0.84 fm is already closer to the form factor result.

Concerning the neutron the authors of [11] give a mean square radius of $-0.11\,\mathrm{fm}^2$ in clear disagreement with our result. Consequently we did a re-computation of the neutron electric form factor (see fig. 2.5) and re-analyzed the mean square radius (see fig. 2.6). It must be stated first, that the form factor that we computed using 12 oscillator shells within this model (see fig. 2.5) is in perfect agreement with the one obtained in [11], so the deviation can only be due to the procedure of how to extract its slope at the photon point. A plot of the form factor at low Q^2 (see fig. 2.6) reveals a difficulty here. The form factor takes a non-zero value at $Q^2 = 0$, although it should be zero — the charge of the neutron. This discrepancy may be explained with numerical inaccuracies, however it is surprising, that the values at different Q^2 fit perfectly on a straight line and do not scatter to a greater extent. If we stick to the definition (2.62) of

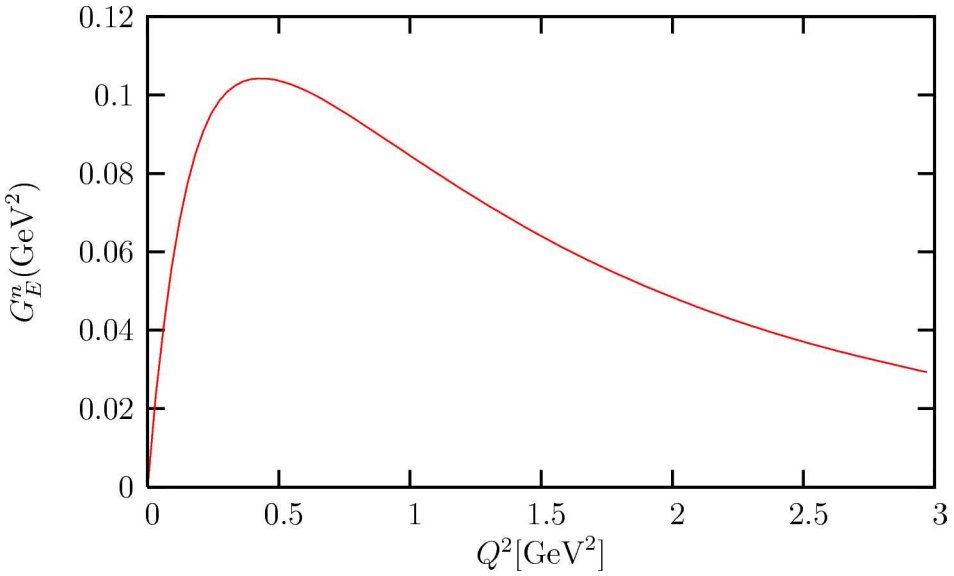

Figure 2.5: The electric form factor of the neutron calculated within the Bethe-Salpeter model using a basis size of 12 oscillator shells.

the charge radius as the slope of the form factor at zero momentum transfer and ignore the aforementioned problem, the radius that we extract amounts to $-0.224\,\mathrm{fm}^2$. This has to be compared to the value that we calculate using a basis size of 12 oscillator shells, namely $-0.188\,\mathrm{fm}^2$. Clearly both values are now in better coincidence. The remaining deviation may be due to numerical uncertainties, which undoubtedly spoil the predictability of small quantities like the neutron charge radius. The reanalysis of the form factor however showed that the extraction of the neutron radius in [11] is erroneous.

2.5.2 Hyperon charge radii

In addition to the nucleon charge radii we have also computed those of the strange octet baryons, although empirical values are naturally hard to find here. In this spirit the hyperon radii should be mainly considered as predictions. Table 2.1 lists the results for the hyperons. The Σ^- charge radius has been measured by the SELEX collaboration [23] by elastic scattering of Σ^- off electrons in a space-like Q^2 regime of $0.035\,\mathrm{GeV}^2 - 0.105\,\mathrm{GeV}^2$. The charge radius can be extracted from the differential cross section which up to order $m_e^2/(s - M_{\Sigma^-}^2)$ (s being the square of the center of mass energy) takes the form:

$$\frac{\mathrm{d}\sigma}{\mathrm{d}Q^2} = \frac{4\pi\alpha^2}{Q^4}\left(1 - \frac{Q^2}{Q^2_{\mathrm{max}}}\right) F^2(Q^2), \tag{2.97}$$

where Q_{max} depends on the beam momentum. $F(Q^2)$ is a combination of the electric and magnetic form factor both of which are then parameterized by a dipole shape in which the mean square charge radius enters as a parameter. By fitting to the measured

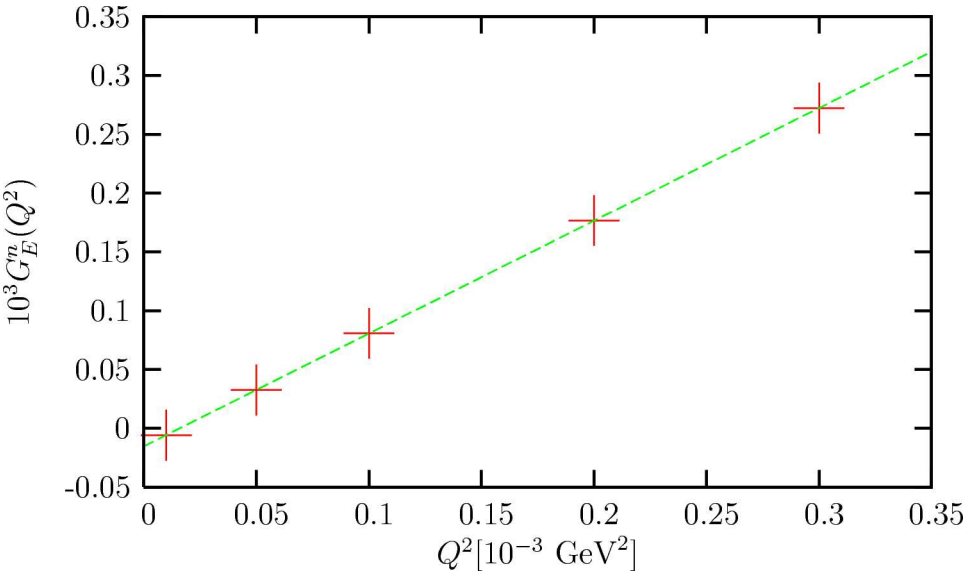

Figure 2.6: The electric form factor of the neutron at five different values of low momentum transfer to extract its slope at $Q^2 = 0$.

Q^2-distribution the radius can be extracted. The authors of [23] give a value of

$$\langle r^2 \rangle_{\Sigma^-} = (0.61 \pm 0.12(\text{stat.}) \pm 0.09(\text{syst.}))\text{fm}^2, \tag{2.98}$$

whose statistical and systematical errors make it compatible with our result of $0.42\,\text{fm}^2$.

In much the same way the Σ^--charge radius has been measured by the WA89 hyperon beam experiment at CERN [24] by elastically scattering high energy Σ^- off electrons in carbon and copper targets. The charge radius thus extracted from the Q^2-distribution of the reaction leads to a charge radius of:

$$\langle r^2 \rangle_{\Sigma^-} = (0.91 \pm 0.32(\text{stat.}) \pm 0.4(\text{syst.}))\text{fm}^2. \tag{2.99}$$

The large systematical and statistical errors in both analysis call for much improved experiments. Also the measurement of other hyperon charge radii would be advantageous in the future.

Comparison with form factor calculations

The hyperon charge radii have also been extracted from electric form factors by the authors of [12] within the same model extended to also include strange form factors. In table 2.1 these results are compared with ours. There are larger discrepancies especially with the neutral hyperons culminating in a large deviation of the Λ-charge radius. It should be noted however that the charge radii of the neutral baryons are anyway small and the computation of moments of a charge distribution with no net charge may pose numerical problems, especially when extracting it from a form factor calculation which is prone to numerical errors as shown in the previous subsection in case of the neutron and has also been discussed with the authors of ref. [12].

baryon	this calculation [fm^2]	Form factors [12] [fm^2]
Λ	0.0086	0.038
Σ^+	0.64	0.79
Σ^0	0.11	0.15
Σ^-	0.42	0.49
Ξ^0	0.075	0.14
Ξ^-	0.40	0.47

Table 2.1: Charge radii of the hyperons. The last column shows the results from form factor calculations performed within the same model [12].

2.5.3 The nonrelativistic limit

To underline the importance of a relativistic treatment of baryons we want to study the influence of relativistic effects on the charge radii. We therefore take the nonrelativistic limit of the relativistic expression (2.87) by setting $\omega_i \to m_i$:

$$\langle r^2 \rangle_{\rm nr} = \frac{1}{\langle \Phi_M^\Lambda | \Phi_M^\Lambda \rangle} \langle \Phi_M^\Lambda | \sum_{\alpha=1}^{3} \hat{q}^\alpha \left[\mathrm{i}\boldsymbol{\nabla}_{\boldsymbol{p_\alpha}} - \frac{\sum_{\beta=1}^{3} m_\beta \, \mathrm{i}\boldsymbol{\nabla}_{\boldsymbol{p_\beta}}}{m_1 + m_2 + m_3} \right]^2 | \Phi_M^\Lambda \rangle. \tag{2.100}$$

This expression is well known. One would write it down in nonrelativistic quantum mechanics. To demonstrate relativistic effects we computed the baryon octet charge radii with this expression taking the same wavefunctions as in the preceding sections. The results are compiled in table 2.2 together with the relativistic results and the ratio between both. Note that this calculation was performed using a basis size of 12 oscillator shells, which is sufficient to show the effect but explains the deviation from the results in subsections 2.5.1 and 2.5.2. The nonrelativistic radii are only about half the size of their relativistic counterparts, which emphasizes the importance of a relativistic treatment of baryons.

Comparison with other models

In table 2.3 we compare our results to other models or approaches to charge radii. The values in the third column stem from a calculation performed in fourth order in relativistic chiral perturbation theory with infrared regularization (see ref. [25]). Here, the experimental radii of proton and neutron have been taken to fit two low energy constants, such that the radii of the hyperons can be considered as predictions. The errors are obtained from the uncertainty in the theoretical description of the magnetic moments, which have also been used to fix low energy constants. They do however not contain errors that are due to higher order corrections. In the fourth column we

baryon	rel. [fm^2]	nonrel. [fm^2]	nonrel./rel. [%]
proton	0.71	0.3	42
neutron	−0.185	−0.08	43
Λ	0.0086	0.002	23
Σ^+	0.64	0.3	47
Σ^0	0.11	0.043	36
Σ^-	0.42	0.22	52
Ξ^0	0.075	0.044	59
Ξ^-	0.40	0.26	65

Table 2.2: Charge radii in the nonrelativistic limit (3rd column). Also shown are the relativistic results (2nd column) and the ratios (4th column) between the nonrelativistic and relativistic treatment. The analysis was performed using a basis size of 12 oscillator shells

have cited the charge radii from a constituent quark model (CQM) that incorporates interactions induced by Goldstone boson exchange (GBE) taken from ref. [26].

baryon	this calculation [fm^2]	χPT [25] [fm^2]	GBE-CQM [26] [fm^2]
proton	0.71	0.717	0.82
neutron	−0.185	−0.113	−0.13
Λ	0.0086	0.11 ± 0.02	0.03
Σ^+	0.64	0.60 ± 0.02	1.13
Σ^0	0.11	-0.03 ± 0.01	0.20
Σ^-	0.42	0.67 ± 0.03	0.72
Ξ^0	0.075	0.13 ± 0.03	−0.19
Ξ^-	0.40	0.49 ± 0.05	0.72

Table 2.3: Charge radii computed in the Bethe-Salpeter framework compared to other models.

2.6 Summary

We have presented two different derivations for an analytic expression of the charge radius in the Bethe-Salpeter framework, both resulting in the same formula. In the first approach we started from a very basic definition of the charge radius of a charge distribution taken from classical electrodynamics. By inserting the time component of the current matrix element derived in chapter 1 we made a connection to the Bethe-Salpeter formalism. After evaluating the Laplacian of the current matrix element and taking the static limit, we integrated out the dependence on the relative energy variables. Symmetrizing the resulting expression over the three fermions, we arrived at the final expression, which turned out to be an expectation value with respect to Salpeter amplitudes. Before interpreting this result, we followed the second approach, which was based on the definition of the charge radius as the slope of the electric form factor at vanishing four-momentum transfer squared. We first showed that this definition is equivalent to our first approach in a generic way. Following this definition we had to find the Q^2-dependence of the current matrix element, which was accomplished by expanding the boost of the incoming Salpeter amplitude as an exponential. It was then easy to compute the first derivative with respect to Q^2 and to follow the same steps of the first approach to end up with the identical expression. The interpretation of the result revealed an interesting physical structure. We obviously found the relativistic generalization of the nonrelativistic charge radius operator. The fermion masses are replaced by the relativistic kinetic energies and the center of mass motion is subtracted. In addition an overall relativistic weight factor multiplies the operator. These features appeared naturally, nothing was inserted by hand.

To test this analytic result we turned to the quark model described in chapter 1 and computed the charge radii of the complete baryon octet, taking the Salpeter amplitudes as they emerged from the computation of the baryon mass spectra, *i.e.* no further parameters were introduced. The proton mean square charge radius fit the empirical value very accurately, whereas the neutron charge radius was to large by almost 80%. To clarify this observation we studied the dependence of these numbers on the size of the instanton cutoff parameter. Although it was known that changing this parameter while readjusting the instanton coupling accordingly affects the mass spectrum only slightly, it was not clear that the same is true for the charge radii. Indeed we found a strong dependence of the neutron charge radius on the cutoff size and moderate dependence of the proton charge radius. Since the neutron radius is anyway small this observation is not astonishing. It was then argued that there is a choice of the instanton parameters which minimizes the error in the neutron charge radius while making the proton charge radius deviate from the empirical value by about a few percent. This parameter set will be tested in a subsequent chapter also on the nucleon magnetic moments and form factors. We then moved on to compare our results with form factor calculations that were carried out in the same model. We found a large discrepancy in the neutron form factor. After reproducing the form factor calculation and the extraction of the charge radius we could show, that there was indeed an error in the original analysis of the form factor. The discrepancy was thus removed. To underline the importance of a relativistic treatment of baryon properties, we also computed the nonrelativistic limit of the obtained operator with unaltered Salpeter amplitudes. The

resulting charge radii where to small by about a factor of two. Our results on the hyperon charge radii have a more predictive character since conclusive experimental results do not exist at present. The comparison with form factor calculations shows deviations which might originate from numerical instabilities. The deviating values are anyway very small.

To conclude this chapter, we note that the analytic derivation of the charge radius in the context of the Bethe-Salpeter formalism has lead to new insights into the structure of this observable, which could never be obtained from a form factor calculations alone. The result found its successful application with the computation of the baryon octet charge radii.

Chapter 3

Magnetic moments

The new approach to static properties of relativistic three-fermion systems being successful in the case of charge radii, it is worthwhile extend it to magnetic moments. Since this has already been done in ref. [16] however starting from the energy of a magnetic dipole in a magnetic field, we take a different approach starting from form factors. This has already proven to be a suitable starting point in the preceding chapter on charge radii. As was done there, we also apply the analytic results of this chapter to the computation of baryon magnetic moments.

3.1 Introduction and overview

The magnetic moment encodes information about the response of a classical or quantum mechanical system to an applied external magnetic field. Classically a charge q with mass m that is forced on a circular trajectory produces a magnetic moment that is given by:

$$\boldsymbol{\mu} = \frac{q}{2m}\boldsymbol{L}, \tag{3.1}$$

where $\boldsymbol{L}$ is its angular momentum. The energy of this magnetic dipole in a magnetic field is given by $E = -\boldsymbol{\mu} \cdot \boldsymbol{B}$. If we make the transition to quantum mechanics, the angular momentum in eq. (3.1) is promoted to an operator according to the correspondence principle and the magnetic moment is given by the expectation value of the operator (3.1) with respect to Schrödinger wavefunctions. If we also take the spin of the particle into account, we have to add a term to the orbital angular momentum $\boldsymbol{L}$ that represents the interaction of the particles spin with external magnetic fields. This term is given for free spin-$\frac{1}{2}$ particles by $2\boldsymbol{S}$, where $\boldsymbol{S}$ is the canonical spin operator. Since the spin is a genuinely relativistic quantity, the orbital angular momentum as defined above however is not, this procedure constitutes no real relativistic generalization. On the other hand in field theoretic descriptions one defines the magnetic moment as the value of the magnetic form factor at vanishing momentum transfer squared of the probing photon. This approach however clouds the mechanisms that result in the total magnetic moment. In particular it does not distinguish between contributions of the orbital angular momentum and the intrinsic spins of the constituents that make up a bound state. As with the charge radius, we seek for a synthesis of both approaches. In

ref. [16] the magnetic moment of a bound state in a field theoretic description based on the Bethe-Salpeter equation has successfully been expressed as an expectation value with respect to Salpeter amplitudes. The resulting operator could be assigned a natural physical interpretation. The starting point for the derivation of this operator in ref. [16] was the comparison of the energy of a magnetic dipole in an external magnetic field $E = -\boldsymbol{\mu} \cdot \boldsymbol{B}$ with the interaction energy $E_{\rm int} = \int \mathrm{d}^3x \langle\psi|\mathcal{H}_{\rm int}(x)|\psi\rangle$ from the coupling of an electromagnetic current with an external field $\mathcal{H}_{\rm int}(x) = j_\mu(x)A^\mu(x)$.

In the present work we want to give a different derivation that starts with the magnetic form factor. As already mentioned, in this context the magnetic moment is defined as the value of this form factor at the photon point. As we will show in section 3.2, care must be taken when evaluating the limit $Q^2 \to 0$, since the current matrix element that enters the form factor is divided by $\sqrt{Q^2}$. We isolate the Q^2-dependence by expanding the boost of the incoming vertex function as an exponential, utilizing the results of the charge radius derivation. Because of parity the lowest order term of this expansion is of order $\sqrt{Q^2}$ and the static limit is well defined. After the relative energy integration, the expression is made an expectation value with the help of the Wigner-Eckart theorem. When symmetrizing over the three fermions we exactly get the result of ref. [16]. The expression turns indeed out as the relativistic generalization of the nonrelativistic prescription discussed above, *i.e.* the sum of orbital angular momentum corrected by the center of mass motion and a spin contribution with fermion masses replaced by the relativistic single-particle energies. Since an extensive interpretation of this result has already been given there, we restrict ourselves to a short description of its prominent features in section 3.2.1.

We also want to make an application to magnetic moments of baryons, whose mass spectra have been calculated in a relativistic quark model based on the Bethe-Salpeter equation in refs. [6, 7]. A numerical implementation of the analytic result has been given for the baryon octet in ref. [16], however with a wrong strange/non-strange instanton coupling, which spoiled the result for the hyperon magnetic moments. We therefore show the correct results in section 3.3 and also compare them to form factor calculations which recently have been performed within the same model. We study relativistic effects by computing the expectation value of the nonrelativistic limit of the fully relativistic operator. An important advantage of the method presented here over the form factor approach is the fact that the decomposition into orbital angular momentum and spin contributions to the net magnetic moment is preserved, which allows for a systematical study of these contributions. We will see that the overwhelming part stems from the fermion spins, at least for the ground states. This result is however only true if we work with constituent quark masses. When making the quark masses nearly as small as the current masses and at the same time adjusting the coupling strengths accordingly to keep the ground states at their empirical values, both contributions become in fact comparable in magnitude. Since efforts are being made to measure also magnetic moments of excited nucleon states, we contribute some selected predictions here. In the same spirit, our results on the decuplet magnetic moments which close this section are sole predictions.

3.2 From magnetic form factors to magnetic moments

To derive magnetic moments from form factors in an analogous way as the charge radius in chapter 2 we start from the parameterization (2.56) of the electromagnetic vector current:

$$\langle \mathcal{P}P, \lambda' | j_+(0) | P, \lambda \rangle = e \left[F_1(Q^2) + F_2(Q^2) \right] \bar{u}_{\lambda'}(\mathcal{P}P) \gamma_+ u_\lambda(P), \tag{3.2}$$

where the "+"-component of the current is defined by:

$$j_+(0) = j_1(0) + \mathrm{i} j_2(0). \tag{3.3}$$

Note that this definition deviates from the definition of a spherical tensor operator of rank 1 shown in the appendix (C.2). The baryon makes a spin flip of course so we have $\lambda' \neq \lambda$. The spin polarizations will be fixed later. Evaluation of the spinorial part of this equation yields:

$$\begin{aligned} \bar{u}_{\lambda'}(\mathcal{P}P)\gamma_+ u_\lambda(P) &= \left(\xi^\dagger_{\lambda'} \sqrt{\sigma(P)}, \xi^\dagger_{\lambda'} \sqrt{\bar{\sigma}(P)} \right) \cdot \begin{pmatrix} 0 & -\sigma^+ \\ \sigma^+ & 0 \end{pmatrix} \cdot \begin{pmatrix} \sqrt{\sigma(P)}\xi_\lambda \\ \sqrt{\bar{\sigma}(P)}\xi_\lambda \end{pmatrix} \\ &= 4\sqrt{|\boldsymbol{P}|^2} = 2\sqrt{Q^2} \end{aligned} \tag{3.4}$$

The last line can be shown by introducing a specific orthonormal spin basis like $\xi_{\lambda'} = (1,0)$ and $\xi_\lambda = (0,1)$ and using the explicit representation for the square root of $\sigma(P)$. Together with the definition of the magnetic Sachs form factor (2.61a) we then get from (3.2) the relation

$$G_M(Q^2) = \frac{\langle \mathcal{P}P, \lambda' | j_+(0) | P, \lambda \rangle}{2\sqrt{Q^2}}, \tag{3.5}$$

which expresses the magnetic form factor in terms of spatial components of the current matrix element. The magnetic moment of a baryon is defined as the value of the magnetic form factor at the photon point:

$$\mu := G_M(Q^2 = 0). \tag{3.6}$$

Because of the denominator in (3.5) taking this limit requires some care. We need to know the Q^2-dependence of the current matrix element rather precisely. But first let us choose the three momentum transfer to point in the 3-direction from now on:

$$\boldsymbol{q} := \begin{pmatrix} 0 \\ 0 \\ q_3 \end{pmatrix} = \sqrt{Q^2}\, \boldsymbol{e_3}. \tag{3.7}$$

As is obvious from the definition of $\hat{P}$ (1.102) we then have $\hat{P}^+ = 0$ so that the current matrix element (1.107) now becomes:

$$\begin{aligned} \langle \mathcal{P}P | j^+(0) | P \rangle = -3 \int \frac{d^4 p_\xi}{(2\pi)^4} \int \frac{d^4 p_\eta}{(2\pi)^4} \bar{\Gamma}^\Lambda_M(\boldsymbol{p_\xi}, \boldsymbol{p_\eta}) \\ \times \left[S_F^1(p_\xi + \tfrac{1}{2} p_\eta) \otimes S_F^2(-p_\xi + p_\eta) \otimes S_F^3(M - p_\eta) \right] \left[S^2_{\Lambda_P} \otimes S^2_{\Lambda_P} \otimes S^2_{\Lambda_P} \right] \\ \times \left[\mathbb{1} \otimes \mathbb{1} \otimes \hat{q}\gamma^+ S_F^3(M - \Lambda_P^{-1^2} p_\eta) \right] \Gamma^\Lambda_M(\overrightarrow{\Lambda_P^{-1^2} p_\xi}, \overrightarrow{\Lambda_P^{-1^2} p_\eta}) \end{aligned} \tag{3.8}$$

To extract the Q^2-dependence of this expression we express the boost as an exponential just like in the previous chapter on charge radii:

$$\langle \mathcal{P}P,\lambda'|j^+(0)|P,\lambda\rangle = -3\int\frac{d^4p_\xi}{(2\pi)^4}\int\frac{d^4p_\eta}{(2\pi)^4}\bar{\Gamma}^\Lambda_{M,\lambda'}(\boldsymbol{p_\xi},\boldsymbol{p_\eta})$$
$$\times\left[S_F^1(p_\xi+\tfrac{1}{2}p_\eta)\otimes S_F^2(-p_\xi+p_\eta)\otimes S_F^3(M-p_\eta)\right]\exp(-2\mathrm{i}\,\boldsymbol{\eta}(P)\cdot\hat{\boldsymbol{K}})$$
$$\times\left[\mathbb{1}\otimes\mathbb{1}\otimes\hat{q}\gamma^+S_F^3(M-p_\eta)\right]\Gamma^\Lambda_{M,\lambda}(\boldsymbol{p_\xi},\boldsymbol{p_\eta}). \quad (3.9)$$

This time however the boost generator also acts on the Dirac space of the third quark as can be seen from the current matrix element (3.8):

$$\hat{K}^i = \mathrm{i}\left[-p^0_\xi\tfrac{\partial}{\partial p^i_\xi}-p^i_\xi\tfrac{\partial}{\partial p^0_\xi}-p^0_\eta\tfrac{\partial}{\partial p^i_\eta}-p^i_\eta\tfrac{\partial}{\partial p^0_\eta}+\tfrac{1}{2}\left(\alpha^i\otimes\mathbb{1}\otimes\mathbb{1}+\text{cycl. perm.}\right)\right] \quad (3.10)$$

Since γ^+ is odd under parity it follows that terms with even powers of $\boldsymbol{\eta}(P)$ from the exponential vanish, if we again assume that the vertex functions represent states with definite parity. This leads to the following expression:

$$\langle \mathcal{P}P,\lambda'|j^+(0)|P,\lambda\rangle = -3\int\frac{d^4p_\xi}{(2\pi)^4}\int\frac{d^4p_\eta}{(2\pi)^4}\bar{\Gamma}^\Lambda_{M,\lambda'}(\boldsymbol{p_\xi},\boldsymbol{p_\eta})$$
$$\times\left[S_F^1(p_\xi+\tfrac{1}{2}p_\eta)\otimes S_F^2(-p_\xi+p_\eta)\otimes S_F^3(M-p_\eta)\right]\left[-2\mathrm{i}\,\boldsymbol{\eta}(P)\cdot\hat{\boldsymbol{K}}\right]$$
$$\times\left[\mathbb{1}\otimes\mathbb{1}\otimes\hat{q}\gamma^+S_F^3(M-p_\eta)\right]\Gamma^\Lambda_{M,\lambda}(\boldsymbol{p_\xi},\boldsymbol{p_\eta})+\mathcal{O}(\boldsymbol{\eta}^3). \quad (3.11)$$

Inserting this into (3.5) and taking the limit $Q^2\to 0$ then shows that terms with $\mathcal{O}(\boldsymbol{\eta})>1$ vanish because $\boldsymbol{\eta}(P)$ is of order $\sqrt{Q^2}$. Concerning the first order term we find with the special choice of the three momentum transfer (3.7) and the definition of the rapidity (2.68):

$$\lim_{Q^2\to0}\frac{\boldsymbol{\eta}(P)}{\sqrt{Q^2}}=\lim_{Q^2\to0}\frac{-\sqrt{Q^2}}{2\sqrt{M^2+Q^2/4}\sqrt{Q^2}}\boldsymbol{e}_3=\frac{-1}{2M}\boldsymbol{e}_3. \quad (3.12)$$

Therefore the static limit can safely be taken and we find for the magnetic moment:

$$\mu=-\frac{3}{4M^2}\int\frac{d^4p_\xi}{(2\pi)^4}\int\frac{d^4p_\eta}{(2\pi)^4}\bar{\Gamma}^\Lambda_{M,\lambda'}(\boldsymbol{p_\xi},\boldsymbol{p_\eta})$$
$$\times\left[S_F^1(p_\xi+\tfrac{1}{2}p_\eta)\otimes S_F^2(-p_\xi+p_\eta)\otimes S_F^3(M-p_\eta)\right]$$
$$\times\mathrm{i}\hat{K}_3\left[\mathbb{1}\otimes\mathbb{1}\otimes\hat{q}\gamma^+S_F^3(M-p_\eta)\right]\Gamma^\Lambda_{M,\lambda}(\boldsymbol{p_\xi},\boldsymbol{p_\eta}). \quad (3.13)$$

We inserted a factor $1/2M$ in this expression since the wavefunctions are normalized to $2M$ as can be seen from (1.60). As was shown in the previous chapter, there exists a relation (2.77) between $\hat{K}_i$ and A_i which allows us to use the results of appendix B

regarding the integration over the relative energies:

$$\mu = \frac{3}{8M}\int\frac{d^3p_\xi}{(2\pi)^3}\int\frac{d^3p_\eta}{(2\pi)^3}\bar{\Gamma}^\Lambda_{M,\lambda'}(\boldsymbol{p_\xi},\boldsymbol{p_\eta})\Big\{ \\ \frac{\Lambda^{+++}}{(M-\Omega)}[\gamma^0\otimes\gamma^0\otimes\mathbb{1}]A^3_+[\mathbb{1}\otimes\mathbb{1}\otimes\hat{q}\alpha^+]\frac{\mathbb{1}\otimes\mathbb{1}\otimes\Lambda^+}{(M-\Omega)} \\ + \frac{\Lambda^{---}}{(M+\Omega)}[\gamma^0\otimes\gamma^0\otimes\mathbb{1}]A^3_-[\mathbb{1}\otimes\mathbb{1}\otimes\hat{q}\alpha^+]\frac{\mathbb{1}\otimes\mathbb{1}\otimes\Lambda^-}{(M+\Omega)}\Big\}[\mathbb{1}\otimes\mathbb{1}\otimes\gamma^0]\Gamma^\Lambda_{M,\lambda}(\boldsymbol{p_\xi},\boldsymbol{p_\eta}), \tag{3.14}$$

with

$$A^i_\pm := -\tfrac{2}{M}\left[\pm\tfrac{1}{2}(\omega_1-\omega_2)\tfrac{\partial}{\partial p^i_\xi}\pm(\omega_1+\omega_2)\tfrac{\partial}{\partial p^i_\eta}+\tfrac{1}{2}(\alpha^i\otimes\mathbb{1}\otimes\mathbb{1}+\text{cycl. perm.})\right]. \tag{3.15}$$

We ultimately want to replace the vertex functions in (3.14) by Salpeter amplitudes. First by making use of the anti-commutator $\{\gamma^0,\alpha^i\}_+=0$, we obtain:

$$\mu = \frac{3}{8M}\int\frac{d^3p_\xi}{(2\pi)^3}\int\frac{d^3p_\eta}{(2\pi)^3}\bar{\Gamma}^\Lambda_{M,\lambda'}(\boldsymbol{p_\xi},\boldsymbol{p_\eta})\Big\{\frac{\Lambda^{+++}}{(M-\Omega)}B^3_+[\mathbb{1}\otimes\mathbb{1}\otimes\hat{q}\alpha^+]\frac{\mathbb{1}\otimes\mathbb{1}\otimes\Lambda^+}{(M-\Omega)} \\ + \frac{\Lambda^{---}}{(M+\Omega)}B^3_-[\mathbb{1}\otimes\mathbb{1}\otimes\hat{q}\alpha^+]\frac{\mathbb{1}\otimes\mathbb{1}\otimes\Lambda^-}{(M+\Omega)}\Big\}[\gamma^0\otimes\gamma^0\otimes\gamma^0]\Gamma^\Lambda_{M,\lambda}(\boldsymbol{p_\xi},\boldsymbol{p_\eta}), \tag{3.16}$$

where $B^i_\pm$ originates from $A^i_\pm$ by reversing the sign of $\frac{1}{2}(\alpha^i\otimes\mathbb{1}\otimes\mathbb{1})$ and $\frac{1}{2}(\mathbb{1}\otimes\alpha^i\otimes\mathbb{1})$:

$$B^i_\pm := -\tfrac{2}{M}\Big[\pm\tfrac{1}{2}(\omega_1-\omega_2)\tfrac{\partial}{\partial p^i_\xi}\pm(\omega_1+\omega_2)\tfrac{\partial}{\partial p^i_\eta} \\ -\tfrac{1}{2}(\alpha^i\otimes\mathbb{1}\otimes\mathbb{1}+\mathbb{1}\otimes\alpha^i\otimes\mathbb{1}-\mathbb{1}\otimes\mathbb{1}\otimes\alpha^i)\Big]. \tag{3.17}$$

Next we complete $\mathbb{1}\otimes\mathbb{1}\otimes\Lambda^\pm$ to eventually obtain a Salpeter projector. We make use of the projector structure of the vertex functions, namely that they only contain pure energy components:

$$\mu = \frac{3}{8M}\int\frac{d^3p_\xi}{(2\pi)^3}\int\frac{d^3p_\eta}{(2\pi)^3}\bar{\Gamma}^\Lambda_{M,\lambda'}(\boldsymbol{p_\xi},\boldsymbol{p_\eta})\Big\{\frac{\Lambda^{+++}}{(M-\Omega)}C^3_+[\mathbb{1}\otimes\mathbb{1}\otimes\hat{q}\alpha^+]\frac{\Lambda^{+++}}{(M-\Omega)} \\ + \frac{\Lambda^{---}}{(M+\Omega)}C^3_-[\mathbb{1}\otimes\mathbb{1}\otimes\hat{q}\alpha^+]\frac{\Lambda^{---}}{(M+\Omega)}\Big\}[\gamma^0\otimes\gamma^0\otimes\gamma^0]\Gamma^\Lambda_{M,\lambda}(\boldsymbol{p_\xi},\boldsymbol{p_\eta}). \tag{3.18}$$

We obtain $C^i_\pm$ from $B^i_\pm$ by applying the commutation rule (2.43):

$$C^i_\pm := -\tfrac{2}{M}\left[\pm\tfrac{1}{2}(\omega_1-\omega_2)\tfrac{\partial}{\partial p^i_\xi}\pm(\omega_1+\omega_2)\tfrac{\partial}{\partial p^i_\eta}\mp\frac{p^i_1}{\omega_1}\mp\frac{p^i_2}{\omega_2}+\tfrac{1}{2}\mathbb{1}\otimes\mathbb{1}\otimes\alpha^i\right]. \tag{3.19}$$

We still cannot replace the vertex functions because of the changing signs in $C^i_\pm$. So (2.42) has to be applied to commute $\Lambda^\pm_3$ with α^+ and get an additional changing sign.

Before we can do so however, $\Lambda_3^{\pm}$ has to be commuted with the derivative terms of $C_{\pm}^i$:

$$\mu = \frac{3}{8M}\int\frac{d^3p_\xi}{(2\pi)^3}\int\frac{d^3p_\eta}{(2\pi)^3}\bar{\Gamma}^{\Lambda}_{M,\lambda'}(\boldsymbol{p_\xi},\boldsymbol{p_\eta})\Big\{ \\ \frac{\Lambda^{+++}}{(M-\Omega)}[\mathbb{1}\otimes\mathbb{1}\otimes\hat{q}(D_+^3\Lambda^+ + E^3)\alpha^+]\frac{\Lambda^{+++}}{(M-\Omega)} \\ + \frac{\Lambda^{---}}{(M+\Omega)}[\mathbb{1}\otimes\mathbb{1}\otimes\hat{q}(D_-^3\Lambda^- + E^3)\alpha^+]\frac{\Lambda^{---}}{(M+\Omega)}\Big\}[\gamma^0\otimes\gamma^0\otimes\gamma^0]\Gamma^{\Lambda}_{M,\lambda}(\boldsymbol{p_\xi},\boldsymbol{p_\eta}), \quad (3.20)$$

We get $D_{\pm}^i$ and E^i from $C_{\pm}^i$ by applying the derivatives in $C_{\pm}^i$ to $\Lambda_{\pm}(\boldsymbol{p_3})$:

$$D_{\pm}^i := -\tfrac{2}{M}\left[\pm\tfrac{1}{2}(\omega_1-\omega_2)\tfrac{\partial}{\partial p_\xi^i}\pm(\omega_1+\omega_2)\tfrac{\partial}{\partial p_\eta^i}\mp\frac{p_1^i}{\omega_1}\mp\frac{p_2^i}{\omega_2}\mp\frac{\omega_1+\omega_2}{2\omega_3^2}p_\eta^i\right] \quad (3.21)$$

$$E^i := \frac{\omega_1+\omega_2+\omega_3}{M\omega_3}(\mathbb{1}\otimes\mathbb{1}\otimes\alpha^i). \quad (3.22)$$

Finally by applying (2.42) we obtain the desired result:

$$\mu = \frac{3}{2M}\int\frac{d^3p_\xi}{(2\pi)^3}\int\frac{d^3p_\eta}{(2\pi)^3}\bar{\Gamma}^{\Lambda}_{M,\lambda'}(\boldsymbol{p_\xi},\boldsymbol{p_\eta})\left[\frac{\Lambda^{+++}}{(M-\Omega)}+\frac{\Lambda^{---}}{(M+\Omega)}\right] \\ \times \mathrm{i}F^{3+}\hat{q}_3\left[\frac{\Lambda^{+++}}{(M-\Omega)}+\frac{\Lambda^{---}}{(M+\Omega)}\right][\gamma^0\otimes\gamma^0\otimes\gamma^0]\Gamma^{\Lambda}_{M,\lambda}(\boldsymbol{p_\xi},\boldsymbol{p_\eta}), \quad (3.23)$$

with the tensor operator:

$$F^{ij} := \frac{1}{2M}\Big\{\frac{p_3^j}{2\omega_3}\left[\tfrac{1}{2}(\omega_1-\omega_2)\,\mathrm{i}\tfrac{\partial}{\partial p_\xi^i}+(\omega_1+\omega_2)\,\mathrm{i}\tfrac{\partial}{\partial p_\eta^i}-\text{h. c.}\right] \\ + \frac{\omega_1+\omega_2+\omega_3}{2\omega_3}\left(\mathbb{1}\otimes\mathbb{1}\otimes\mathrm{i}\alpha^i\alpha^j\right)+\frac{\omega_1+\omega_2}{2\omega_3^2}p_3^ip_3^j\Big\} \quad (3.24)$$

Note that the "+"-component in the second index of F^{ij} in (3.23) has to be taken in the sense of (3.3). Before we analyze this expression further let us replace the vertex functions in (3.23) by using the relations (A.13) and (A.14) to arrive at the compact notation:

$$\begin{aligned}\mu &= \frac{3}{2M}\int\frac{d^3p_\xi}{(2\pi)^3}\int\frac{d^3p_\eta}{(2\pi)^3}\Phi^{\Lambda}_{M,\lambda'}{}^{\dagger}(\boldsymbol{p_\xi},\boldsymbol{p_\eta})\,F^{3+}\hat{q}_3\Phi^{\Lambda}_{M,\lambda}(\boldsymbol{p_\xi},\boldsymbol{p_\eta}) \\ &= \frac{3}{2M}\langle\Phi^{\Lambda}_{M,\lambda'}|F^{3+}\hat{q}_3|\Phi^{\Lambda}_{M,\lambda}\rangle\end{aligned} \quad (3.25)$$

Since F^{ij} is a product of two vector operators it constitutes a Cartesian tensor operator of rank 2, which can be decomposed into irreducible representations of the rotation group according to (2.80). Just as we did when deriving the charge radius, we may show that the contributions of certain representations vanish. The scalar representation

gives no contribution because of the m-selection rule of the Wigner-Eckart theorem, which states that

$$\langle j_1, m_1 | F_q^{[k]} | j_2, m_2 \rangle = 0 \quad \text{unless} \quad m_1 - m_2 = q. \tag{3.26}$$

In our case $m_1 = \frac{1}{2}$, $m_2 = -\frac{1}{2}$ and $q = 0$. The spin 2 representation vanishes for spin-$\frac{1}{2}$ particles because of the triangularity relation:

$$\langle \tfrac{1}{2}, \tfrac{1}{2} | T_q^{[2]} | \tfrac{1}{2}, -\tfrac{1}{2} \rangle = 0. \tag{3.27}$$

We are thus left with the antisymmetric representation belonging to spin 1 which we may write as a vector product:

$$\begin{aligned} F^{3+[1]} &= \left(F^{31} + \mathrm{i}F^{32}\right)^{[1]} \\ &= \tfrac{1}{2}\left(F^{31} - F^{13} + \mathrm{i}F^{32} - \mathrm{i}F^{23}\right) \\ &= \tfrac{1}{2}\sum_{j,k=1}^{3}\left(\epsilon_{2jk}F^{jk} - \mathrm{i}\epsilon_{1jk}F^{jk}\right) \\ &= \tfrac{\mathrm{i}}{\sqrt{2}}\sum_{j,k=1}^{3}\epsilon_{+jk}F^{jk} \end{aligned} \tag{3.28}$$

where in the last line it is understood to take the spherical "+1"-component of the vector product as defined in eq. (C.2). Note that since F^{ij} is contracted with the skew tensor ϵ_{ijk}, the last term in (3.24) that is proportional to $p_3^i p_3^j$ vanishes. Inserting (3.28) back into (3.25) and choosing the spin projections $\lambda' = \frac{1}{2}$ and $\lambda = -\frac{1}{2}$ then yields:

$$\mu = \frac{3}{2M}\langle \Phi^{\Lambda}_{M,1/2} | \tfrac{1}{\sqrt{2}} \sum_{j,k=1}^{3} \epsilon_{+jk} F^{jk} \hat{q}_3 | \Phi^{\Lambda}_{M,-1/2} \rangle. \tag{3.29}$$

By using the Wigner-Eckart theorem (C.10):

$$\begin{aligned} \langle \tfrac{1}{2}, \tfrac{1}{2} | T^{[1]}_{+1} | \tfrac{1}{2}, -\tfrac{1}{2} \rangle &= \begin{pmatrix} \frac{1}{2} & 1 & \frac{1}{2} \\ -\frac{1}{2} & 1 & -\frac{1}{2} \end{pmatrix} \langle \tfrac{1}{2} || T^{[1]} || \tfrac{1}{2} \rangle \\ &= -\sqrt{2}\begin{pmatrix} \frac{1}{2} & 1 & \frac{1}{2} \\ -\frac{1}{2} & 1 & \frac{1}{2} \end{pmatrix} \langle \tfrac{1}{2} || T^{[1]} || \tfrac{1}{2} \rangle \\ &= -\sqrt{2}\langle \tfrac{1}{2}, \tfrac{1}{2} | T^{[1]}_0 | \tfrac{1}{2}, \tfrac{1}{2} \rangle, \end{aligned} \tag{3.30}$$

we remove the spin-flip and turn the expression in an expectation value:

$$\mu = -\frac{3}{2M}\langle \Phi^{\Lambda}_{M,1/2} | \sum_{j,k=1}^{3} \epsilon_{3jk} F^{jk} \hat{q}_3 | \Phi^{\Lambda}_{M,1/2} \rangle, \tag{3.31}$$

To simplify (3.24) further we replace the relative coordinates by single-particle coordinates according to (2.52):

$$F^{ij} := \frac{1}{2M}\left\{\frac{1}{2}\left[-\frac{\Omega}{\omega_3}p_3^j\left(\mathrm{i}\tfrac{\partial}{\partial p_3^i} - \frac{1}{\Omega}\sum_{\alpha=1}^{3}\omega_\alpha \mathrm{i}\tfrac{\partial}{\partial p_\alpha^i}\right) - \text{h. c.}\right] + \frac{\Omega}{2\omega_3}\left(\mathbb{1}\otimes\mathbb{1}\otimes\mathrm{i}\alpha^i\alpha^j\right)\right\}. \tag{3.32}$$

Since in the expectation value (3.31) F^{jk} is contracted with the skew symmetric tensor ϵ_{ijk} it is suggestive to define:

$$\hat{L}^i_{R\alpha} := \epsilon_{ijk} p^k_\alpha \left(\mathrm{i} \frac{\partial}{\partial p^j_\alpha} - \hat{R}^j \right). \tag{3.33}$$

Furthermore we identify the spin operator $\boldsymbol{S} = \frac{1}{2}\boldsymbol{\Sigma}$ in the following contraction:

$$\sum_{j,k=1}^{3} \epsilon_{ijk} \alpha^j \alpha^k = 2\mathrm{i} \begin{pmatrix} \sigma_i & \mathbb{1} \\ \mathbb{1} & \sigma_i \end{pmatrix} = 2\mathrm{i}\Sigma^i. \tag{3.34}$$

We then have:

$$\sum_{j,k=1}^{3} \epsilon_{ijk} F^{jk} = -\frac{\Omega}{4M\omega_3} \left(\hat{L}^3_{Ri} + \mathbb{1} \otimes \mathbb{1} \otimes \Sigma^i + \text{h. c.} \right). \tag{3.35}$$

This expression is still not symmetric in the three quarks, so in the final step we symmetrize over the three quarks in the same way as we did already when deriving the charge radius:

$$\mu = \frac{\langle \Phi^\Lambda_M | \hat{\mu} | \Phi^\Lambda_M \rangle}{2M}, \tag{3.36}$$

where we defined the magnetic moment operator $\hat{\mu}$ which follows from symmetrizing (3.35):

$$\hat{\mu} = \frac{1}{2} \left[\frac{\Omega}{M} \sum_{\alpha=1}^{3} \frac{\hat{q}_\alpha}{2\omega_\alpha} \left(\hat{L}^3_{R\alpha} + 2S^3_\alpha \right) + \text{h. c.} \right]. \tag{3.37}$$

with the single-particle spin operators:

$$\begin{aligned} \boldsymbol{S}_1 &:= \boldsymbol{\Sigma}/2 \otimes \mathbb{1} \otimes \mathbb{1} \\ \boldsymbol{S}_2 &:= \mathbb{1} \otimes \boldsymbol{\Sigma}/2 \otimes \mathbb{1} \\ \boldsymbol{S}_3 &:= \mathbb{1} \otimes \mathbb{1} \otimes \boldsymbol{\Sigma}/2. \end{aligned} \tag{3.38}$$

3.2.1 Interpretation

An interpretation of the operator $\hat{\mu}$ as defined in (3.37) has already been given in ref. [16]. We therefore want to mention its features in brevity here. As has already been shown in the interpretation of the charge radius, the term

$$\mathrm{i}\boldsymbol{\nabla}_{\boldsymbol{p_\alpha}} - \hat{\boldsymbol{R}} = \hat{\boldsymbol{x}}_{\boldsymbol{\alpha}} - \frac{1}{\Omega} \sum_{\beta=1}^{3} \omega_\beta \hat{\boldsymbol{x}}_{\boldsymbol{p_\beta}} \tag{3.39}$$

corresponds to the position of particle α as measured from the center of mass of the system. One is thus naturally led to interpret $\hat{\boldsymbol{L}}_{\boldsymbol{R\alpha}}$ defined in (3.33) as the angular momentum of the three-quark system with the correct center of mass motion removed. As already mentioned $\boldsymbol{S_1}$, $\boldsymbol{S_2}$ and $\boldsymbol{S_3}$ are single-particle spin operators. We therefore

conclude that the magnetic moment of a baryon can be decomposed in contributions of the quark angular momenta and their spins:

$$\langle \mu \rangle = \langle \mu_L \rangle + 2\langle \mu_S \rangle, \tag{3.40}$$

with $\langle \mu_L \rangle$ being the contribution of the angular momenta of the three quarks:

$$\langle \mu_L \rangle := \frac{1}{2M} \langle \Phi^{\Lambda}_{M,1/2}| \, \frac{1}{2} \left(\frac{\Omega}{M} \sum_{\alpha=1}^{3} \frac{\hat{q}_\alpha}{2\omega_\alpha} \hat{L}^3_{R\alpha} + \text{h. c.} \right) |\Phi^{\Lambda}_{M,1/2}\rangle \tag{3.41}$$

and $\langle \mu_S \rangle$ the contribution of the quark spins:

$$\langle \mu_S \rangle := \frac{1}{2M} \langle \Phi^{\Lambda}_{M,1/2}| \, \frac{\Omega}{M} \sum_{\alpha=1}^{3} S^3_\alpha \, |\Phi^{\Lambda}_{M,1/2}\rangle. \tag{3.42}$$

Such a decomposition into spin and angular momentum contributions is not possible by extracting the magnetic moment from a form factor. It is thus another benefit of the approach to static properties presented in this work. In (3.37) we discover the same relativistic weight factor Ω/M as has already been found in the charge radius. When taking the nonrelativistic limit, the operator $\hat{\mu}$ (3.37) becomes:

$$\hat{\mu}_{\text{n.r.}} = \sum_{\alpha=1}^{3} \frac{\hat{q}_\alpha}{2m_\alpha} \left[\epsilon_{3jk} p^j_\alpha \left(\mathrm{i} \tfrac{\partial}{\partial p^k_\alpha} - \frac{1}{M} \sum_{\beta=1}^{3} m_\beta \mathrm{i} \tfrac{\partial}{\partial p^i_\beta} \right) + 2S^3_\alpha \right]. \tag{3.43}$$

Except for the center of mass correction this expression is well known. The nonrelativistic magnetic moment operator stemming from the orbital motion of a particle with charge q and mass m is given by:

$$\hat{\mu}_{L\text{n.r.}} = \frac{q}{2m} \hat{L}^3, \tag{3.44}$$

where $\hat{L}$ is the angular momentum operator. The spin of a nonrelativistic particle generates a magnetic moment that is given by:

$$\hat{\mu}_{S\text{n.r.}} = \frac{q}{m} \sigma^3. \tag{3.45}$$

In both cases the axis of quantization has been chosen to point in the 3-direction. We are thus led to conclude that we have found the relativistic generalization of the nonrelativistic magnetic moment operator.

3.3 Results on the baryon magnetic moments

On the basis of the theoretical considerations of the preceding section we present in this section numerical results for the baryon magnetic moments of both the octet and the decuplet. Again we work with the model described in section 1.5. The model parameters are fixed by the spectra and no further parameterization is adopted. We begin with the octet and compare our results to experiment and form factor calculations. For the decuplet one has to consider mixed energy contributions, which have been derived in ref. [16] but not numerically implemented there. We show that the inclusion of these terms enlarge the magnetic moments by roughly a factor of two. Unfortunately the empirical situation here is very poor.

3.3.1 Baryon octet magnetic moments

The magnetic moments of the octet baryons have already been computed in the framework presented here in [16], however mistakenly without including the instanton force coupling strange to non-strange quarks. It is appropriate to give the correct results here which are presented in table 3.1. A short discussion on the numerical implementation and the stability of these results can be found in appendix D and ref. [16]. The nucleon magnetic moments were computed using a basis size of 18, the hyperons using 14 oscillator shells. The limitation on these numbers comes essentially from the available computer main memory. The smaller number with the hyperons is due to their higher dimensional spin/flavor basis. The experimental data is reproduced with an average accuracy of roughly ten percent. The worst match is seen with the Ξ^- with a deviation of 14 %. In total the results are in good agreement with experiment.

baryon	experiment [15] $[\mu/\mu_N]$	this calculation $[\mu/\mu_N]$	form factors [11, 12] $[\mu/\mu_N]$
p	2.793	2.77	2.74
n	-1.913	-1.71	-1.70
Λ	-0.613 ± 0.004	-0.61	-0.61
Σ^+	2.458 ± 0.01	2.51	2.47
Σ^0	–	0.75	–
Σ^-	-1.16 ± 0.025	-1.02	-0.99
Ξ^0	-1.25 ± 0.014	-1.33	-1.33
Ξ^-	-0.6507 ± 0.0025	-0.56	-0.57

Table 3.1: Baryon octet magnetic moments. Nucleon magnetic moments are known up to the 7th digit.

In the preceding chapter on charge radii we found that by varying the instanton cutoff parameter simultaneously with the coupling strength we could describe both the proton and the neutron charge radius with a relative error of 14 % compared to the empirical values, leaving at the same time the spectrum largely unaltered. With the "standard" parameter set as listed in table 1.1 which also accounts for the magnetic moments as given by table 3.1 only the proton radius could be described well, the neutron radius being much too big. In the following we analyze the effect of a varied cutoff on the magnetic moments. We computed the nucleon magnetic moments with the "new" parameters, *i.e.* an instanton cutoff parameter of 0.6 fm and a coupling strength of 263 MeV fm^3. For the proton we find $\mu_p = 2.75\,\mu_N$ which is slightly worse than the value obtained with the standard parameters (see table 1.1). For the neutron we find $\mu_n = -1.73\,\mu_N$ which is slightly better. One is led to conclude that the nucleon magnetic moments hardly change with a variation in the cutoff parameter and are almost insensitive to the effective instanton size in contrast to the charge radii. Since

we neither see an improvement in the magnetic moments nor a degradation a judgment in favor of the "new" parameter set cannot be given by this analysis.

Comparison with form factor calculations

The nucleon magnetic moments have also been computed within this quark model and using the same parameters by the authors of [11]. The hyperon magnetic moments have been computed by the authors of [12]. As can be seen from the last column of table 3.1 the coincidence with the values from these calculations is very good for both the nucleon and the hyperons.

Nonrelativistic limit

Also for the magnetic moments we want to demonstrate the effect of a relativistic approach. We took the same Salpeter amplitudes as before but this time computed the expectation value of the nonrelativistic limit of the operator (3.36), which is given by eq. (3.43). Table 3.2 compares the results of the fully relativistic computation with the nonrelativistic limit. The effect is less pronounced than with the charge radius,

baryon	$\langle\hat{\mu}_{\text{n.r.}\rangle}$ $[\mu/\mu_N]$	$\langle\hat{\mu}\rangle$ $[\mu/\mu_N]$	$\langle\hat{\mu}\rangle_{\text{n.r.}}/\langle\hat{\mu}\rangle$ [%]
p	2.41	2.79	86
n	−1.52	−1.71	89
Λ	−0.48	−0.61	79
Σ^+	2.56	2.51	102
Σ^0	0.74	0.75	99
Σ^-	−1.08	−1.02	98
Ξ^0	−1.35	−1.33	102
Ξ^-	−0.42	−0.56	75

Table 3.2: Comparison between the magnetic moments computed fully relativistically and in the nonrelativistic limit. The last column shows the ratio between both computations.

nevertheless it amounts to a good more than ten percent for the nucleon magnetic moments and 25 % for the Ξ^- magnetic moment. For the Σ^+ and Ξ^0 it curiously has a slightly converse impact, *i.e.* their magnetic moments become bigger in magnitude in the nonrelativistic limit.

Spin and orbital angular momentum decomposition

As has already been shown in the derivation of the magnetic moment operator, the magnetic moment may be decomposed in spin and orbital angular momentum contributions according to:

$$\langle \mu \rangle = \langle \mu_L \rangle + 2\langle \mu_S \rangle, \tag{3.46}$$

with $\langle \mu_L \rangle$ as defined in (3.41) being the contribution of the angular momenta of the three quarks and $\langle \mu_S \rangle$ as defined in (3.42) the contribution of the quark spins. This decomposition enables us to carry out a numerical analysis of the magnitudes of both contributions — spin and angular momentum — within the model described in section 1.5. Note that such a study is not possible by relying on form factor calculations because there only the total magnitude of the magnetic moment can be extracted. Table 3.3 lists the contributions of spin and angular momentum to the magnetic moments of the baryon octet. The analysis shows, that the contribution of the quark spins exceeds

baryon	$2\langle \mu_S \rangle$ $[\mu/\mu_N]$	$\frac{2\langle \mu_S \rangle}{\langle \mu \rangle}$ [%]	$\langle \mu_L \rangle$ $[\mu/\mu_N]$	$\frac{\langle \mu_L \rangle}{\langle \mu \rangle}$ [%]
p	2.53	91	0.24	9
n	−1.59	93	−0.12	7
Λ	−0.6	98	−0.01	2
Σ^+	2.33	93	0.23	7
Σ^0	0.7	94	0.05	6
Σ^-	−0.91	89	−0.11	11
Ξ^0	−1.27	94	−0.06	6
Ξ^-	−0.55	98	−0.013	2

Table 3.3: Contributions of quark spins ($2\langle \mu_S \rangle$) and angular momentum ($\langle \mu_L \rangle$) to the net magnetic moments of the octet baryons.

the contribution of the quark angular momenta by far. One can state that a good 90% of the magnetic moment is coming from quark spins which is due to the fact that the quarks are dominantly in a relative S-wave. This result also explains in part the success of the nonrelativistic quark model in predicting the magnetic moments. Our analysis shows that by neglecting the angular motion of the quarks by assuming that the quarks are in a relative S-wave, the induced error is in the percent region. The preceding discussion is however only true if we work with a constituent quark mass of 330 MeV.

Evolution of quark spin and angular momentum contributions

We may however carry this analysis further by studying the change of the spin/angular momentum distribution with decreasing quark masses. As already mentioned we assume isospin symmetry between up- and down-quark and thus there is only one mass parameter for the nucleon, namely m_n from table 1.1. At different magnitudes of this mass parameter we have now fitted the remaining six parameters of the model to the baryon spectra. We might of course not expect to reproduce the spectra as well as with the original value of 330 MeV but at least we are able to keep the ground states i. e. the nucleon and the Δ-particle at the empirical values. Figure 3.1 shows the nucleon spectrum at a quark mass of $m_n = 25\,\mathrm{MeV}$. The mass gap between the ground state and exited states becomes so huge that the spectrum below 3 GeV is depleted. We achieved a quark mass as small as 25 MeV before numerical restrictions impeded us to go any further. Figure 3.2 shows the effect on the spin and angular momentum contribution to the magnetic moment of proton and neutron. We see an almost linear decrease of the spin contribution from its original value of a good 90 % at 330 MeV to roughly 60 % at 25 MeV. At the same time the angular momentum contribution gains in magnitude correspondingly to roughly 40 %. We have also plotted the total magnetic moment of proton and neutron as a function of the quark mass parameter in fig. 3.3. It shows that both decrease in absolute magnitude by roughly one nuclear magneton as the quark mass is decreased from 330 MeV to 25 MeV.

The foregoing discussion is not academic. In fact the constituent quark mass is not precisely fixed by QCD. What is fixed is the mass function and much more is now known about its momentum dependence from lattice QCD [27] since the earliest QCD computation in 1976 [28]. In the region between 0 GeV and 2 GeV it varies as a function of momentum between $\sim$ 400 MeV and $\sim$ 50 MeV. One may define the constituent quark mass as the value of the mass function at $p \approx 0$ but this is not compulsory; constituent quark models which aim at a description of high mass resonances (up 3 GeV) may even be forced to use a mass value at larger momenta in order to take the full momentum dependence effectively better into account.

Magnetic moments of nucleon resonances

Since efforts are being made to measure also magnetic moments of excited nucleon states like the $S^{11}(1535)$ as mentioned in ref. [14], we contribute some selected predictions here, which are shown in table 3.4. We observe that for the $S^{11}(1535)$ the absolute value of the spin contribution is only a quarter of the angular momentum contribution and opposite in sign. Since this resonance is dominantly a P-wave, the spin has to be aligned anti-parallel to the angular momentum to result in a state with total spin 1/2.

3.3.2 Baryon decuplet magnetic moments

In ref. [16] a derivation for the magnetic moment has been given in the case of vanishing two-particle kernels. As has been mentioned already, the vertex functions then also contain mixed energy contributions. Since in ref. [16] these additional terms have not

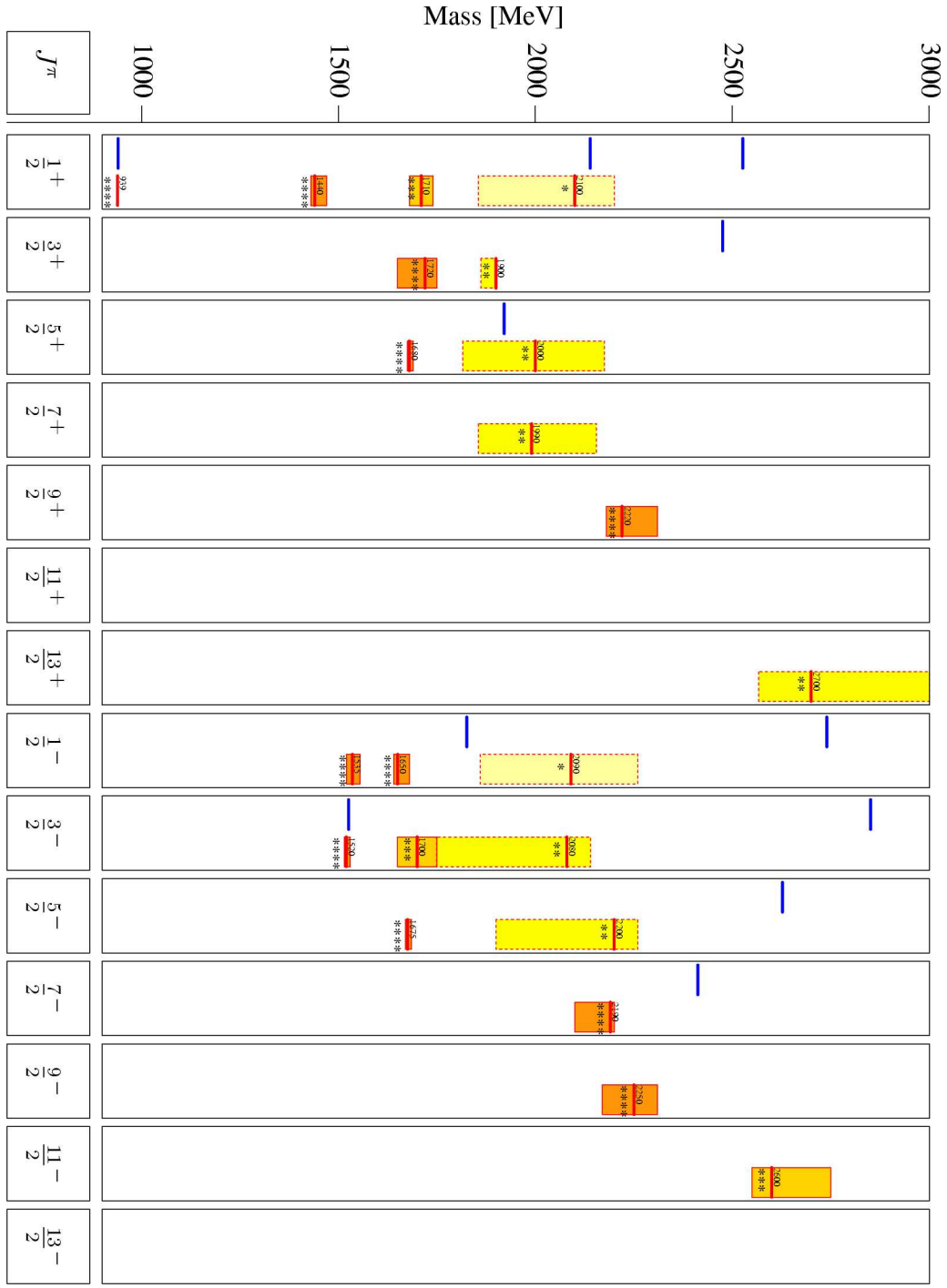

Figure 3.1: The nucleon-spectrum at a non-strange quark mass of 25 MeV.

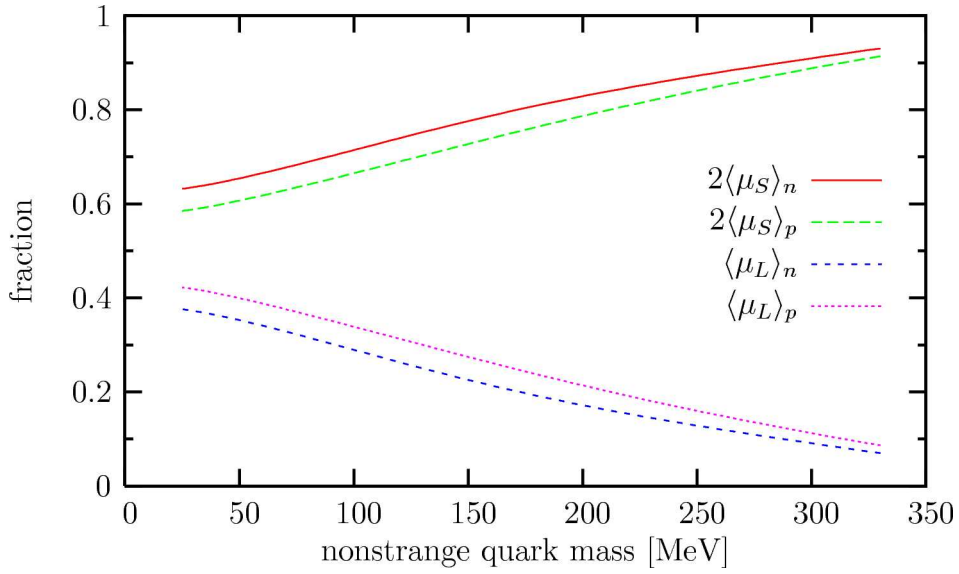

Figure 3.2: Fraction of the total magnetic moment carried by quark spin and angular momentum resp. of proton and neutron resp. as a function of the non-strange quark mass.

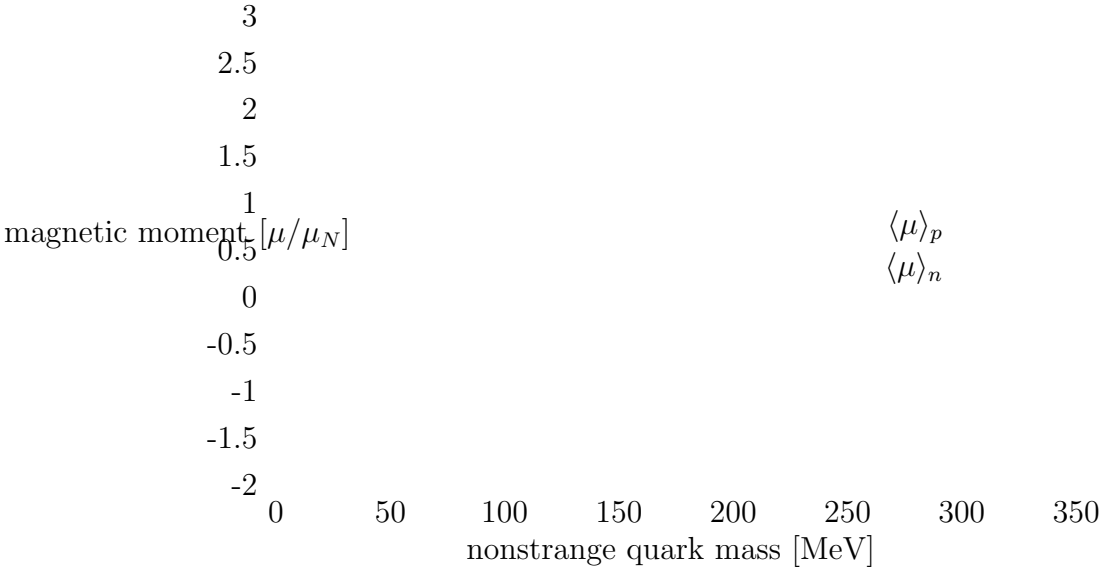

Figure 3.3: Evolution of total magnetic moment of proton and neutron with non-strange quark mass.

been implemented numerically due to their complexity we do so in this work. The result from ref. [16] looks as follows:

$$\langle\mu\rangle = \frac{3}{4M}\mathrm{i}\,\epsilon_{3jk}\int\frac{\mathrm{d}^3p_\xi}{(2\pi)^3}\int\frac{\mathrm{d}^3p_\eta}{(2\pi)^3}\overline{\Gamma}^{\Lambda}_{M}(p_\xi,p_\eta)\,\hat{q}_3\hat{\mu}^{jk}\,\gamma^0\otimes\gamma^0\otimes\gamma^0\,\Gamma^{\Lambda}_{M}(p_\xi,p_\eta) \tag{3.47}$$

nucleon resonance	T_3 $[\mu/\mu_N]$	magnetic moment $[\mu/\mu_N]$	$\langle\mu\rangle_S$ $[\mu/\mu_N]$	$\langle\mu\rangle_L$ $[\mu/\mu_N]$
$P^{11}(1440)$	1/2	1.55	1.39	0.16
	−1/2	-0.98	-0.9	-0.08
$S^{11}(1535)$	1/2	0.37	-0.14	0.51
	−1/2	-0.1	0.034	-0.134
$S^{11}(1650)$	1/2	1.85	1.70	0.15
	−1/2	-0.69	-0.44	-0.25
$D^{13}(1520)$	1/2	1.44	0.51	0.93
	−1/2	-0.166	0.019	-0.185
$D^{15}(1675)$	1/2	1.74	1.52	0.22
	−1/2	0.32	-0.22	0.54

Table 3.4: Prediction of magnetic moments of selected excited nucleon states as well as their decomposition into spin- ($\langle\mu\rangle_S$) and orbital angular momentum contributions ($\langle\mu\rangle_L$). T_3 denotes the third isospin component.

where the operator $\hat{\mu}^{jk}$ takes the following form:

$$
\begin{aligned}
\hat{\mu}^{jk} \;:=\; & - \frac{\Lambda^{+++}}{M-\omega_1-\omega_2-\omega_3}\, \mathbb{1}\otimes\mathbb{1}\otimes \hat{e}\alpha^k\, \frac{\omega_1+\omega_2}{M}\frac{\partial}{\partial p_\eta^j}\, \frac{\Lambda^{+++}}{M-\omega_1-\omega_2-\omega_3} \\
& - \frac{\Lambda^{+++}}{M-\omega_1-\omega_2-\omega_3}\, \mathbb{1}\otimes\mathbb{1}\otimes \hat{e}\alpha^k\, \frac{\omega_1-\omega_2}{2M}\frac{\partial}{\partial p_\xi^j}\, \frac{\Lambda^{+++}}{M-\omega_1-\omega_2-\omega_3} \\
& - \frac{\Lambda^{+++}}{M-\omega_1-\omega_2-\omega_3}\, \mathbb{1}\otimes\mathbb{1}\otimes \hat{e}\alpha^k\, \frac{\frac{1}{\omega_1}-\frac{1}{\omega_2}}{2M} p_\xi^j\, \frac{\Lambda^{+++}}{M-\omega_1-\omega_2-\omega_3} \\
& + \frac{\Lambda^{+++}}{M-\omega_1-\omega_2-\omega_3}\, \mathbb{1}\otimes\mathbb{1}\otimes \hat{e}\alpha^k\alpha^j\, \frac{1}{2M}\, \frac{\Lambda^{+++}}{M-\omega_1-\omega_2-\omega_3} \\
& + \frac{\Lambda^{---}}{M+\omega_1+\omega_2+\omega_3}\, \mathbb{1}\otimes\mathbb{1}\otimes \hat{e}\alpha^k\, \frac{\omega_1+\omega_2}{M}\frac{\partial}{\partial p_\eta^j}\, \frac{\Lambda^{---}}{M+\omega_1+\omega_2+\omega_3} \\
& + \frac{\Lambda^{---}}{M+\omega_1+\omega_2+\omega_3}\, \mathbb{1}\otimes\mathbb{1}\otimes \hat{e}\alpha^k\, \frac{\omega_1-\omega_2}{2M}\frac{\partial}{\partial p_\xi^j}\, \frac{\Lambda^{---}}{M+\omega_1+\omega_2+\omega_3} \\
& + \frac{\Lambda^{---}}{M+\omega_1+\omega_2+\omega_3}\, \mathbb{1}\otimes\mathbb{1}\otimes \hat{e}\alpha^k\, \frac{\frac{1}{\omega_1}-\frac{1}{\omega_2}}{2M} p_\xi^j\, \frac{\Lambda^{---}}{M+\omega_1+\omega_2+\omega_3} \\
& + \frac{\Lambda^{---}}{M+\omega_1+\omega_2+\omega_3}\, \mathbb{1}\otimes\mathbb{1}\otimes \hat{e}\alpha^k\alpha^j\, \frac{1}{2M}\, \frac{\Lambda^{---}}{M+\omega_1+\omega_2+\omega_3}
\end{aligned}
$$

$$
\begin{aligned}
&- \frac{\Lambda^{+++}}{M-\omega_1-\omega_2-\omega_3}\ \mathbb{1}\otimes\mathbb{1}\otimes\hat{e}\alpha^k\,\frac{M-\omega_3}{2\omega_3 M}\frac{\partial}{\partial p_\eta^j}\ \Lambda^{++-}\\
&- \frac{\Lambda^{+++}}{M-\omega_1-\omega_2-\omega_3}\ \mathbb{1}\otimes\mathbb{1}\otimes\hat{e}\alpha^k\,\frac{\omega_1-\omega_2}{4\omega_3 M}\frac{\partial}{\partial p_\xi^j}\ \Lambda^{++-}\\
&- \frac{\Lambda^{+++}}{M-\omega_1-\omega_2-\omega_3}\ \mathbb{1}\otimes\mathbb{1}\otimes\hat{e}\alpha^k\left(\frac{\frac{p_1^j}{\omega_1}+\frac{p_2^j}{\omega_2}}{8M\omega_3}+\frac{p_3^j}{4\omega_3^3}\right)\Lambda^{++-}\\
&- \frac{\Lambda^{+++}}{M-\omega_1-\omega_2-\omega_3}\ \mathbb{1}\otimes\mathbb{1}\otimes\hat{e}\alpha^k\alpha^j\frac{1}{2M(M-\omega_1-\omega_2-\omega_3)}\Lambda^{++-}\\
&- \frac{\Lambda^{---}}{M+\omega_1+\omega_2+\omega_3}\ \mathbb{1}\otimes\mathbb{1}\otimes\hat{e}\alpha^k\,\frac{M+\omega_3}{2\omega_3 M}\frac{\partial}{\partial p_\eta^j}\ \Lambda^{--+}\\
&- \frac{\Lambda^{---}}{M+\omega_1+\omega_2+\omega_3}\ \mathbb{1}\otimes\mathbb{1}\otimes\hat{e}\alpha^k\,\frac{\omega_1-\omega_2}{4\omega_3 M}\frac{\partial}{\partial p_\xi^j}\ \Lambda^{--+}\\
&- \frac{\Lambda^{---}}{M+\omega_1+\omega_2+\omega_3}\ \mathbb{1}\otimes\mathbb{1}\otimes\hat{e}\alpha^k\left(\frac{\frac{p_1^j}{\omega_1}+\frac{p_2^j}{\omega_2}}{8M\omega_3}-\frac{p_3^j}{4\omega_3^3}\right)\Lambda^{--+}\\
&- \frac{\Lambda^{---}}{M+\omega_1+\omega_2+\omega_3}\ \mathbb{1}\otimes\mathbb{1}\otimes\hat{e}\alpha^k\alpha^j\frac{1}{2M(M+\omega_1+\omega_2+\omega_3)}\Lambda^{--+}\\
&- \Lambda^{++-}\ \mathbb{1}\otimes\mathbb{1}\otimes\hat{e}\alpha^k\,\frac{M-\omega_3}{2\omega_3 M}\frac{\partial}{\partial p_\eta^j}\ \frac{\Lambda^{+++}}{M-\omega_1-\omega_2-\omega_3}\\
&- \Lambda^{++-}\ \mathbb{1}\otimes\mathbb{1}\otimes\hat{e}\alpha^k\,\frac{\omega_1-\omega_2}{4\omega_3 M}\frac{\partial}{\partial p_\xi^j}\ \frac{\Lambda^{+++}}{M-\omega_1-\omega_2-\omega_3}\\
&- \Lambda^{++-}\ \mathbb{1}\otimes\mathbb{1}\otimes\hat{e}\alpha^k\left(\frac{\frac{p_1^j}{\omega_1}+\frac{p_2^j}{\omega_2}}{8M\omega_3}+\frac{p_3^j}{4\omega_3^3}\right)\frac{\Lambda^{+++}}{M-\omega_1-\omega_2-\omega_3}\\
&- \Lambda^{--+}\ \mathbb{1}\otimes\mathbb{1}\otimes\hat{e}\alpha^k\,\frac{M+\omega_3}{2\omega_3 M}\frac{\partial}{\partial p_\eta^j}\ \frac{\Lambda^{---}}{M+\omega_1+\omega_2+\omega_3}\\
&- \Lambda^{--+}\ \mathbb{1}\otimes\mathbb{1}\otimes\hat{e}\alpha^k\,\frac{\omega_1-\omega_2}{4\omega_3 M}\frac{\partial}{\partial p_\xi^j}\ \frac{\Lambda^{---}}{M+\omega_1+\omega_2+\omega_3}\\
&- \Lambda^{--+}\ \mathbb{1}\otimes\mathbb{1}\otimes\hat{e}\alpha^k\left(\frac{\frac{p_1^j}{\omega_1}+\frac{p_2^j}{\omega_2}}{8M\omega_3}-\frac{p_3^j}{4\omega_3^3}\right)\frac{\Lambda^{---}}{M+\omega_1+\omega_2+\omega_3}\\
&- \Lambda^{+--}\ \alpha^j\otimes\mathbb{1}\otimes\hat{e}\alpha^k\frac{1}{8M\omega_3\omega_1}\Lambda^{--+}-\Lambda^{-+-}\ \mathbb{1}\otimes\alpha^j\otimes\hat{e}\alpha^k\frac{1}{8M\omega_3\omega_2}\Lambda^{--+}
\end{aligned}
$$

$$
\begin{aligned}
- \;& \Lambda^{+-+}\, \alpha^j \otimes \mathbb{1} \otimes \hat{e}\alpha^k \frac{1}{8M\omega_3\omega_1} \Lambda^{---} - \Lambda^{-++}\, \mathbb{1} \otimes \alpha^j \otimes \hat{e}\alpha^k \frac{1}{8M\omega_3\omega_2} \Lambda^{---} \\
+ \;& \Lambda^{--+}\, \alpha^j \otimes \mathbb{1} \otimes \hat{e}\alpha^k \frac{1}{8M\omega_3\omega_1} \Lambda^{+--} + \Lambda^{--+}\, \mathbb{1} \otimes \alpha^j \otimes \hat{e}\alpha^k \frac{1}{8M\omega_3\omega_2} \Lambda^{-+-} \\
+ \;& \Lambda^{---}\, \alpha^j \otimes \mathbb{1} \otimes \hat{e}\alpha^k \frac{1}{8M\omega_3\omega_1} \Lambda^{+-+} + \Lambda^{---}\, \mathbb{1} \otimes \alpha^j \otimes \hat{e}\alpha^k \frac{1}{8M\omega_3\omega_2} \Lambda^{+-+} \\
- \;& \Lambda^{-+-}\, \alpha^j \otimes \mathbb{1} \otimes \hat{e}\alpha^k \frac{1}{8M\omega_3\omega_1} \Lambda^{+++} - \Lambda^{+--}\, \mathbb{1} \otimes \alpha^j \otimes \hat{e}\alpha^k \frac{1}{8M\omega_3\omega_2} \Lambda^{+++} \\
- \;& \Lambda^{-++}\, \alpha^j \otimes \mathbb{1} \otimes \hat{e}\alpha^k \frac{1}{8M\omega_3\omega_1} \Lambda^{++-} - \Lambda^{+-+}\, \mathbb{1} \otimes \alpha^j \otimes \hat{e}\alpha^k \frac{1}{8M\omega_3\omega_2} \Lambda^{++-} \\
+ \;& \Lambda^{+++}\, \alpha^j \otimes \mathbb{1} \otimes \hat{e}\alpha^k \frac{1}{8M\omega_3\omega_1} \Lambda^{-+-} + \Lambda^{+++}\, \mathbb{1} \otimes \alpha^j \otimes \hat{e}\alpha^k \frac{1}{8M\omega_3\omega_2} \Lambda^{+--} \\
+ \;& \Lambda^{++-}\, \alpha^j \otimes \mathbb{1} \otimes \hat{e}\alpha^k \frac{1}{8M\omega_3\omega_1} \Lambda^{-++} + \Lambda^{++-}\, \mathbb{1} \otimes \alpha^j \otimes \hat{e}\alpha^k \frac{1}{8M\omega_3\omega_2} \Lambda^{+-+}.
\end{aligned}
\tag{3.48}
$$

The first eight terms only involve pure energy components. After application of the commutation rules (2.42) and (2.43), replacement of the vertex functions by Salpeter amplitudes and symmetrizing over the three fermions we recover the result (3.36). All that has been said about its natural physical interpretation in subsection 3.2.1 also applies here of course. If we denote the remaining 30 terms in eq. (3.48) which involve mixed energy components by $\hat{\mu}^{jk}_{\text{mixed}}$, we arrive at:

$$
\begin{aligned}
\langle \mu \rangle = \frac{\langle \Phi^\Lambda_M | \hat{\mu} | \Phi^\Lambda_M \rangle}{\langle \Phi_M | \Phi_M \rangle} + \frac{3}{\langle \Phi_M | \Phi_M \rangle} \int \frac{\mathrm{d}^3 p_\xi}{(2\pi)^3} \int \frac{\mathrm{d}^3 p_\eta}{(2\pi)^3} \overline{\Gamma}^\Lambda_M(p_\xi, p_\eta) \\
\times \frac{\mathrm{i}}{2} \sum_{j,k=1}^{3} \epsilon_{3jk}\, \hat{\mu}^{jk}_{\text{mixed}}\, \hat{q}_3 \gamma^0 \otimes \gamma^0 \otimes \gamma^0\, \Gamma^\Lambda_M(p_\xi, p_\eta)
\end{aligned}
\tag{3.49}
$$

This expression decomposes the magnetic moment into a contribution from the pure energy components of the vertex functions and the mixed ones. To have a shorter notation we denote the contribution to the total magnetic moment of the first by $\langle \mu \rangle_{\text{pure}}$ and of the latter by $\langle \mu \rangle_{\text{mixed}}$ such that the decomposition reads $\langle \mu \rangle = \langle \mu \rangle_{\text{pure}} + \langle \mu \rangle_{\text{mixed}}$. The sum of the pure energy components of the vertex function may then be replaced by projected Salpeter amplitudes like in the first term of eq. (3.49). The occurrence of mixed energy components in the second term of eq. (3.49) forbids such a replacement. Also it is not possible to give a natural physical interpretation to the terms which contribute to $\langle \mu \rangle_{\text{mixed}}$ even after symmetrizing over the three quarks.

We have computed the magnetic moments of the decuplet baryons according to formula (3.49). The results are summarized in table 3.5. We find a rather large magnetic moment for the Δ^{++} of 7.62 nuclear magnetons. Also we observe exact isospin relations between the Δ magnetic moments:

$$
\langle \mu_\Delta \rangle = \left(T_3(\Delta) + \tfrac{1}{2} \right) \langle \mu_{\Delta^+} \rangle. \tag{3.50}
$$

baryon	$\langle\mu\rangle_{\text{pure}}$ $[\mu/\mu_N]$	$\langle\mu\rangle_{\text{mixed}}$ $[\mu/\mu_N]$	$\langle\mu\rangle$ $[\mu/\mu_N]$	$\langle\mu\rangle_{\text{pure}}/\langle\mu\rangle$ [%]	$\langle\mu\rangle_{\text{exp}}$ [15] $[\mu/\mu_N]$
Δ^{++}	4.14	3.48	7.62	54	3.7–7.5
Δ^{+}	2.07	1.74	3.81	54	$2.7^{1.0}_{-1.3} \pm 1.5 \pm 3$
Δ^{0}	0	0	0	–	
Δ^{-}	-2.07	-1.74	-3.81	54	
Σ^{*+}	2.51	2.22	4.73	53	
Σ^{*0}	0.27	0.41	0.68	40	
Σ^{*-}	-1.97	-1.29	-3.26	60	
Ξ^{*0}	0.59	1.09	1.68	35	
Ξ^{*-}	-1.83	-1.08	-2.91	63	
Ω^{-}	-1.66	-0.62	-2.28	73	2.02 ± 0.05

Table 3.5: Baryon decuplet magnetic moments $\langle\mu\rangle$ (4th column). Contribution of purely positive and negative energy components $\langle\mu\rangle_{\text{pure}}$ (2nd column) and mixed components $\langle\mu\rangle_{\text{mixed}}$ (3rd column). Ratio of pure component contributions and the total magnetic moments $\langle\mu\rangle_{\text{pure}}/\langle\mu\rangle$ (5th column). Also shown are the experimentally measured magnetic moments (last column) from ref. [15].

Since the Δ has isospin $\frac{3}{2}$, its isospin wavefunction is totally symmetric with respect to S_3-permutations. To combine it with the totally antisymmetric color wavefunction to a totally antisymmetric state, the product of spin- and spatial wavefunctions has to be totally symmetric. The Δ-wavefunction then looks as follows after separation of the totally antisymmetric color wavefunction:

$$|\Delta; T = \tfrac{3}{2}, T_3\rangle = |\phi^{\Delta}_{\mathcal{S}}; T = \tfrac{3}{2}, T_3\rangle \otimes \left[|\psi^{L+}_{R_L}\rangle \otimes |\chi^{S}_{R_S}\rangle\right]^{3/2}_{\mathcal{S}}, \tag{3.51}$$

where ϕ^{Δ}_{S}, $\psi^{L+}_{R_L}$ and $\chi^{S}_{R_S}$ denote wavefunctions in flavor-, position/momentum-, and spin-space respectively. Inside the bracket $[\dots]^{3/2}_{\mathcal{S}}$, the spin wavefunctions with spin S and S_3-symmetry R_S combine with the spatial wavefunctions with orbital angular momenta L and S_3-symmetry R_L to form a product state with total spin $\frac{3}{2}$ that is totally symmetric ($\mathcal{S}$) under the interchange of any two quark pairs. Obviously the flavor wavefunction separates because of its total symmetry. The magnetic moment operator that we found consists of a product of operators in flavor-, spin- and position/momentum-space, of which the flavor part separates. The flavor part is given by the charge operator acting on the third quark. Let us denote the product of operators in spin- and position/momentum-space with $\hat{\mu}_{LS}$. We then have for the magnetic

moment of the Δ-baryons:

$$\begin{aligned}\langle\mu_\Delta\rangle &= \langle\Delta; T=\tfrac{3}{2}, T_3|\,\hat{q}_3\,\hat{\mu}_{LS}\,|\Delta; T=\tfrac{3}{2}, T_3\rangle \\ &= \langle\phi^\Delta_{\mathcal{S}}; T=\tfrac{3}{2}, T_3|\,\hat{q}_3\,|\phi^\Delta_{\mathcal{S}}; T=\tfrac{3}{2}, T_3\rangle \left[\langle\psi^{L+}_{R_L}|\otimes\langle\chi^S_{R_S}|\right]^{3/2}_{\mathcal{S}}\hat{\mu}_{LS}\left[|\psi^{L+}_{R_L}\rangle\otimes|\chi^S_{R_S}\rangle\right]^{3/2}_{\mathcal{S}}. \quad (3.52)\end{aligned}$$

The flavor part can easily be evaluated according to the Gell-Mann/Nishijima formula (1.64) and noting that the Δ-baryons have one unit of hyper-charge, since their baryon number is one and strangeness is zero. Thus the flavor matrix element is

$$\langle\phi^\Delta_{\mathcal{S}}; T=\tfrac{3}{2}, T_3|\,\hat{q}_3\,|\phi^\Delta_{\mathcal{S}}; T=\tfrac{3}{2}, T_3\rangle = T_3+\tfrac{1}{2}, \quad (3.53)$$

which explains our observed relation (3.50).

The magnetic moment of the Δ^+ has been measured at MAMI with the TAPS calorimeter in a pilot experiment in the reaction $\gamma p \to \pi^0\gamma' p$ (see ref. [14]). The proton is excited by a photon to the Δ^+-resonance, which subsequently radiates a photon and then decays into a pion and a proton. The electromagnetic transition within the Δ is a magnetic dipole transition (M1) because of parity and spin conservation, whose amplitude is proportional to the magnetic moment of the Δ^+. This reaction is however hardly to distinguish from bremsstrahlung emitted by the intermediate Δ and the proton. An accurate theoretical knowledge about all processes contributing to the reaction is mandatory. This also explains the large theoretical uncertainty in the measured magnetic moment of

$$\mu_{\Delta^+} = \left(2.7^{+1.0}_{-1.3}(\text{stat.}) \pm 1.5(\text{syst.}) \pm 3(\text{theo.})\right)\mu_N. \quad (3.54)$$

Surely the uncertainties in this number do not allow for a conclusive comparison with model calculations and call for both an experimental refinement, which is already underway at MAMI involving the Crystall Ball detector (see ref. [29]), as well as a reduction of the theoretical errors.

The Particle Data Group (see ref. [15]) quotes a magnetic moment of the Δ^{++} in the range of $(3.7-7.5)\,\mu_N$. This has been extracted from experiments performed at UCLA (see ref. [30]) and SIN (now PSI) (see ref. [31]) from the reaction $\pi^+ p \to \pi^+\gamma' p$. Large errors are induced by π^+ bremsstrahlung, which is much larger than in the experiment described above, and theoretical uncertainties.

For the Ω^- magnetic moment the Particle Data Group gives a value of -2.02 ± 0.05, which is an average of the experimental results cited from refs. [32, 33]. Our value of $-2.28\,\mu_N$ is too large in magnitude by about 13 %.

Table 3.5 also shows the contributions of pure and mixed energy components of the vertex functions to the total magnetic moments. Both contributions account for about half of the total value, *i.e.* are of comparable size. The largest deviations from this rule are seen with the Ξ^0 where the mixed components contribute roughly 2/3 and the Ω^- where they account only for 23 % of the total magnetic moment.

3.4 Summary

In this chapter we have given a derivation of an analytic expression for the magnetic moment of a three-fermion system in the context of the Bethe-Salpeter formalism. We started from the definition of the magnetic moment as the value of the magnetic form factor at vanishing four-momentum transfer squared. The connection to the Bethe-Salpeter formalism was made through the current matrix element derived in section 1.4. Since this matrix element is divided by $\sqrt{Q^2}$ in the expression for the magnetic moment, we had to figure out the Q^2-dependence of the current matrix element. This was accomplished by the exponential representation of the boost transformation of the incoming vertex function. Because of parity the lowest order term was of order $\sqrt{Q^2}$, and thus the static limit could safely be taken. After integrating out the dependence on the relative energies and replacement of the vertex functions by Salpeter amplitudes, we used the Wigner-Eckart theorem to transform the matrix element into a true expectation value. Symmetrizing the resulting expression in the three fermions then confirmed the result of ref. [16] which was obtained by starting from the energy of a magnetic dipole in a magnetic field. Because the result was already interpreted there, we only discussed its main features briefly, which are: relativistic generalization of the well-known nonrelativistic expression, decomposition in orbital angular momentum and spin contribution to the total magnetic moment and removement of the center of mass motion.

Using the analytic result we computed first the magnetic moments of the baryon octet. This was already done in ref. [16] however using a wrong strange/non-strange instanton coupling such that the hyperon results were wrong. Using the correct parameters resulted in a better description of the hyperon magnetic moments, which now coincide with the results of form factor calculation performed within the same model. We also studied the nucleon magnetic moments with the parameters that we found to describe both nucleon charge radii in a better way. However the magnetic moment turned out to be almost insensitive to a variation of the instanton cutoff size. Taking the nonrelativistic limit of the operator showed that relativistic effects are less pronounced here than with the charge radius. However they account still for roughly ten percent of the nucleon magnetic moments. Since the analytic result allows for a decomposition into spin and orbital angular momentum contributions we exploited this to study their magnitudes. It turned out that the largest contribution of roughly 90 % is made by the quark spins. To study the effect of the quark mass on this decomposition we computed it at smaller quark masses as well. The result is interesting and shows that when approaching the current quark masses both contributions become roughly equally large. Of course we were not able to reproduce the spectrum at such small quark masses but at least were able to fit the ground state masses. Since at present preparations are made to also measure the magnetic moments of nucleon resonances we added a few selected predictions. To compute also the magnetic moments of the decuplet baryons, terms have to be added which involve mixed energy contributions. These terms have been derived in ref. [16] but due to their complexity have not been numerically implemented, which we did in the present work. Unfortunately they lack a sensible physical interpretation so far.

Concluding this chapter we annotate, that the analysis of the magnetic moment of

a three-fermion system based on the Bethe-Salpeter formalism revealed new insights into the structure of this observable. Especially the decomposition into spin and orbital angular momentum contributions is an information not to be extracted from a form factor. Within the given model we were able to describe the empirical values quite well and conducted interesting studies concerning the aforementioned decomposition.

Chapter 4

Notes on higher moments and form factors

The successful treatment of static properties so far, poses the question, whether a generalization to arbitrary moments is possible. The answer to this question shows that there are also some implications for the computation of form factors, which we study in this chapter.

4.1 Introduction and overview

We have shown in the foregoing two chapters how the magnetic moment and the charge radius of a three-fermion system can be computed on a field theoretical background, leading to new insights into the underlying structure of these static observables. As already mentioned, both quantities constitute the first moments of the charge and magnetization distribution respectively. It is thus a consequential question to pose, whether an extension to higher moments is possible in an analogous way. The answer to this question is given in section 4.2 of this chapter exemplary for the charge distribution of a three-fermion system. Starting from a very basic definition — a generalization of our starting expression of section 2.2 — we take similar steps to a arrive at a generalized formula for an arbitrary moment of the charge distribution. The resulting expression resembles the charge radius in its structure and contains it as a special case. It is thus fully relativistic and also contains a correction for the center of mass motion of the fermions in a natural way.

The successful extension of the method to higher moments motivates to study whether it is applicable to the computation of form factors as well, which is the content of section 4.3. Form factors provide crucial information about the electromagnetic structure of a bound state. With some care, the Fourier transforms of the electric and magnetic form factors in the Breit frame may be interpreted as the spatial charge and magnetization distribution. In usual field theoretical descriptions form factors are calculated by means of a current matrix element in which a boosted wavefunction enters. This calls for a correct boost prescription but also makes the numerical implementation involved, since simplifying theorems like the Wigner-Eckart theorem are

not applicable. In contrast to that the expressions that we found for static observables are expectation values of operators with well known symmetries taken with respect to wavefunctions with well defined transformation laws under symmetry transformations. Therefore parity selection rules and the Wigner-Eckart theorem can be fully exploited to simplify the numerical implementation considerably. To apply this method to form factors we need a way to separate their Q^2-dependence from the current matrix element. A solution to this problem has already been applied twice in this work. The boost acting on the incoming Salpeter amplitude is expanded as an exponential. In each order of the expansion parameter — which is the rapidity — we obtain a static matrix element, where both Salpeter amplitudes are given in the rest frame of the baryon. The Q^2-dependence separates and enters each order as a factor via the square of the rapidity. We show how the matrix elements can be recoupled to obtain operators with well defined transformation properties under rotations. To estimate whether we have a chance to succeed with this method in computing a form factor, we take the well known dipole parameterization of the electric proton form factor and expand it in powers of the rapidity. Unfortunately we will see, that the expansion is not suited to approximate the form factor by its lowest order terms. Nevertheless the expansion shows that higher order terms are given by similar expression as the charge radius which motivates us to study the sensitivity of the nucleon form factors on the choice of the instanton cutoff parameter and coupling strength. We already found an especially pronounced dependence on these parameters when we studied the neutron charge radius. It will turn out that this sensitivity extends to higher momentum transfers as well, resulting in a much improved description of the empirical data with suitably adjusted instanton interaction parameters. The electric proton form factor only shows a slight dependence on a parameter variation in accordance to the observation we already made with its charge radius. We also study the effect of the adjusted parameters on the nucleon-delta transition, which is commonly badly described by quark models.

4.2 Extension to higher moments

The formalism presented so far paves the way for the calculation of higher moments as well. We take the electric form factor as an example and work accordingly with the "time"-component of the current matrix element (1.100). An arbitrary moment $\langle m \rangle$ of a charge distribution is then given in general by:

$$\langle m \rangle = \sum_{i_1,i_2,\ldots,i_n=1}^{3} O_{i_1 i_2 \ldots i_n} \int \mathrm{d}^3x \, x^{i_1} x^{i_2} \cdots x^{i_n} \rho(\boldsymbol{x}), \tag{4.1}$$

where $O_{i_1,i_2,\ldots,i_n}$ is a tensor of rank n, which depends on the moment to be computed. For example for the charge radius, considered so far, O is simply:

$$O_{i_1 i_2} = \frac{1}{q} \delta_{i_1 i_2}, \tag{4.2}$$

where q is the net charge of the system given by eq. (2.3). By similar steps leading from eq. (2.2) to eq. (2.17) we get:

$$\langle m\rangle = \frac{1}{2M}\left(\frac{-\mathrm{i}}{2}\right)^n \sum_{i_1,i_2,\ldots,i_n=1}^{3} O_{i_1 i_2 \ldots i_n} \frac{\partial}{\partial P^{i_1}}\frac{\partial}{\partial P^{i_2}}\cdots\frac{\partial}{\partial P^{i_n}} \langle \mathcal{P}P|j^0(0)|P\rangle\Big|_{\boldsymbol{P}=0}. \tag{4.3}$$

The current matrix element appearing here is defined in eq. (1.100). As before its P-dependent part is given by an exponential of infinitesimal boosts as in eq. (2.67). Because

$$\lim_{\boldsymbol{P}\to 0}\eta(P) = 0 \quad \text{and} \quad \frac{\partial}{\partial P^i}\eta^j(P)\Big|_{\boldsymbol{P}=0} = \frac{\delta_{ij}}{M}, \tag{4.4}$$

we find:

$$\frac{\partial}{\partial P^{i_1}}\frac{\partial}{\partial P^{i_2}}\cdots\frac{\partial}{\partial P^{i_n}} \exp(-2\mathrm{i}\boldsymbol{\eta}(P)\cdot\hat{\boldsymbol{K}})\Big|_{\boldsymbol{P}=0} = \frac{(-2\mathrm{i})^n}{M^n}\hat{K}^{i_1}\hat{K}^{i_2}\cdots\hat{K}^{i_n} \tag{4.5}$$

Note that to every x^i from our starting equation (4.1) there now corresponds a boost generator $\hat{K}^i$. Using this result we get from eq. (4.3):

$$\begin{aligned}\langle m\rangle = \frac{1}{2M}\sum_{i_1,i_2,\ldots,i_n=1}^{3} O_{i_1 i_2\ldots i_n}\,(-3)\int\frac{d^4p_\xi}{(2\pi)^4}\int\frac{d^4p_\eta}{(2\pi)^4}\,\overline{\Gamma}^{\Lambda}_M(\boldsymbol{p_\xi},\boldsymbol{p_\eta})\\ \times\left[S_F^1(p_\xi+\tfrac{1}{2}p_\eta)\otimes S_F^2(-p_\xi+p_\eta)\otimes S_F^3(M-p_\eta)\right]\frac{1}{M^n}\hat{K}^{i_1}\hat{K}^{i_2}\cdots\hat{K}^{i_n}\\ \times\left[\mathbb{1}\otimes\mathbb{1}\otimes\gamma^0\hat{q}S_F^3(M-p_\eta)\right]\Gamma^{\Lambda}_M(\boldsymbol{p_\xi},\boldsymbol{p_\eta}).\end{aligned} \tag{4.6}$$

Integrating out the dependence on the relative energies after replacing the propagators according to eq. (1.36) then results in:

$$\begin{aligned}\langle m\rangle = \frac{3}{\langle\Phi^{\Lambda}_M|\Phi^{\Lambda}_M\rangle}\sum_{i_1,i_2,\ldots,i_n=1}^{3} O_{i_1 i_2\ldots i_n}\,\langle\Phi^{\Lambda}_M|\frac{1}{M^n}\hat{K}'_{i_1}\hat{K}'_{i_2}\ldots\hat{K}'_{i_n}\hat{q}_3|\Phi^{\Lambda}_M\rangle\\ +\ \text{off-diagonal matrix elements}\end{aligned} \tag{4.7}$$

where $\hat{K}'_i$ is defined in eq. (2.79). For $n > 2$ we also find terms involving matrix elements between different energy components of the vertex function, *i.e.* between the subspaces of purely positive and negative energy components (denoted "off-diagonal matrix elements" in eq. (4.7)). Unfortunately these terms cannot be expressed in a generic way and have to be calculated explicitly for the moment under consideration. One might however expect that these additional contributions are in fact small; first because the negative energy components correspond to the "small" components of the Dirac equation and thus vanish in the nonrelativistic limit and second because both energy subspaces are orthogonal. Note that although the first term of eq. (4.7) also involves matrix elements between different energy subspaces of the Salpeter amplitudes, one can show with relation (2.43) that these do in fact vanish.

Finally we may symmetrize the expectation value in eq. (4.7) over the three fermions to obtain:

$$\langle m\rangle = \frac{1}{\langle\Phi_M^\Lambda|\Phi_M^\Lambda\rangle}\sum_{i_1,i_2,\ldots,i_n=1}^{3} O_{i_1 i_2\ldots i_n}\,\langle\Phi_M^\Lambda|\sum_{\alpha=1}^{3}\hat{K}''_{i_1\,\alpha}\hat{K}''_{i_2\,\alpha}\ldots\hat{K}''_{i_n\,\alpha}\hat{q}_\alpha|\Phi_M^\Lambda\rangle$$

$$+\ \text{off-diagonal matrix elements}, \quad (4.8)$$

where $\hat{K}''_{i\,\alpha}$ is defined as:

$$\hat{K}''_{i\,\alpha} = \frac{1}{2}\left[\frac{\Omega}{M}\left(\mathrm{i}\frac{\partial}{\partial p_\alpha^i} - \hat{\boldsymbol{R}}\right) + \text{h. c.}\right]. \quad (4.9)$$

If we insert eq. (4.2) into the final result (4.8) we instantly obtain the charge radius expression (2.87). What has been said about its interpretation also applies to eq. (4.8) in its general form.

In this sense a generalization of the formalism presented in this work to arbitrary moments is possible, although the ones discussed in detail, namely the charge radius and the magnetic moment are by far the most interesting, having in addition the soundest empirical basis.

4.3 Form factors

The preceding section showed that an extension to the computation of arbitrary moments of the charge distribution of a given three-quark system is possible. One might then ask whether the method is also applicable to the computation of form factors. Let us first sketch the general idea before we show why one might put this question at all.

4.3.1 Elastic form factors

Equation (2.60) allows us to express the electric form factor through the current matrix element of the electromagnetic vector currents "time"-component:

$$G_E^B(Q^2) = \frac{\langle B,\mathcal{P}P,\lambda|j^0(0)|B,P,\lambda\rangle}{2eM_B}. \quad (4.10)$$

As was shown, this matrix element is given in our formalism by eq. (1.100). The boost appearing here can be expanded in an exponential according to eq. (2.72), where the boost generators are defined by eq. (2.71). Because of parity this expansion only contains even powers of the infinitesimal boost:

$$G_E^B(Q^2) = \frac{-3}{2M_B}\int\frac{d^4p_\xi}{(2\pi)^4}\int\frac{d^4p_\eta}{(2\pi)^4}\bar{\Gamma}_M^{(\Lambda)}(\boldsymbol{p_\xi},\boldsymbol{p_\eta})$$

$$\times\left[S_F^1(p_\xi+\tfrac{1}{2}p_\eta)\otimes S_F^2(-p_\xi+p_\eta)\otimes S_F^3(M-p_\eta)\right]\exp\left(-4(\boldsymbol{\eta}(P)\cdot\hat{\boldsymbol{K}})^2\right)$$

$$\times\left[\mathbb{1}\otimes\mathbb{1}\otimes\gamma^0\hat{q}S_F^3(M-p_\eta)\right]\Gamma_M^{(\Lambda)}(\boldsymbol{p_\xi},\boldsymbol{p_\eta}). \quad (4.11)$$

This is an expansion of the electric form factor in powers of the rapidity $\boldsymbol{\eta}(P)$. Every term in this expansion is a matrix element with respect to vertex functions in the rest frame of the baryon. As is shown in appendix B the integration over the relative energies for an arbitrary numbered product of such boosts can be performed. If we apply that to eq. (4.11) and then make use of relation (2.43) we arrive at:

$$G_E^B(Q^2) = \frac{3}{2M_B}\langle\Phi_M|\hat{q}_3 \exp\left(-4(\boldsymbol{\eta}(P)\cdot\hat{\boldsymbol{K}}')^2\right)|\Phi_M\rangle + \text{off-diagonal matrix elements}, \quad (4.12)$$

where $\hat{K}'_i$ is defined in eq. (2.79). As we already mentioned the terms involving matrix elements between different energy components (denoted "off-diagonal matrix elements" in the above expansion) are expected to be small; so let us concentrate on the first term of eq. (4.12). In the following we sketch how the expansion 4.12 can be computed in any order of $(\boldsymbol{\eta}(P)\cdot\hat{\boldsymbol{K}}')^2$, *i.e.* how a matrix element of the form

$$\langle\Phi_M,\tfrac{1}{2}|\hat{q}_3\left(\boldsymbol{\eta}(P)\cdot\hat{\boldsymbol{K}}'\right)^{2n}|\Phi_M,\tfrac{1}{2}\rangle = \sum_{i_1,i_2,\ldots,i_2n}^{3}\eta_{i_1}(P)\eta_{i_2}(P)\cdots\eta_{i_{2n}}(P)\langle\Phi_M,\tfrac{1}{2}|\hat{q}_3\hat{K}'_{i_1}\hat{K}'_{i_2}\cdots\hat{K}'_{i_{2n}}|\Phi_M,\tfrac{1}{2}\rangle \quad (4.13)$$

may be evaluated. Since Φ_M represents a state with a defined transformation property under rotations it is advisable to decompose $\hat{K}'_{i_1}\hat{K}'_{i_2}\cdots\hat{K}'_{i_{2n}}$ into irreducible representations of the rotation group. The triangularity relation rules out any contributions of tensor operators with a higher rank than 1 because $|\Phi_M\rangle$ represents a particle with total spin 1/2:

$$\langle\Phi_M,\tfrac{1}{2}|T_q^{[k]}|\Phi_M,\tfrac{1}{2}\rangle = 0 \quad \text{unless} \quad 0 \le k \le 1. \quad (4.14)$$

Also because a spherical tensor of rank 1 is always skew symmetric with respect to a permutation of its indices, but $\eta_{i_1}(P)\eta_{i_2}(P)\cdots\eta_{i_{2n}}(P)$ clearly is symmetric, the spin 1 representation makes no contribution at all. So fortunately, we only need to find the scalar representations. It must be noted here that a Cartesian tensor of rank $k > 2$ contains the scalar representation more than just once. Let us sketch the general procedure for the first order $n = 1$: The usual scalar product of two vectors can be written in terms of their spherical components like

$$\boldsymbol{U}\cdot\boldsymbol{V} = -U_{+1}^{[1]}V_{-1}^{[1]} - U_{-1}^{[1]}V_{+1}^{[1]} + U_0^{[1]}V_0^{[1]}. \quad (4.15)$$

With this relation we express the scalar product $\boldsymbol{\eta}(P)\cdot\hat{\boldsymbol{K}}'$ through the spherical components of the vectors $\boldsymbol{\eta}$ and $\boldsymbol{K}'$:

$$\begin{aligned}(\boldsymbol{\eta}\cdot\hat{\boldsymbol{K}}')(\boldsymbol{\eta}\cdot\hat{\boldsymbol{K}}') &= (-\eta_{+1}\hat{K}'_{-1} - \eta_{-1}\hat{K}'_{+1} + \eta_0\hat{K}'_0)(-\eta_{+1}\hat{K}'_{-1} - \eta_{-1}\hat{K}'_{+1} + \eta_0\hat{K}'_0)\\ &= \eta_{-1}\eta_{-1}\hat{K}'_{+1}\hat{K}'_{+1} + \eta_{-1}\eta_{+1}\hat{K}'_{+1}\hat{K}'_{-1} - \eta_{-1}\eta_0\hat{K}'_{+1}\hat{K}'_0\\ &\quad + \eta_{+1}\eta_{-1}\hat{K}'_{-1}\hat{K}'_{+1} + \eta_{+1}\eta_{+1}\hat{K}'_{-1}\hat{K}'_{-1} - \eta_{+1}\eta_0\hat{K}'_{-1}\hat{K}'_0\\ &\quad - \eta_0\eta_{-1}\hat{K}'_0\hat{K}'_{+1} - \eta_0\eta_{+1}\hat{K}'_0\hat{K}'_{-1} + \eta_0\eta_0\hat{K}'_0\hat{K}'_0\end{aligned} \quad (4.16)$$

A product of two spherical tensor operators can be coupled to a tensor product, yielding a sum of spherical tensor operators according to the following formula (see *e.g.* refs. [34, 35]):

$$T_1{}^{[j_1]}_{m_1} T_2{}^{[j_2]}_{m_2} = \sum_{J=|j_1-j_2|}^{j_1+j_2} C^{J\,(m_1+m_2)}_{j_1 m_1, j_2 m_2} \left[T_1{}^{[j_1]} \otimes T_2{}^{[j_2]} \right]^{[J]}_{m_1+m_2} . \tag{4.17}$$

By making use of this formula, eq. (4.16) becomes:

$$\begin{aligned}(\boldsymbol{\eta}\cdot\hat{\boldsymbol{K}}')(\boldsymbol{\eta}\cdot\hat{\boldsymbol{K}}') = {} & \left(\tfrac{2}{\sqrt{3}}\,\eta_{-1}\eta_1 - \tfrac{1}{\sqrt{3}}\,|\eta_0|^2\right)\left[\hat{K}'^{[1]}\otimes\hat{K}'^{[1]}\right]^{[0]}_0 + \eta_0^2\left[\hat{K}'^{[1]}\otimes\hat{K}'^{[1]}\right]^{[2]}_2 \\ & - \sqrt{2}\,\eta_{-1}\eta_0\left[\hat{K}'^{[1]}\otimes\hat{K}'^{[1]}\right]^{[2]}_1 + \sqrt{\tfrac{2}{3}}\,(\eta_0^2+\eta_{-1}\eta_1)\left[\hat{K}'^{[1]}\otimes\hat{K}'^{[1]}\right]^{[2]}_0 \\ & - \sqrt{2}\,\eta_1\eta_0\left[\hat{K}'^{[1]}\otimes\hat{K}'^{[1]}\right]^{[2]}_{-1} + \eta_1^2\left[\hat{K}'^{[1]}\otimes\hat{K}'^{[1]}\right]^{[2]}_{-2} .\end{aligned} \tag{4.18}$$

Note that this sum does not contain a representation of spin 1, since it vanishes due to skewness as already mentioned. If we take the expectation value of this operator with respect to Salpeter amplitudes, the contributions of the tensors with rank 2 vanish due to the triangularity relation. Thus the only contribution is made by the scalar tensor operator $\left[\hat{K}'^{[1]}\otimes\hat{K}'^{[1]}\right]^{[0]}_0$:

$$\langle\Phi_M,\tfrac{1}{2}|\hat{q}_3\left(\boldsymbol{\eta}(P)\cdot\hat{\boldsymbol{K}}'\right)^2|\Phi_M,\tfrac{1}{2}\rangle = -\tfrac{1}{\sqrt{3}}\,|\boldsymbol{\eta}(P)|^2\langle\Phi_M,\tfrac{1}{2}|\hat{q}_3\left[\hat{K}'^{[1]}\otimes\hat{K}'^{[1]}\right]^{[0]}_0|\Phi_M,\tfrac{1}{2}\rangle. \tag{4.19}$$

Note that we made use of eq. (4.15) here. The generalization to higher orders is now obvious: First express the vectors $\boldsymbol{\eta}$ and $\hat{\boldsymbol{K}}'$ in $\left(\boldsymbol{\eta}(P)\cdot\hat{\boldsymbol{K}}'\right)^{2n}$ by spherical components, then couple products of infinitesimal boosts $\hat{\boldsymbol{K}}'$ to spherical tensor operators according to eq. (4.17). Because spherical tensors corresponding to odd spin are skew, their contributions vanish, since the product $\eta_{i_1}\eta_{i_2}\cdots\eta_{i_{2n}}$ is symmetric under the exchange of indices. Finally when taking the expectation value with respect to Salpeter amplitudes the triangularity relation rules out any contribution of tensor operators with a higher rank than 1 and thus only the scalar tensors contribute. We thus obtain:

$$\begin{aligned}\langle\Phi_M,\tfrac{1}{2}|\hat{q}_3\left(\boldsymbol{\eta}(P)\cdot\hat{\boldsymbol{K}}'\right)^{2n}|\Phi_M,\tfrac{1}{2}\rangle = {} & |\boldsymbol{\eta}(Q^2)|^{2n}\sum_{\{j_n\}} C_{j_1 j_2\ldots j_{2n-3}} \\ & \times\langle\Phi_M,\tfrac{1}{2}|\,\hat{q}_3\left[T^{[j_1]}\otimes\left[T^{[j_2]}\otimes\cdots\otimes\left[T^{[j_3]}\otimes T^{[j_4]}\right]^{[j_5]}\ldots\right]^{[j_1]}\right]^{[0]}|\Phi_M,\tfrac{1}{2}\rangle.\end{aligned} \tag{4.20}$$

For the sake of a better readability we have defined:

$$T^{[j]} := \left[\hat{K}'\otimes\hat{K}'\right]^{[j]} . \tag{4.21}$$

The sum in the above equation runs over a set of $(2n-3)$-tuples $(j_1, j_2, \ldots, j_{2n-3})$, where j_i is either 0 or 2. This set depends of course on the order n. We have listed

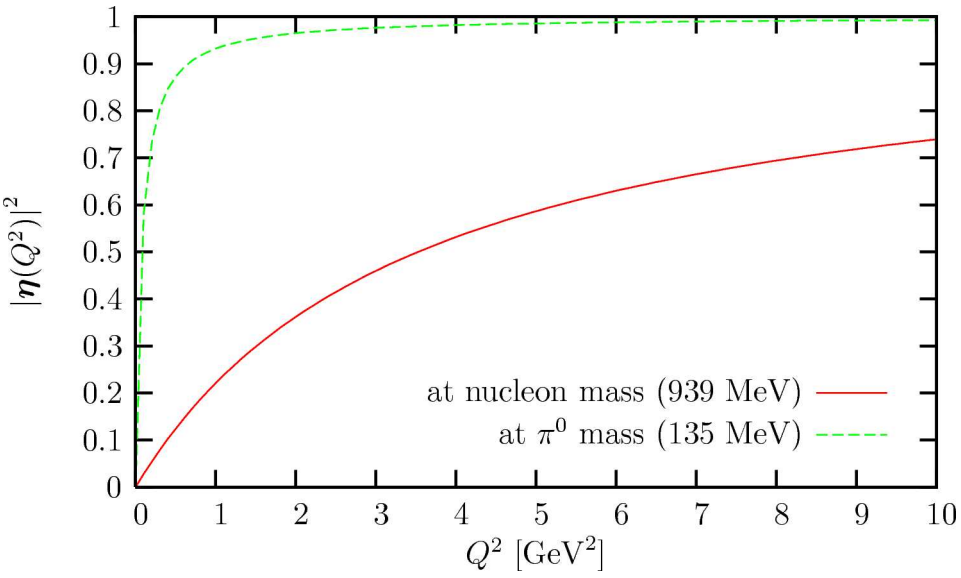

Figure 4.1: Square of the rapidity as function of Q^2 for the nucleon and the neutral pion as comparison.

the sets $\{j_n\}$ and the coefficients $C_{j_1 j_2 \cdots j_{2n-3}}$ in table 4.1 up to fourth order $n = 4$. The number of scalar representations that contribute increases quite rapidly with the order n. In fourth order we already have 14 scalar tensors.

With eqs. (4.20) and (4.12) we get an expansion of the electric form factor in powers of $|\boldsymbol{\eta}(Q^2)|^2$. We should motivate now, why we are interested in such an expansion at all. The reason is that $|\boldsymbol{\eta}(P)|^2$ is a bounded function of Q^2:

$$\lim_{Q^2\to\infty} |\boldsymbol{\eta}(Q^2)|^2 = \lim_{Q^2\to\infty} \frac{Q^2}{4(M^2 + Q^2/4)} = 1. \tag{4.22}$$

In fig. 4.1 we have plotted $|\boldsymbol{\eta}|^2$ as a function of Q^2 up to $10\,\mathrm{GeV}^2$ for elastic scattering off the nucleon and for the much lighter pion as a comparison. Apparently it stays well below one, exceeding 1/2 around $3\,\mathrm{GeV}^2$. So if the matrix elements in eq. (4.20) do not grow exponentially with increasing order n it may be sufficient to compute the expansion (4.12) up to some low order n. We want to study the quality of the expansion for the proton form factor. To this end we take the well known but purely phenomenological dipole parameterization:

$$G_D(Q^2) = \frac{1}{\left(1 + Q^2/0.71\mathrm{GeV}^2\right)^2}. \tag{4.23}$$

Although it is known, that this parameterization results in a mean square charge radius of 0.81 fm which is too small compared to the empirical value of 0.87 ± 0.008 fm, and that it also overestimates the electric proton form factor at high energies, it should fit the data sufficiently well for the present analysis. From the definition of the rapidity (2.68) we immediately get $Q^2 = 4M^2/|\boldsymbol{\eta}|^2(1 - |\boldsymbol{\eta}|^2)$ which we insert in the parameterization (4.23) to expand it in powers of $|\boldsymbol{\eta}|^2$:

$$G_E^p(Q^2) = 1 - 9.935\,\boldsymbol{\eta}^2 + 64.09\,\boldsymbol{\eta}^4 - 352.2\,\boldsymbol{\eta}^6 + 1786\,\boldsymbol{\eta}^8 - 8625\,\boldsymbol{\eta}^{10} + \mathcal{O}(\boldsymbol{\eta}^{12}) \tag{4.24}$$

A glance at this expansion up to tenth order unfortunately reveals, that it is not sufficient to know its lowest order terms only. Obviously the coefficients increase exponentially with the order n which renders the expansion useless at least for the computation of the electric proton form factor.

In the chapter on charge radii we found a strong dependence of the neutron charge radius on the size of the instanton cutoff parameter. The foregoing discussion showed that the electric form factor can be expanded in powers of the squared rapidity. The Q^2-dependence thus factorizes and all information about the shape of the form factor is encoded in static matrix element of the form

$$\langle \Phi_M, \tfrac{1}{2}|\, \hat{q}_3 \left[T^{[j_1]} \otimes \left[T^{[j_2]} \otimes \cdots \otimes \left[T^{[j_3]} \otimes T^{[j_4]} \right]^{[j_5]} \ldots \right]^{[j_1]} \right]^{[0]} |\Phi_M, \tfrac{1}{2}\rangle. \tag{4.25}$$

We are thus led to conclude that if the charge radius, which is nothing but the first order $n = 1$ of the expansion (4.12), varies strongly with the instanton cutoff size, the same may be true for the higher order matrix elements (4.25) and so the behavior of the electric form factor at high Q^2 may also be affected by a variation of the cutoff. We have computed the electric form factors for both proton and neutron with the "standard" parameter set of table 1.1, *i.e.* an instanton cutoff of 0.4 fm and a coupling strength of 136 MeV fm^3 and the "new" parameters with a cutoff of 0.6 fm and a coupling strength of 263 MeV fm^3. The proton form factor is shown in fig. 4.2. We hardly see

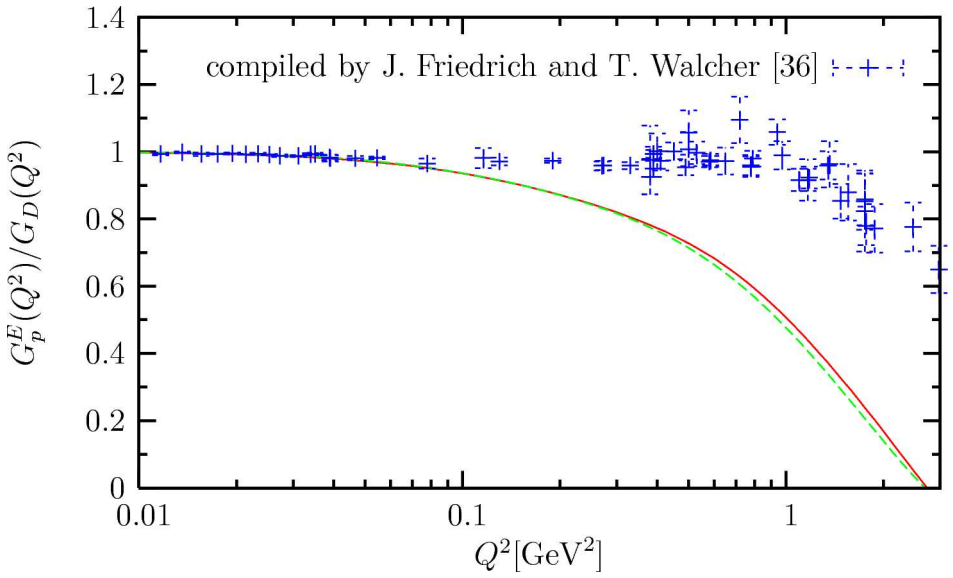

Figure 4.2: The calculated electric proton form factor divided by the dipole parameterization (4.23) with the standard parameter set (full curve) and an instanton cutoff of 0.6 fm and a coupling strength of 263 MeV fm^3 (dashed curve).

a variation with the instanton cutoff size here. Especially at low Q^2 both parameter sets result in almost identical form factors. Above 0.5 GeV^2 the larger instanton cutoff enforces the steep fall-off of the calculated form factor. The almost unaffected shape at low momentum transfer is in concord with the observation, that the relative change in the proton charge radius was also quite moderate. The situation is different for

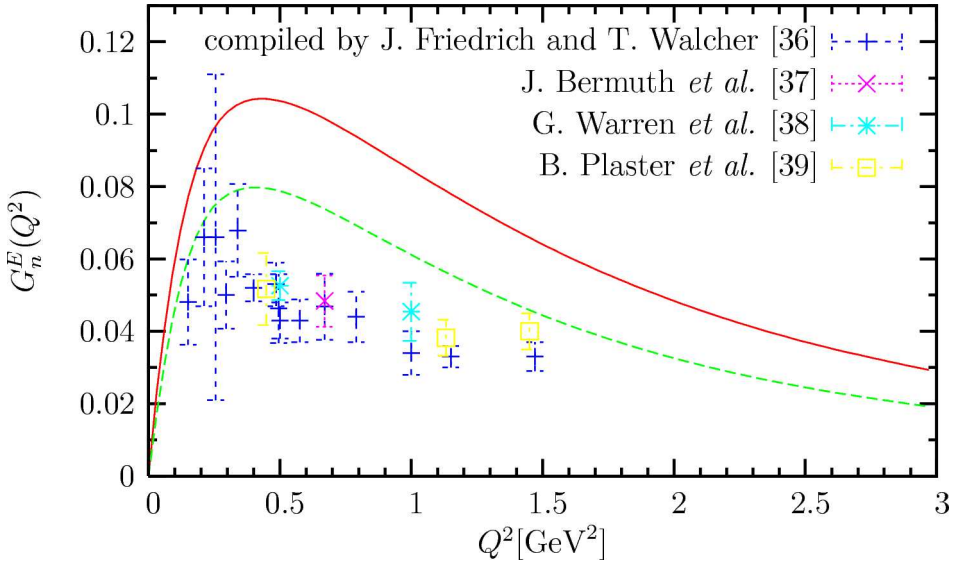

Figure 4.3: The calculated electric neutron form factor with the standard parameter set (full curve) and an instanton cutoff of 0.6 fm and a coupling strength of 263 MeV fm^3 (dashed curve).

the neutron form factor, which we have plotted in fig. 4.3. The dependence on the cutoff size is rather pronounced here. Fortunately the description of the data is much improved with the "new" parameter set.

4.3.2 Nucleon-Delta transition form factor

Motivated by the above analysis, we also want to study the dependence of the nucleon-delta transition on the choice of the instanton parameters. Let us therefore briefly introduce the necessary formalism. The photon spin can be aligned parallel or anti-parallel to the target spin, resulting in two different helicity amplitudes $A^N_{3/2}$ and $A^N_{1/2}$ respectively, that is four amplitudes for the nucleon:

$$A^N_{1/2} := k\langle N^*, \bar{P}', \tfrac{1}{2}|j_+(0)|N, \bar{P}, -\tfrac{1}{2}\rangle \tag{4.26}$$

$$A^N_{3/2} := k\langle N^*, \bar{P}', \tfrac{3}{2}|j_+(0)|N, \bar{P}, \tfrac{1}{2}\rangle, \tag{4.27}$$

where N is either p (proton) or n (neutron). Concerning the normalization of these transversal amplitudes we use the convention of ref. [40]:

$$k := \sqrt{\frac{2\pi\alpha M_{N^*}}{M^2_{N^*} - M^2_N}}. \tag{4.28}$$

It must be noted however that there is only one restriction on the normalization, namely that at $Q^2 = 0$ the electro-production amplitude coincides with the photo-coupling amplitude. With the above choice this is guaranteed. One also defines the following longitudinal amplitude:

$$S^N_{1/2} := k\langle N^*, \bar{P}', \tfrac{1}{2}|j_0(0)|N, \bar{P}, \tfrac{1}{2}\rangle. \tag{4.29}$$

Conventionally one introduces nucleon-delta transition form factors, which are defined as linear combinations of the helicity amplitudes according to ref. [40]. Similar to the elastic form factors of the nucleon one obtains electric and magnetic transition form factors:

$$G_E^*(Q^2) = F(Q^2)\left(\frac{1}{\sqrt{3}}A_{\frac{3}{2}}^N - A_{\frac{1}{2}}^N\right) \tag{4.30}$$

$$G_M^*(Q^2) = F(Q^2)\left(\frac{1}{\sqrt{3}}A_{\frac{3}{2}}^N + A_{\frac{1}{2}}^N\right). \tag{4.31}$$

The normalization of these form factors is given by (see ref. [40]):

$$F(Q^2) := \frac{1}{\sqrt{2\pi\alpha}} M_N \sqrt{\frac{M_N(M_N^* - M_N)}{(M_N^* + M_N)\left((M_N^* - M_N)^2 + Q^2\right)}}. \tag{4.32}$$

G_M^* has already been studied within the present quark model in ref. [11] and was found to be too small, especially at low momentum transfers. Our result on G_M^* is shown in fig. 4.4. We have computed the form factor with two different sets of confinement parameters. The first set is listed in table 1.1, the second consists in a modification of the instanton cutoff size and coupling strength as found to give improvements on the neutron charge radius and form factor. We modified the cutoff to 0.6 fm and the coupling strength to 263 MeV^3. A well known problem of quark models

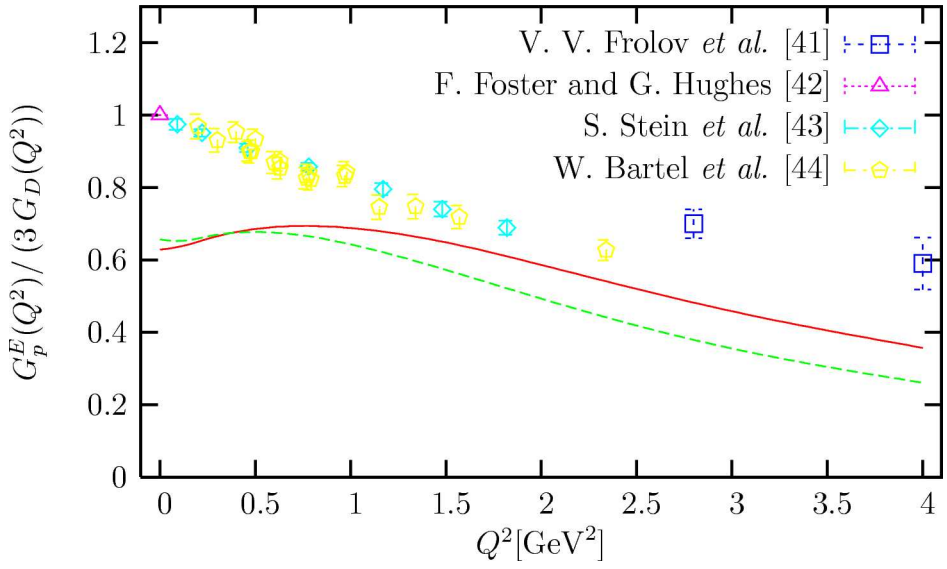

Figure 4.4: The calculated magnetic transition form factor divided by $3\,G_D(Q^2)$ with the standard parameter set (full curve) and an instanton cutoff of 0.6 fm and a coupling strength of 263 MeV fm^3 (dashed curve).

is the correct description of this form factor at low momentum transfer. Especially at the photon point quark models tend to be to small by a factor of two. Also in our computation the form factor comes out to small. With the "new" parameter set we can only improve the situation slightly at low momentum transfer at the price of a pronounced underestimation of the form factor above 0.5 GeV^2.

The situation is even worse with the longitudinal helicity amplitude $S^N_{1/2}(Q^2)$ of the $P^{33}(1232)$ resonance which we have plotted in fig. 4.5. The amplitude that we obtain

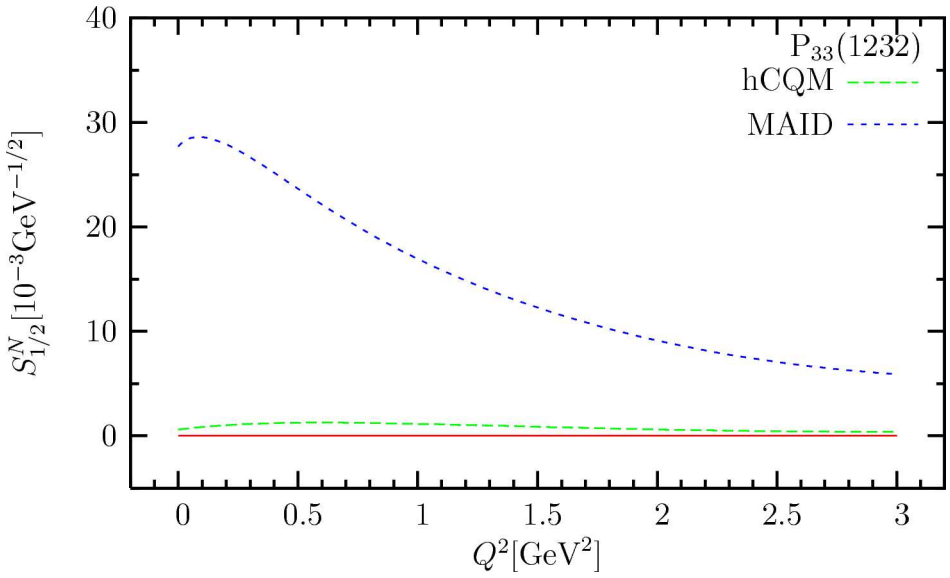

Figure 4.5: Longitudinal helicity amplitude $S^N_{1/2}(Q^2)$ of the Δ-baryon $P^{33}(1232)$ as compared to a MAID fit to the experimental data and a quark model calculation.

is compatible with zero. The same is true if we take the other parameter set, such that we have not even included it in the figure. For comparison with the empirical results, we have included a MAID fit to the experimental data in the figure, which was taken from ref. [45]. The computed amplitude is much too small as compared to the empirical one. The same can also be said for the hypercentral constituent quark model (hCQM) of ref. [46], whose results on this amplitude we have also included in the figure. The discrepancy in the description of this transition is commonly ascribed to pion cloud contributions, which are missing in quark models (see *e.g.* ref. [45]). The pion cloud gives rise to a correction of the electromagnetic vertex, whereas the quark model only includes the bare vertex.

4.4 Summary

This chapter commenced with the question whether the formalism developed in the two preceding chapters on charge radii and magnetic moments can be extended to higher moments as well. To answer this question we started with an arbitrary moment of a charge distribution which is the generalization of the charge radius. Following similar steps as in the case of the charge radius derivation we found indeed a formula generalizing the preceding results and showing a similar structure. We then asked whether the method could be applied to the computation of form factors as well. Because of energy-momentum conservation at least one of the wavefunctions entering the form factor has to be boosted, which is a numerical disadvantage. We then showed that the electric form factor can be expanded in powers of the rapidity squared, which made

a separation of the Q^2-dependence possible in each order of the expansion. The remaining matrix elements only involve wavefunctions in the rest frame of the system thus facilitating the computation by the use of symmetries. To study whether this expansion is applicable to the computation of the electric proton form factor, we expanded its dipole parameterization in powers of the rapidity. The resulting coefficients unfortunately grew exponentially with the order of the expansion, such that it may not be cut at low orders. We however found that higher orders are given by similar matrix elements as the charge radius, which motivated us to study the dependence of the nucleon form factors on the instanton parameters. Indeed we found that the neutron form factor varies strongly with this parameters, whereas the proton form factor mainly stays unaffected. Both observations are in accordance with the results on the charge radii. We then proposed a new parameter set, which makes the neutron form factor better fit the experimental data, while leaving the mass spectrum largely unchanged. The description of the nucleon-delta transition is however not improved with a different choice of the parameters.

To conclude we would like to remark that the extension to higher moments becomes important, when new experiments are completed, which measure those observables like *e.g.* quadrupole moments. Likewise the expansion that we found for the form factors may not be in vain, although not applicable to nucleon form factors. It might be useful to study for example decay observables between states with a small mass gap, where the rapidity is small and thus becomes a good expansion parameter.

order n	coupling scheme	$\{j_n\}$	$C_{j_1 j_2 \dots j_{2n-3}}$
1	$T^{[j]}$	j_1	
		0	$-1/\sqrt{3}$
2	$\left[T^{[j]} \otimes T^{[j]}\right]^{[0]}$	j_1	
		0	$1/3$
		2	$2/(3\sqrt{5})$
3	$\left[T^{[j_1]} \otimes \left[T^{[j_2]} \otimes T^{[j_3]}\right]^{[j_1]}\right]^{[0]}$	j_1 j_2 j_3	
		0 0 0	$-1/(3\sqrt{3})$
		0 2 2	$-2/(3\sqrt{15})$
		2 0 2	$-2/(3\sqrt{15})$
		2 2 0	$-2/(3\sqrt{15})$
		2 2 2	$-4/(3\sqrt{105})$
4	$\left[T^{[j_1]} \otimes \left[T^{[j_2]} \otimes \left[T^{[j_3]} \otimes T^{[j_4]}\right]^{[j_5]}\right]^{[j_1]}\right]^{[0]}$	j_1 j_2 j_3 j_4 j_5	
		0 0 0 0 0	$1/9$
		0 0 2 2 0	$2/(9\sqrt{5})$
		0 2 0 2 2	$2/(9\sqrt{5})$
		0 2 2 0 2	$2/(9\sqrt{5})$
		0 2 2 2 2	$4/(9\sqrt{35})$
		2 0 0 2 2	$2/(9\sqrt{5})$
		2 0 2 0 2	$2/(9\sqrt{5})$
		2 0 2 2 2	$4/(9\sqrt{35})$
		2 2 0 0 0	$2/(9\sqrt{5})$
		2 2 2 2 0	$4/45$
		2 2 0 2 2	$4/(9\sqrt{35})$
		2 2 2 0 2	$4/(9\sqrt{35})$
		2 2 2 2 2	$8/(63\sqrt{5})$
		2 2 2 2 4	$8/105$

Table 4.1: Coupling schemes and coefficients up to fourth order in $\boldsymbol{\eta}^2$.

Summary and outlook

The main objective of this work was to find new access to static observables of three-fermion systems. Especially it was devoted to the computation of charge radii and magnetic moments of baryons. The analytic derivations founded on the Bethe-Salpeter formalism, which is the usual way to treat bound states in quantum field theory. Because of conceptual problems stemming from retardation effects this equation is however seldom used as such. Instead the instantaneous approximation is adopted consisting in the neglect of these retardation effects. The resulting Salpeter equation has successfully been used as a starting point for the development of a relativistic quark model for baryons. The interaction kernels consisted of a linearly rising confinement potential together with a residual instanton induced interaction. The model gives a quite satisfactory description of the experimentally observed baryon spectra and constitutes the basis for the numerical calculations of this work.

We started our analysis with charge radii of three-fermion systems. There are at least two different approaches to this observable, both of which were used here. The first approach consisted in a definition of the charge radius taken from classical electrodynamics and the second started from form factors, where the charge radius is defined as the slope of the electric form factor at the photon point. Both approaches turned out to be equivalent and also resulted in the same final expression for the charge radius in the Bethe-Salpeter framework. The result is the relativistic generalization of the nonrelativistic expression, naturally incorporating a center of mass correction. The result was then applied to the computation of baryon octet radii using the Salpeter amplitudes of the quark model described in detail in ref. [6]. The computed charge radius of the proton is in excellent agreement whereas the neutron radius is too large and also showed to be rather sensitive to the particular choice of the instanton cutoff parameter. Since the proton radius only depends slightly on this parameter, we found a parameter set, which describes both radii equally well. Unfortunately the experimental situation with the hyperon radii is rather sparse and calls for refined experiments.

We then moved on to apply the formalism also to magnetic moments. Since this had already been done partly in ref. [16], we started from a different approach, namely from form factors. The resulting expression allows for a distinction between spin- and angular momentum contributions to the net magnetic moment, a fact which we exploited in the numerical treatment of baryon magnetic moments. The computation indicated, that roughly 90 % of the baryon octet magnetic moments are due to the quark spins. For the nucleon we also analyzed the dependence of this decomposition on the quark mass. At quark masses nearly as small as current quark masses both contributions roughly become of the same magnitude. The octet magnetic moments are

experimentally well measured. The model is able to describe them quite accurately. For the decuplet, one also has to include mixed energy contributions of the vertex function due to the missing two-body interaction. This has been done in ref. [16] analytically but not implemented numerically, so we did that here. The experimental situation is however such that only the Ω^- magnetic moment allows for a sensible discussion. The model misses this value by about 13 %.

Inspired by successfully expressing charge radius and magnetic moment of a relativistic three-fermion system as an expectation value, we extended the method to higher moments. The resulting expression is indeed a generalization of the aforementioned lowest moments, but in addition also matrix elements between mixed energy components of the vertex functions appear, which are however expected to be small. We then showed a way to also apply the method to the computation of form factors, by expanding the boost of the incoming Salpeter amplitude that enters the current matrix element in an exponential. Indeed we were able to separate the Q^2-dependence from the static matrix elements in all orders of the resulting expansion in the rapidity. A fit of the expansion to the dipole parameterization of the proton form factor however revealed, that the expansion is not suited to compute the proton form factor. Instead we computed the form factors the classical way, inspired by the foregoing analysis to study the effect of a change in the instanton parameters on the nucleon form factors. The dependence of the electric proton form factor on variations of these parameters is only slightly, but the neutron form factor shows a rather large dependence, fitting the empirical data indeed much better, when we use the parameter set proposed in the treatment of the nucleon charge radii.

The generalizing results of the last chapter pave the way for future work on static hadron properties like magnetic radii and electric polarizabilities, which we mention here because efforts have already been made to measure them at least for the nucleon. Also when deriving the current matrix element we neglected so far the first order contribution of the residual kernel due to its complexity. Although the resulting expressions for the charge radius and magnetic moment seem to be “complete” and in its most natural form, it remains to study the effect of these contributions.

Appendix A

Reconstruction of the Bethe-Salpeter amplitude

In the case of vanishing two-body interactions, we have a reconstruction prescription for the Bethe-Salpeter amplitudes from the Bethe-Salpeter equation itself. By performing the integration over the relative energies p_ξ^0 and p_η^0 on the right-hand side of the Bethe-Salpeter equation (1.33), which is possible because of the instantaneous three-body kernel $V^{(3)}$, we get:

$$\chi_M = -\mathrm{i}\, G_{0M}\, V^{(3)}\, \phi_M^\Lambda. \tag{A.1}$$

In this case, the Bethe-Salpeter amplitudes contain also mixed energy components, because $V^{(3)}$ does not commute with the Salpeter projector (1.43) in general.

In the presence of a two-body force, we need a reconstruction scheme that is consistent with the approximations that entered the Salpeter equation. To this end we first isolate the instantaneous part $V_\Lambda^{(3)} + \sum_{i=1}^k V_M^{\mathrm{eff}(i)}$ of the Bethe-Salpeter equation:

$$\chi_M = -\mathrm{i} G_{0M} \left(\bar{K}_M^{(2)} + V_R^{(3)} - \sum_{i=1}^k V_M^{\mathrm{eff}(i)} + V_\Lambda^{(3)} + \sum_{i=1}^k V_M^{\mathrm{eff}(i)} \right) \chi_M. \tag{A.2}$$

This allows for a reformulation of the Bethe-Salpeter equation

$$\chi_M = -\mathrm{i} \mathcal{G}_M^{R,k} \left(V_\Lambda^{(3)} + \sum_{i=1}^k V_M^{\mathrm{eff}(i)} \right) \chi_M, \tag{A.3}$$

by the introduction of a resolvent $\mathcal{G}_M^{R,k}$ which must fulfill the following integral equation to guarantee the equivalence of (A.2) and (A.3):

$$\mathcal{G}_M^{R,k} = G_{0M} - \mathrm{i} G_{0M} \left(\bar{K}_M^{(2)} + V_R^{(3)} - \sum_{i=1}^k V_M^{\mathrm{eff}(i)} \right) \mathcal{G}_M^{R,k}. \tag{A.4}$$

After integrating over p_ξ^0 and p_η^0 on both sides of (A.3) and projecting onto pure energy components we get the Salpeter equation:

$$\Phi_M^\Lambda = -\mathrm{i} \langle \mathcal{G}_M^{R,k} \rangle_\Lambda \left(V_\Lambda^{(3)} + \sum_{i=1}^k V_M^{\mathrm{eff}(i)} \right) \Phi_M^\Lambda. \tag{A.5}$$

Performing the same with the resolvent $\mathcal{G}_M^{R,k}$ (A.4) yields:

$$\langle \mathcal{G}_M^{R,k} \rangle_\Lambda = \langle G_{0M} \rangle - \mathrm{i} \langle G_{0M} \rangle \sum_{i=k+1}^{\infty} V_M^{\mathrm{eff}(i)} \langle \mathcal{G}_M^{R,k} \rangle_\Lambda. \tag{A.6}$$

The kernel of this integral equation is at least of order $k+1$ in the residual kernel $V_R^{(3)} + \bar{K}_M^{(2)}$. Expanding (A.6) in a Neumann series and taking accordingly to the effective kernel V_M^{eff} only terms up to order k then leaves us with:

$$\left\langle \sum_{i=0}^{k} \mathcal{G}_M^{R,k(i)} \right\rangle_\Lambda = \langle G_{0M} \rangle \tag{A.7}$$

Thus it is possible to give an approximation to the exact Bethe-Salpeter equation

$$\chi_M^{(k)} = -\mathrm{i} \sum_{i=0}^{k} \mathcal{G}_M^{R,k} \left(V_\Lambda^{(3)} + \sum_{i=1}^{k} V_M^{\mathrm{eff}(i)} \right) \chi_M^{(k)} \tag{A.8}$$

which is consistent with the approximated Salpeter equation (1.57), because the accordingly reduced Bethe-Salpeter amplitude

$$\Phi_M^{\Lambda\ (k)}(\boldsymbol{p_\xi}, \boldsymbol{p_\eta}) := \Lambda(\boldsymbol{p_\xi}, \boldsymbol{p_\eta}) \int \frac{\mathrm{d}p_\xi^0}{2\pi} \frac{\mathrm{d}p_\eta^0}{2\pi} \chi_M^{(k)}(p_\xi, p_\eta) \tag{A.9}$$

is a solution to the approximated Salpeter equation. A reconstruction prescription for the Bethe-Salpeter amplitude $\chi_M^{(k)}$ is obtained by performing the p_ξ^0- and p_η^0-integration in the instantaneous part of (A.8):

$$\chi_M^{(k)} = -\mathrm{i} \sum_{i=0}^{k} \mathcal{G}_M^{R,k} \left(V_\Lambda^{(3)} + \sum_{i=1}^{k} V_M^{\mathrm{eff}(i)} \right) \Phi_M^{\Lambda\ (k)}. \tag{A.10}$$

From the approximated Salpeter equation (A.5) and the reduction of the resolvent $\mathcal{G}_M^{R,k}$ (A.4) we get an important relation between the vertex function defined in (1.87) and the Salpeter amplitude. By using the partial fraction decomposition of the propagators:

$$S_F^i(p_i) = \mathrm{i} \left(\frac{\Lambda^+(\boldsymbol{p_i})}{p_i^0 - \omega_i(\boldsymbol{p_i}) + \mathrm{i}\epsilon} + \frac{\Lambda^-(\boldsymbol{p_i})}{p_i^0 + \omega_i(\boldsymbol{p_i}) - \mathrm{i}\epsilon} \right) \gamma^0 \tag{A.11}$$

we may use the residue theorem to perform the p_ξ^0- and p_η^0-integration in $\langle G_{0M} \rangle$:

$$\begin{aligned} &\langle G_{0M} \rangle(\boldsymbol{p_\xi}, \boldsymbol{p_\eta}; \boldsymbol{p'_\xi}, \boldsymbol{p'_\eta}) = \\ &\quad \mathrm{i} \left[\frac{\Lambda(\boldsymbol{p_1}) \otimes \Lambda(\boldsymbol{p_2}) \otimes \Lambda(\boldsymbol{p_3})}{M - \omega_1(\boldsymbol{p_i}) - \omega_2(\boldsymbol{p_i}) - \omega_3(\boldsymbol{p_i})} + \frac{\Lambda(\boldsymbol{p_1}) \otimes \Lambda(\boldsymbol{p_2}) \otimes \Lambda(\boldsymbol{p_3})}{M + \omega_1(\boldsymbol{p_i}) + \omega_2(\boldsymbol{p_i}) + \omega_3(\boldsymbol{p_i})} \right] \\ &\qquad \times \gamma^0 \otimes \gamma^0 \otimes \gamma^0 (2\pi)^3 \delta^{(3)}(\boldsymbol{p_\xi} - \boldsymbol{p'_\xi}) (2\pi)^3 \delta^{(3)}(\boldsymbol{p_\eta} - \boldsymbol{p'_\eta}), \end{aligned} \tag{A.12}$$

where $\boldsymbol{p_i} = \boldsymbol{p_i}(\boldsymbol{p_\xi}, \boldsymbol{p_\eta})$ as has been defined in eq. (1.11). This allows us to express the Salpeter amplitudes through vertex functions:

$$\Phi^{\Lambda}_{M}(\boldsymbol{p_\xi}, \boldsymbol{p_\eta}) = \mathrm{i}\left[\frac{\Lambda(\boldsymbol{p_1}) \otimes \Lambda(\boldsymbol{p_2}) \otimes \Lambda(\boldsymbol{p_3})}{M - \omega_1(\boldsymbol{p_i}) - \omega_2(\boldsymbol{p_i}) - \omega_3(\boldsymbol{p_i})} + \frac{\Lambda(\boldsymbol{p_1}) \otimes \Lambda(\boldsymbol{p_2}) \otimes \Lambda(\boldsymbol{p_3})}{M + \omega_1(\boldsymbol{p_i}) + \omega_2(\boldsymbol{p_i}) + \omega_3(\boldsymbol{p_i})}\right] \times \gamma^0 \otimes \gamma^0 \otimes \gamma^0 \Gamma^{\Lambda}_{M}(\boldsymbol{p_\xi}, \boldsymbol{p_\eta}). \quad \text{(A.13)}$$

Accordingly for the adjoint vertex function we find:

$$\Phi^{\Lambda\,\dagger}_{M}(\boldsymbol{p_\xi}, \boldsymbol{p_\eta}) = -\mathrm{i}\,\overline{\Gamma}^{\Lambda}_{M}(\boldsymbol{p_\xi}, \boldsymbol{p_\eta}) \left[\frac{\Lambda(\boldsymbol{p_1}) \otimes \Lambda(\boldsymbol{p_2}) \otimes \Lambda(\boldsymbol{p_3})}{M - \omega_1(\boldsymbol{p_i}) - \omega_2(\boldsymbol{p_i}) - \omega_3(\boldsymbol{p_i})} + \frac{\Lambda(\boldsymbol{p_1}) \otimes \Lambda(\boldsymbol{p_2}) \otimes \Lambda(\boldsymbol{p_3})}{M + \omega_1(\boldsymbol{p_i}) + \omega_2(\boldsymbol{p_i}) + \omega_3(\boldsymbol{p_i})}\right]. \quad \text{(A.14)}$$

Both relations are important, if we want to express static observables as expectation values with respect to Salpeter amplitudes, since they allow the replacement of the vertex functions by the latter after the integration over the relative energies has been performed.

Appendix B

Integrating out the relative energy dependence

Integrating out the dependence on the relative energies p_ξ^0 and p_η^0 in static matrix elements can be done in a generic way, that is for an n-fold product of $A(\bar{M})$ as it is defined in (2.30). To be definite we want to evaluate the following double integral:

$$
\begin{aligned}
I := \int \frac{\mathrm{d}p_\xi^0}{2\pi} \int \frac{\mathrm{d}p_\eta^0}{2\pi} \bar{\Gamma}_M^\Lambda(\boldsymbol{p_\xi}, \boldsymbol{p_\eta}) \\
\left[\frac{\Lambda_1^+ \otimes \Lambda_2^+ \otimes \Lambda_3^+}{(p_\xi^0 + \frac{1}{2}p_\eta^0 - \omega_1 + \mathrm{i}\epsilon)(-p_\xi^0 + \frac{1}{2}p_\eta^0 - \omega_2 + \mathrm{i}\epsilon)(M - p_\eta^0 - \omega_3 + \mathrm{i}\epsilon)} \right. \\
\left. + \frac{\Lambda_1^- \otimes \Lambda_2^- \otimes \Lambda_3^-}{(p_\xi^0 + \frac{1}{2}p_\eta^0 + \omega_1 - \mathrm{i}\epsilon)(-p_\xi^0 + \frac{1}{2}p_\eta^0 + \omega_2 - \mathrm{i}\epsilon)(M - p_\eta^0 + \omega_3 - \mathrm{i}\epsilon)} \right] \\
[\gamma^0 \otimes \gamma^0 \otimes \mathbb{1}] A_{i_1}(\bar{M}) \cdots A_{i_n}(\bar{M}) \\
\left[\frac{\mathbb{1} \otimes \mathbb{1} \otimes \Lambda_3^+}{(M - p_\eta^0 - \omega_3 + \mathrm{i}\epsilon)} + \frac{\mathbb{1} \otimes \mathbb{1} \otimes \Lambda_3^-}{(M - p_\eta^0 + \omega_3 - \mathrm{i}\epsilon)} \right] [\mathbb{1} \otimes \mathbb{1} \otimes \gamma^0] \Gamma_M^\Lambda(\boldsymbol{p_\xi}, \boldsymbol{p_\eta}), \quad \text{(B.1)}
\end{aligned}
$$

where $i_1, \ldots, i_n \in \{1, 2, 3\}$. When using the residue theorem here one is faced with the following difficulty: The denominator of the integrand is of second order in p_ξ^0 and of fourth order in p_η^0 but $A_i(\bar{M})$ is of first order in p_ξ^0 and p_η^0 respectively as can be seen from (2.30). So the contour of integration can not be closed. Even worse for $n > 1$ the integral diverges and so is not well-defined at all. We observe however that as soon as we make the momentum transfer of the photon finite by an arbitrary small amount, whose three-component we call $\boldsymbol{P}$, the integral is regular. This can be seen as follows: From (1.101) and (1.103) we first find for the square of the three-components of a boosted four-vector x:

$$
\left| \overrightarrow{\Lambda_P x} \right|^2 = |\boldsymbol{x}|^2 + 4(x^0)^2(\hat{P}^0)^2|\hat{\boldsymbol{P}}|^2 + 2x^0\hat{P}^0(\boldsymbol{x} \cdot \hat{\boldsymbol{P}}) + \mathcal{O}(|\boldsymbol{P}|^4) \quad \text{(B.2a)}
$$

$$
\left| \overrightarrow{\Lambda_P^{-1} x} \right|^2 = |\boldsymbol{x}|^2 + 4(x^0)^2(\hat{P}^0)^2|\hat{\boldsymbol{P}}|^2 - 2x^0\hat{P}^0(\boldsymbol{x} \cdot \hat{\boldsymbol{P}}) + \mathcal{O}(|\boldsymbol{P}|^4). \quad \text{(B.2b)}
$$

If we boost the incoming and outgoing vertex functions in eq. (B.1) by a small momentum $\boldsymbol{P}$ in opposite directions — corresponding to a small momentum transfer of the photon — we find according to the boost prescription of the vertex functions:

$$\Gamma_P(p_\xi, p_\eta) = [S_{\Lambda_P} \otimes S_{\Lambda_P} \otimes S_{\Lambda_P}]\, \Gamma_M(\overrightarrow{\Lambda_P p_\xi}, \overrightarrow{\Lambda_P p_\eta}) \tag{B.3a}$$

$$\overline{\Gamma}_{\mathcal{P}P}(p_\xi, p_\eta) = \overline{\Gamma}_M(\overrightarrow{\Lambda_P p_\xi}, \overrightarrow{\Lambda_P p_\eta})\, [S_{\Lambda_P} \otimes S_{\Lambda_P} \otimes S_{\Lambda_P}]\,. \tag{B.3b}$$

The last line is explicitly shown in eq. (1.96). As is briefly touched in appendix D, the vertex functions are expanded in a basis of the harmonic three-particle oscillator, whose radial part is given by the product $R_{n_\xi l_\xi}(\beta|\boldsymbol{p_\xi}|)R_{n_\eta l_\eta}(\beta|\boldsymbol{p_\eta}|)$ with the radial functions of the harmonic one-particle oscillator defined in eq. (D.2). As can be seen from these equations by inserting (B.3), the integral (B.1) is always finite, when the vertex functions are boosted by an arbitrary small momentum $\boldsymbol{P}$ due to the exponential damping factors in (D.2). To account for the regularizing behavior of the vertex functions, we multiply by a factor that enforces convergence and take the static limit after integration. Let us first apply this method to the p_ξ^0-integration:

$$\begin{aligned} I = \lim_{\boldsymbol{P}\to 0} \int \frac{\mathrm{d}p_\xi^0}{2\pi} \int \frac{\mathrm{d}p_\eta^0}{2\pi} \bar{\Gamma}^\Lambda_M(\boldsymbol{p_\xi}, \boldsymbol{p_\eta}) \\ \left[\frac{\Lambda_1^+ \otimes \Lambda_2^+ \otimes \Lambda_3^+}{(1+\mathrm{i}|\boldsymbol{P}|p_\xi^0)^k (p_\xi^0 + \frac{1}{2}p_\eta^0 - \omega_1 + \mathrm{i}\epsilon)(-p_\xi^0 + \frac{1}{2}p_\eta^0 - \omega_2 + \mathrm{i}\epsilon)(M - p_\eta^0 - \omega_3 + \mathrm{i}\epsilon)} \right. \\ \left. + \frac{\Lambda_1^- \otimes \Lambda_2^- \otimes \Lambda_3^-}{(1-\mathrm{i}|\boldsymbol{P}|p_\xi^0)^k (p_\xi^0 + \frac{1}{2}p_\eta^0 + \omega_1 - \mathrm{i}\epsilon)(-p_\xi^0 + \frac{1}{2}p_\eta^0 + \omega_2 - \mathrm{i}\epsilon)(M - p_\eta^0 + \omega_3 - \mathrm{i}\epsilon)} \right] \\ [\gamma^0 \otimes \gamma^0 \otimes \mathbb{1}] A_{i_1}(\bar{P}) \cdots A_{i_n}(\bar{P}) \\ \left[\frac{\mathbb{1} \otimes \mathbb{1} \otimes \Lambda_3^+}{(M - p_\eta^0 - \omega_3 + \mathrm{i}\epsilon)} + \frac{\mathbb{1} \otimes \mathbb{1} \otimes \Lambda_3^-}{(M - p_\eta^0 + \omega_3 - \mathrm{i}\epsilon)} \right] [\mathbb{1} \otimes \mathbb{1} \otimes \gamma^0] \Gamma^\Lambda_M(\boldsymbol{p_\xi}, \boldsymbol{p_\eta}), \end{aligned} \tag{B.4}$$

where $k > n$ to assure that the contour of integration can be closed. Obviously this expression is the same as (B.1) in the limit $\boldsymbol{P} \to 0$. We close the contour such that the k-fold pole at $\pm\mathrm{i}/|\boldsymbol{P}|$ is never picked up. After integrating over p_ξ^0 we then get:

$$\begin{aligned} I = -\mathrm{i} \int \frac{dp_\eta^0}{2\pi} \bar{\Gamma}^\Lambda_M(\boldsymbol{p_\xi}, \boldsymbol{p_\eta}) \\ \left\{ \frac{\left[\Lambda_1^+ \otimes \Lambda_2^+ \otimes \Lambda_3^+\right] [\gamma^0 \otimes \gamma^0 \otimes \mathbb{1}]}{(p_\eta^0 - \omega_1 - \omega_2 + \mathrm{i}\epsilon)(M - p_\eta^0 - \omega_3 + \mathrm{i}\epsilon)} \left[A_{i_1}(\bar{M}) \cdots A_{i_n}(\bar{M})\right]_{p_\xi^0 = -\frac{1}{2}p_\eta^0 + \omega_1} \right. \\ \left. - \frac{\left[\Lambda_1^- \otimes \Lambda_2^- \otimes \Lambda_3^-\right] [\gamma^0 \otimes \gamma^0 \otimes \mathbb{1}]}{(p_\eta^0 + \omega_1 + \omega_2 - \mathrm{i}\epsilon)(M - p_\eta^0 + \omega_3 - \mathrm{i}\epsilon)} \left[A_{i_1}(\bar{M}) \cdots A_{i_n}(\bar{M})\right]_{p_\xi^0 = -\frac{1}{2}p_\eta^0 - \omega_1} \right\} \\ \left[\frac{\mathbb{1} \otimes \mathbb{1} \otimes \Lambda_3^+}{(M - p_\eta^0 - \omega_3 + \mathrm{i}\epsilon)} + \frac{\mathbb{1} \otimes \mathbb{1} \otimes \Lambda_3^-}{(M - p_\eta^0 + \omega_3 - \mathrm{i}\epsilon)} \right] [\mathbb{1} \otimes \mathbb{1} \otimes \gamma^0] \Gamma^\Lambda_M(\boldsymbol{p_\xi}, \boldsymbol{p_\eta}) \end{aligned} \tag{B.5}$$

We perform the remaining integration over p_η^0 in the same manner:

$$
\begin{aligned}
I = -\mathrm{i}\lim_{\boldsymbol{P}\to 0}\int \frac{dp_\eta^0}{2\pi}\bar{\Gamma}^{\Lambda}_{M}(\boldsymbol{p_\xi},\boldsymbol{p_\eta})
\\
&\left\{\frac{\left[\Lambda_1^+\otimes\Lambda_2^+\otimes\Lambda_3^+\right]\left[\gamma^0\otimes\gamma^0\otimes\mathbb{I}\right]}{(1+\mathrm{i}|\boldsymbol{P}|p_\eta^0)^k(p_\eta^0-\omega_1-\omega_2+\mathrm{i}\epsilon)(M-p_\eta^0-\omega_3+\mathrm{i}\epsilon)}\right.
\\
&\quad\times\left[A_{i_1}(P)\cdots A_{i_n}(P)\right]_{p_\xi^0=-\frac{1}{2}p_\eta^0+\omega_1}\frac{\mathbb{I}\otimes\mathbb{I}\otimes\Lambda_3^+}{(M-p_\eta^0-\omega_3+\mathrm{i}\epsilon)}
\\
&+\frac{\left[\Lambda_1^+\otimes\Lambda_2^+\otimes\Lambda_3^+\right]\left[\gamma^0\otimes\gamma^0\otimes\mathbb{I}\right]}{(1-\mathrm{i}|\boldsymbol{P}|p_\eta^0)^k(p_\eta^0-\omega_1-\omega_2+\mathrm{i}\epsilon)(M-p_\eta^0-\omega_3+\mathrm{i}\epsilon)}
\\
&\quad\times\left[A_{i_1}(P)\cdots A_{i_n}(P)\right]_{p_\xi^0=-\frac{1}{2}p_\eta^0+\omega_1}\frac{\mathbb{I}\otimes\mathbb{I}\otimes\Lambda_3^-}{(M-p_\eta^0+\omega_3-\mathrm{i}\epsilon)}
\\
&-\frac{\left[\Lambda_1^-\otimes\Lambda_2^-\otimes\Lambda_3^-\right]\left[\gamma^0\otimes\gamma^0\otimes\mathbb{I}\right]}{(1+\mathrm{i}|\boldsymbol{P}|p_\eta^0)^k(p_\eta^0+\omega_1+\omega_2-\mathrm{i}\epsilon)(M-p_\eta^0+\omega_3-\mathrm{i}\epsilon)}
\\
&\quad\times\left[A_{i_1}(P)\cdots A_{i_n}(P)\right]_{p_\xi^0=-\frac{1}{2}p_\eta^0-\omega_1}\frac{\mathbb{I}\otimes\mathbb{I}\otimes\Lambda_3^+}{(M-p_\eta^0-\omega_3+\mathrm{i}\epsilon)}
\\
&-\frac{\left[\Lambda_1^-\otimes\Lambda_2^-\otimes\Lambda_3^-\right]\left[\gamma^0\otimes\gamma^0\otimes\mathbb{I}\right]}{(1-\mathrm{i}|\boldsymbol{P}|p_\eta^0)^k(p_\eta^0+\omega_1+\omega_2-\mathrm{i}\epsilon)(M-p_\eta^0+\omega_3-\mathrm{i}\epsilon)}
\\
&\quad\times\left.\left[A_{i_1}(P)\cdots A_{i_n}(P)\right]_{p_\xi^0=-\frac{1}{2}p_\eta^0-\omega_1}\frac{\mathbb{I}\otimes\mathbb{I}\otimes\Lambda_3^-}{(M-p_\eta^0+\omega_3-\mathrm{i}\epsilon)}\right\}
\\
&\qquad\times\left[\mathbb{I}\otimes\mathbb{I}\otimes\gamma^0\right]\Gamma^{\Lambda}_{M}(\boldsymbol{p_\xi},\boldsymbol{p_\eta})
\end{aligned}
\tag{B.6}
$$

This time $k > n-2$ to assure that the contour of integration can be closed.

$$
\begin{aligned}
I = -\bar{\Gamma}^{\Lambda}_{M}(\boldsymbol{p_\xi},\boldsymbol{p_\eta})
\\
&\left\{\frac{\Lambda^{+++}}{(M-\Omega)}\left[\gamma^0\otimes\gamma^0\otimes\mathbb{I}\right]\left[A_{i_1}(\bar{M})\cdots A_{i_n}(\bar{M})\right]_{p_\xi^0=\frac{1}{2}(\omega_1-\omega_2),\ p_\eta^0=\omega_1+\omega_2}\frac{\mathbb{I}\otimes\mathbb{I}\otimes\Lambda_3^+}{(M-\Omega)}\right.
\\
&+\frac{\Lambda^{---}}{(M+\Omega)}\left[\gamma^0\otimes\gamma^0\otimes\mathbb{I}\right]\left[A_{i_1}(\bar{M})\cdots A_{i_n}(\bar{M})\right]_{p_\xi^0=-\frac{1}{2}(\omega_1-\omega_2),\ p_\eta^0=-(\omega_1+\omega_2)}\frac{\mathbb{I}\otimes\mathbb{I}\otimes\Lambda_3^-}{(M+\Omega)}
\\
&+\frac{\Lambda_1^{+++}}{(M-\Omega_1)}\left[\gamma^0\otimes\gamma^0\otimes\mathbb{I}\right]\left[A_{i_1}(\bar{M})\cdots A_{i_n}(\bar{M})\right]_{p_\xi^0=-\frac{1}{2}(M-\omega_3)+\omega_1,\ p_\eta^0=M-\omega_3}\frac{\mathbb{I}\otimes\mathbb{I}\otimes\Lambda_3^-}{2\omega_3}
\\
&+\frac{\Lambda^{---}}{(M+\Omega)}\left[\gamma^0\otimes\gamma^0\otimes\mathbb{I}\right]\left[A_{i_1}(\bar{M})\cdots A_{i_n}(\bar{M})\right]_{p_\xi^0=-\frac{1}{2}(M+\omega_3)-\omega_1,\ p_\eta^0=M+\omega_3}\left.\frac{\mathbb{I}\otimes\mathbb{I}\otimes\Lambda_3^+}{2\omega_3}\right\}
\\
&\qquad\left[\mathbb{I}\otimes\mathbb{I}\otimes\gamma^0\right]\Gamma^{\Lambda}_{M}(\boldsymbol{p_\xi},\boldsymbol{p_\eta})
\end{aligned}
\tag{B.7}
$$

We used the shorthand notations $\Lambda^{\pm\pm\pm} := \Lambda_1^{\pm} \otimes \Lambda_2^{\pm} \otimes \Lambda_3^{\pm}$ and $\Omega := \omega_1 + \omega_2 + \omega_3$. Note the structure of this result. The first two terms involve only positive and negative energy projectors respectively whereas in the last two terms mixing occurs. Let us first concentrate on the first two terms and evaluate the operator product $A_{i_1}(\bar{M}) \cdots A_{i_n}(\bar{M})$ at the respective pole positions in p_ξ^0 and p_η^0. We have to be careful here because $A_i(\bar{M})$ contains derivatives with respect to p_ξ^i and p_η^i. To account for that we have to subtract $\frac{\partial p_\xi^0}{\partial p_\xi^i}\frac{\partial}{\partial p_\xi^0} + \frac{\partial p_\eta^0}{\partial p_\xi^i}\frac{\partial}{\partial p_\eta^0}$ from $\frac{\partial}{\partial p_\xi^i}$ and $\frac{\partial p_\xi^0}{\partial p_\eta^i}\frac{\partial}{\partial p_\xi^0} + \frac{\partial p_\eta^0}{\partial p_\eta^i}\frac{\partial}{\partial p_\eta^0}$ from $\frac{\partial}{\partial p_\eta^i}$ according to the chain rule when we plug in the pole positions:

$$
\begin{aligned}
&A(\bar{M})^i\big|_{p_\xi^0=\pm\frac{1}{2}(\omega_1-\omega_2),\ p_\eta^0=\pm(\omega_1+\omega_2)} \\
&\quad = -\tfrac{1}{M}\Big[p_\xi^i\tfrac{\partial}{\partial p_\xi^0} + p_\xi^0(\tfrac{\partial}{\partial p_\xi^i} - \tfrac{\partial p_\xi^0}{\partial p_\xi^i}\tfrac{\partial}{\partial p_\xi^0} - \tfrac{\partial p_\eta^0}{\partial p_\xi^i}\tfrac{\partial}{\partial p_\eta^0}) + p_\eta^i\tfrac{\partial}{\partial p_\eta^0} + p_\eta^0(\tfrac{\partial}{\partial p_\eta^i} - \tfrac{\partial p_\xi^0}{\partial p_\eta^i}\tfrac{\partial}{\partial p_\xi^0} - \tfrac{\partial p_\eta^0}{\partial p_\eta^i}\tfrac{\partial}{\partial p_\eta^0}) \\
&\qquad\qquad - \tfrac{1}{2}(\alpha^i\otimes\mathbb{1}\otimes\mathbb{1} + \mathbb{1}\otimes\alpha^i\otimes\mathbb{1})\Big]_{p_\xi^0=\pm\frac{1}{2}(\omega_1-\omega_2),\ p_\eta^0=\pm(\omega_1+\omega_2)} \\
&\quad = -\tfrac{1}{M}\Big[p_\xi^0\tfrac{\partial}{\partial p_\xi^i} + p_\eta^0\tfrac{\partial}{\partial p_\eta^i} + (p_\xi^i - p_\xi^0\tfrac{\partial p_\xi^0}{\partial p_\xi^i} - p_\eta^0\tfrac{\partial p_\xi^0}{\partial p_\eta^i})\tfrac{\partial}{\partial p_\xi^0} + (p_\eta^i - p_\xi^0\tfrac{\partial p_\eta^0}{\partial p_\xi^i} - p_\eta^0\tfrac{\partial p_\eta^0}{\partial p_\eta^i})\tfrac{\partial}{\partial p_\eta^0} \\
&\qquad\qquad - \tfrac{1}{2}(\alpha^i\otimes\mathbb{1}\otimes\mathbb{1} + \mathbb{1}\otimes\alpha^i\otimes\mathbb{1})\Big]_{p_\xi^0=\pm\frac{1}{2}(\omega_1-\omega_2),\ p_\eta^0=\pm(\omega_1+\omega_2)}
\end{aligned}
\tag{B.8}
$$

The coefficients of $\frac{\partial}{\partial p_\xi^0}$ and $\frac{\partial}{\partial p_\eta^0}$ vanish:

$$
\begin{aligned}
&\Big[p_\xi^i - p_\xi^0\tfrac{\partial p_\xi^0}{\partial p_\xi^i} - p_\eta^0\tfrac{\partial p_\xi^0}{\partial p_\eta^i}\Big]_{p_\xi^0=\pm\frac{1}{2}(\omega_1-\omega_2),\ p_\eta^0=\pm(\omega_1+\omega_2)} \\
&\qquad = p_\xi^i - \tfrac{1}{4}\Big[(\omega_1-\omega_2)(\tfrac{p_1^i}{\omega_1} + \tfrac{p_2^i}{\omega_2}) + (\omega_1+\omega_2)(\tfrac{p_1^i}{\omega_1} - \tfrac{p_2^i}{\omega_2})\Big] \\
&\qquad = p_\xi^i - \tfrac{1}{2}(p_1^i - p_2^i) \\
&\qquad = 0
\end{aligned}
\tag{B.9}
$$

$$
\begin{aligned}
&\Big[p_\eta^i - p_\xi^0\tfrac{\partial p_\eta^0}{\partial p_\xi^i} - p_\eta^0\tfrac{\partial p_\eta^0}{\partial p_\eta^i}\Big]_{p_\xi^0=\pm\frac{1}{2}(\omega_1-\omega_2),\ p_\eta^0=\pm(\omega_1+\omega_2)} \\
&\qquad = p_\eta^i - \tfrac{1}{2}\Big[(\omega_1-\omega_2)(\tfrac{p_1^i}{\omega_1} - \tfrac{p_2^i}{\omega_2}) + (\omega_1+\omega_2)(\tfrac{p_1^i}{\omega_1} + \tfrac{p_2^i}{\omega_2})\Big] \\
&\qquad = p_\eta^i - (p_1^i + p_2^i) \\
&\qquad = 0.
\end{aligned}
\tag{B.10}
$$

So finally we are left with:

$$
\begin{aligned}
&A^i(\bar{M})\big|_{p_\xi^0=\pm\frac{1}{2}(\omega_1-\omega_2),\ p_\eta^0=\pm(\omega_1+\omega_2)} \\
&\quad = -\tfrac{1}{M}\Big[\pm\tfrac{1}{2}(\omega_1-\omega_2)\tfrac{\partial}{\partial p_\xi^i} \pm (\omega_1+\omega_2)\tfrac{\partial}{\partial p_\eta^i} - \tfrac{1}{2}(\alpha^i\otimes\mathbb{1}\otimes\mathbb{1} + \mathbb{1}\otimes\alpha^i\otimes\mathbb{1})\Big]
\end{aligned}
\tag{B.11}
$$

This result suggests to define:

$$A^i_\pm := -\tfrac{1}{M}\left[\pm\tfrac{1}{2}(\omega_1-\omega_2)\tfrac{\partial}{\partial p^i_\xi} \pm (\omega_1+\omega_2)\tfrac{\partial}{\partial p^i_\eta} - \tfrac{1}{2}(\alpha^i\otimes\mathbb{1}\otimes\mathbb{1} + \mathbb{1}\otimes\alpha^i\otimes\mathbb{1})\right] \quad \text{(B.12)}$$

For the last two terms in (B.7) it must be noted that evaluating $\left[A_{i_1}(\bar{M})\cdots A_{i_n}(\bar{M})\right]_{p^0_\xi=-\frac{1}{2}(M+\omega_3)-\omega_1,\ p^0_\eta=M+\omega_3}$ in the same way leads to difficulties:

$$\left[p^i_\xi - p^0_\xi\tfrac{\partial p^0_\xi}{\partial p^i_\xi} - p^0_\eta\tfrac{\partial p^0_\xi}{\partial p^i_\eta}\right]_{p^0_\xi=-\frac{1}{2}(M\mp\omega_3)\pm\omega_1,\ p^0_\eta=M\mp\omega_3} = p^i_\xi \mp \tfrac{1}{2}(M\mp\omega_3)(\tfrac{p^i_1}{\omega_1}+\tfrac{p^i_3}{\omega_3}) \quad \text{(B.13)}$$

$$\left[p^i_\eta - p^0_\xi\tfrac{\partial p^0_\eta}{\partial p^i_\xi} - p^0_\eta\tfrac{\partial p^0_\eta}{\partial p^i_\eta}\right]_{p^0_\xi=-\frac{1}{2}(M\mp\omega_3)\pm\omega_1,\ p^0_\eta=M\mp\omega_3} = p^i_\eta \mp (M\mp\omega_3)\tfrac{p^i_3}{\omega_3}. \quad \text{(B.14)}$$

After inserting the pole positions the derivatives with respect to p^0_ξ and p^0_η do not vanish. The only way out would be to multiply out $A_{i_1}(\bar{M})\cdots A_{i_n}(\bar{M})$ before integration. Fortunately matrix elements between different energy components vanish both in case of the charge radius and the magnetic moments because there $n \leq 2$. Let us summarize the results of this appendix:

$$\begin{aligned} I = -\bar{\Gamma}^\Lambda_M(\boldsymbol{p_\xi},\boldsymbol{p_\eta})\Bigg\{ & \frac{\Lambda^{+++}}{(M-\Omega)}[\gamma^0\otimes\gamma^0\otimes\mathbb{1}]\left[A^{i_1}_+\cdots A^{i_n}_+\right]\frac{\mathbb{1}\otimes\mathbb{1}\otimes\Lambda^+_3}{(M-\Omega)} \\ & + \frac{\Lambda^{---}}{(M+\Omega)}[\gamma^0\otimes\gamma^0\otimes\mathbb{1}]\left[A^{i_1}_-\cdots A^{i_n}_-\right]\frac{\mathbb{1}\otimes\mathbb{1}\otimes\Lambda^-_3}{(M+\Omega)} \\ & + \text{terms with mixed energy components}\Bigg\}[\mathbb{1}\otimes\mathbb{1}\otimes\gamma^0]\Gamma^\Lambda_M(\boldsymbol{p_\xi},\boldsymbol{p_\eta}). \end{aligned} \quad \text{(B.15)}$$

Let us again emphasize that terms with mixed energy components only appear for $n > 2$.

Appendix C

Tensors, coupling formulas and Wigner-Eckart theorem

C.1 Tensor operators

Commutation relations of an operator with the angular momentum operators define the transformation properties under rotations. One defines a tensor operator of rank k, if its $2k+1$ spherical components satisfy the following commutation rules:

$$\left[J_3, T_q^{[k]}\right] = q\, T_q^{[k]} \tag{C.1a}$$

$$\left[J_\pm, T_q^{[k]}\right] = \sqrt{k(k+1) - q(q\pm 1)}\, T_{q\pm 1}^{[k]} \quad q = -k, ...0, ...k. \tag{C.1b}$$

A tensor operator of rank 1 usually is called a vector operator. Its Cartesian components T^i are related to the spherical components $T_q^{[1]}$ via the following relations:

$$T_\pm^{[1]} = \mp\frac{1}{\sqrt{2}} T_\pm \ = \mp\frac{1}{\sqrt{2}}(T_1 \pm \mathrm{i}\, T_2) \tag{C.2a}$$

$$T_0^{[1]} = T_3. \tag{C.2b}$$

With the aid of eqs. (C.2) and the formula for coupling two tensor operators (C.6) one shows by explicit calculation that the common vector product corresponds to the coupling of two vector operators to an operator of rank 1:

$$(T_1 \times T_2)_q^{[1]} = \frac{\sqrt{2}}{i}\left[T_1^{[1]} \otimes T_2^{[1]}\right]_q^{[1]}. \tag{C.3}$$

On the left hand side it is understood to take the spherical components of the vector product according to the definition (C.2). Likewise one shows that the coupling of two vector operators to a scalar tensor operator corresponds to the usual scalar product of two vector operators:

$$\left[T_1^{[1]} \otimes T_2^{[2]}\right]_0^{[0]} = -\tfrac{1}{\sqrt{3}} \boldsymbol{T_1} \cdot \boldsymbol{T_2} \tag{C.4}$$

C.2 Coupling of angular momenta

Let $|j_1, m_1\rangle$ and $|j_2, m_2\rangle$ be eigenstates to two angular momentum operators $\boldsymbol{j_1}$ and $\boldsymbol{j_2}$ respectively. An eigenstate to $\boldsymbol{J} = \boldsymbol{j_1} + \boldsymbol{j_2}$ is obtained by coupling:

$$|JM\rangle = [|j_1\rangle \otimes |j_2\rangle]^J_M = \sum_{m_1,m_2} \langle j_1 m_1, j_2 m_2 | JM\rangle \, |j_1, m_1\rangle \otimes |j_2, m_2\rangle. \tag{C.5}$$

In the same way tensor operators are coupled:

$$\left[T_1^{[k_1]} \otimes T_2^{[k_2]}\right]^{[k]}_q = \sum_{q_1,q_2} \langle k_1 q_1, k_2 q_2 | kq\rangle \, T_{1\,q_1}^{[k_1]} \otimes T_{2\,q_2}^{[k_2]}. \tag{C.6}$$

The numbers $\langle k_1 q_1, k_2 q_2 | kq\rangle$ are Clebsch-Gordan coefficients which are related to the prominent $3j$ symbols:

$$\begin{pmatrix} j_1 & j_2 & J \\ m_1 & m_2 & -M \end{pmatrix} = \frac{(-1)^{j_1 - j_2 + M}}{\hat{J}} \langle j_1 m_1, j_2 m_2 | JM\rangle, \tag{C.7}$$

where $\hat{J} = \sqrt{2J+1}$ is the root of the multiplicity. The $3j$ symbols fulfill the triangularity relation and the m-selection rule:

$$\begin{pmatrix} j_1 & j_2 & j_3 \\ m_1 & m_2 & m_3 \end{pmatrix} \neq 0 \;\Leftrightarrow\; |j_1 - j_2| \leq J \leq j_1 + j_2 \quad \text{and} \quad m_1 + m_2 + m_3 = 0. \tag{C.8}$$

Moreover we have:

$$\begin{pmatrix} j_1 & j_2 & j_3 \\ 0 & 0 & 0 \end{pmatrix} = 0 \;\Leftrightarrow\; j_1 + j_2 + j_3 \text{ odd}. \tag{C.9}$$

C.3 Wigner-Eckart theorem

The Wigner-Eckart theorem allows to factorize the dependence on the geometry *i.e.* m quantum number of a matrix element of a tensor operator with respect to angular momentum eigenstates into a Clebsch-Gordan coefficient and a so called reduced matrix element:

$$\langle j_1, m_1 | T_q^{[k]} | j_2, m_2\rangle = (-1)^{j_1 - m_1} \begin{pmatrix} j_1 & k & j_2 \\ -m_1 & q & m_2 \end{pmatrix} \langle j_1 || T^{[k]} || j_2\rangle. \tag{C.10}$$

For a matrix element of a scalar operator one thus obtains:

$$\langle j, m | T_0^{[0]} | j', m'\rangle = \frac{1}{\hat{j}} \, \delta_{jj'} \, \delta_{mm'} \, \langle j || T^{[0]} || j\rangle. \tag{C.11}$$

The reduced matrix element of a tensor product of tensor operators acting on different spaces can be decomposed:

$$\begin{aligned} &\langle j_1, j_2; J || \left[T_1^{[k_1]} \otimes T_2^{[k_2]}\right]^{[l]} || j_1', j_2', J'\rangle \\ &\qquad = \hat{J}\, \hat{l}\, \hat{J}' \begin{Bmatrix} j_1 & j_2 & J \\ j_1' & j_2' & J' \\ k_1 & k_2 & l \end{Bmatrix} \langle j_1 || T_1^{[k_1]} || j_1'\rangle \, \langle j_2 || T_2^{[k_2]} || j_2'\rangle \end{aligned} \tag{C.12}$$

If both operators however act on the same space, the following identity holds:

$$\langle j|| \left[T_1^{[k_1]} \otimes T_2^{[k_2]}\right]^{[l]} ||j'\rangle = (-1)^{j+l+j'}\, \hat{l} \sum_{\alpha} \left\{ \begin{array}{ccc} j' & j & l \\ k_1 & k_2 & \alpha \end{array} \right\} \langle j||T_1^{[k_1]}||\alpha\rangle \, \langle \alpha||T_2^{[k_2]}||j'\rangle. \tag{C.13}$$

If the states are characterized by additional quantum numbers, α is a multi-index which is summed over. In eqs. (C.12) and (C.13) the the so called $9j$ and 6 symbols respectively appear which are defined by the coupling of four and three angular momentum eigenstates respectively.

Appendix D

Numerical implementation

D.1 General remarks

The numerical implementation of the computation of magnetic moments according to eq. (3.31) has been described in some detail in ref. [16]. We thus want to add some remarks here that are specific to the numerics of the charge radius. The operator that is actually implemented is the one that we obtained before symmetrizing over the three quarks, *i.e.* eq. (2.46) with $\hat{r}^2$ defined in eq. (2.47). This operator is rewritten as a sum of products of scalar tensor operators according to the following identity:

$$\begin{aligned}
&\left[\tfrac{1}{2}(\omega_1-\omega_2)\boldsymbol{\nabla}_{\boldsymbol{p_\xi}}+(\omega_1+\omega_2)\boldsymbol{\nabla}_{\boldsymbol{p_\eta}}+\frac{\boldsymbol{p_1}}{2\omega_1}+\frac{\boldsymbol{p_2}}{2\omega_2}\right]^2 \\
&\qquad=\tfrac{1}{4}(\omega_1-\omega_2)\Delta_{p_\xi}(\omega_1-\omega_2)+(\omega_1+\omega_2)\Delta_{p_\eta}(\omega_1+\omega_2) \\
&\quad+\tfrac{1}{2}(\omega_1-\omega_2)\boldsymbol{\nabla}_{\boldsymbol{p_\xi}}\cdot\boldsymbol{\nabla}_{\boldsymbol{p_\eta}}(\omega_1-\omega_2)+\tfrac{1}{2}(\omega_1+\omega_2)\boldsymbol{\nabla}_{\boldsymbol{p_\xi}}\cdot\boldsymbol{\nabla}_{\boldsymbol{p_\eta}}(\omega_1+\omega_2) \\
&\qquad+\frac{3}{2}\left(\frac{|\boldsymbol{p_1}|^2}{\omega_1^2}+\frac{|\boldsymbol{p_2}|^2}{\omega_2^2}\right)+\frac{\boldsymbol{p_1}\cdot\boldsymbol{p_2}}{\omega_1\omega_2}-3. \qquad \text{(D.1)}
\end{aligned}$$

Owing to a better readability we have omitted the arguments of the relativistic kinetic energies $\omega_1(\boldsymbol{p_1})$ and $\omega_2(\boldsymbol{p_2})$. This version has the advantage, that there are no first order derivatives and thus no scalar products between a momentum and a derivative with respect to a momentum. We may then compute the expectation value of each term in eq. (D.1) by inserting complete sets of states at the appropriate places, such that only matrix elements of scalar operators appear.

D.2 Dependence on the oscillator parameter

As has been described in refs. [16, 48, 49] the Salpeter amplitudes are expanded in a basis of the harmonic three-particle oscillator, whose radial part is given by the product $R_{n_\xi l_\xi}(\beta|\boldsymbol{p_\xi}|)R_{n_\eta l_\eta}(\beta|\boldsymbol{p_\eta}|)$ with the radial functions of the harmonic one-particle

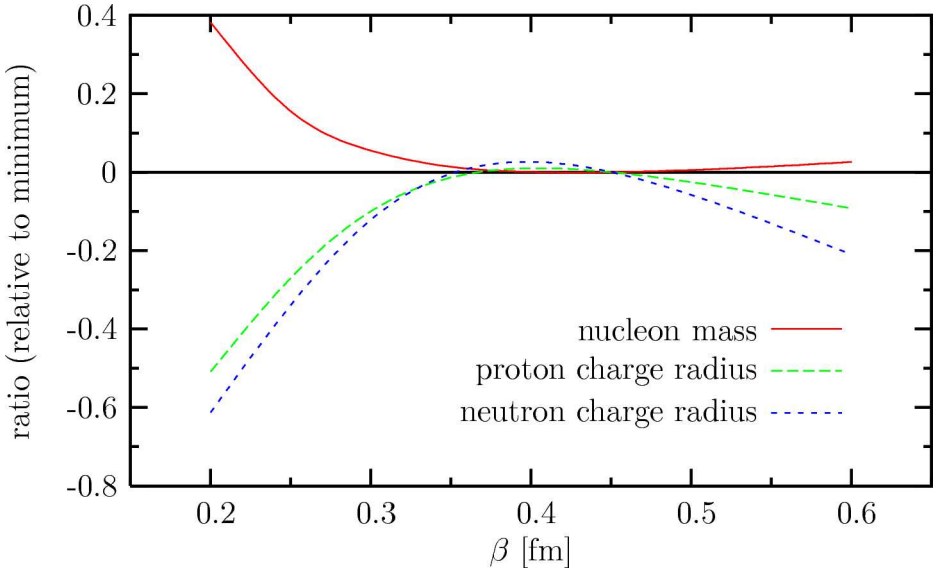

Figure D.1: Dependence of nucleon mass and charge radii on the β-parameter. The variation is relating to the mass minimum at $\beta = 0.45\,\mathrm{fm}$.

oscillator defined by:

$$R_{n_\xi l_\xi}(\beta|\boldsymbol{p_\xi}|) = N_{n_\xi l_\xi} \sum_{\mu=0}^{n} c^{\mu}_{n_\xi l_\xi} (\beta|\boldsymbol{p_\xi}|)^{2\mu+l} e^{-\frac{1}{2}(\beta|\boldsymbol{p_\xi}|)^2} \tag{D.2a}$$

$$R_{n_\eta l_\eta}(\beta|\boldsymbol{p_\eta}|) = N_{n_\eta l_\eta} \sum_{\mu=0}^{n} c^{\mu}_{n_\eta l_\eta} (\beta|\boldsymbol{p_\eta}|)^{2\mu+l} e^{-\frac{1}{2}(\beta|\boldsymbol{p_\eta}|)^2}, \tag{D.2b}$$

where N_{nl} are suitable normalization coefficients and c^{μ}_{nl} summation coefficients. The scale of this oscillator is set by the so called oscillator parameter β. Since the expansion of the Salpeter amplitudes is cut at some finite basis size, which is characterized by the number of oscillator shells, the solutions of the Salpeter equation depend parametrically on the oscillator parameter. The Salpeter equation can be formulated as a variational problem with respect to this parameter (see ref. [48]). One thus has to find a β, such that the mass eigenvalues are minimized. The quality of the approximation can then be checked by plotting the mass as a function of the oscillator parameter as done in fig. D.1. For an infinite basis size the mass does not depend on the variational parameter. For a finite basis size one should see a plateau, which is the broader, the higher the basis size has been chosen. Since we also expect that the charge radius depends on the particular choice of the oscillator parameter, because it directly sets the length scale for the basis functions, we have to check, that it does not vary to much in the region of the mass plateau. From fig. D.1 we see, that the variation of both radii over the mass plateau is in the percent region, related to the values at the mass minimum. The dependence of the neutron charge radius is stronger by about a factor of two compared to that of the proton, which may be due to its smallness.

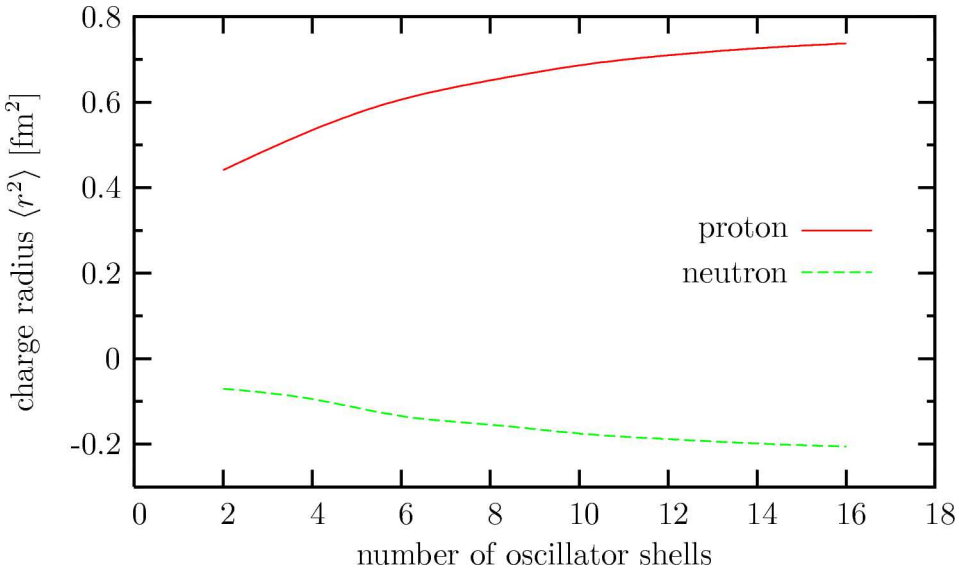

Figure D.2: Charge radii of proton and neutron as a function of the number of oscillator shells to test the effects of a finite basis.

D.3 Testing the convergence

Apart from the analysis above, which studied the dependence of the charge radii on the oscillator parameter, we have to check, if the number of basis states is sufficient to approximate the Salpeter amplitudes well enough. Related to the charge radius this means that its value should converge to some number with increasing basis size. The size of the special oscillator basis that was numerically implemented to approximate the Salpeter amplitudes is expressed in the number of oscillator shells that have been taken into account. The actual number of basis states depends quadratically on the number of oscillator shells and is moreover also a function of the baryons total spin. In fig. D.2 we have plotted the nucleon charge radii as a function of the number of oscillator shells. We see that both radii indeed converge to within a few percent at 16 oscillator shells. The differences from 14 to 16 oscillator shells are 1.6 % in the proton radius and 3.5 % in the neutron radius.

D.4 Concluding remarks

The preceding discussions on the dependence of the charge radii on the oscillator parameter and the basis size shows, that their numerical values can be considered stable. However we must assign a numerical uncertainty of roughly $\pm 5\,\%$ to the results to account for the finite basis size and the induced dependence on the oscillator parameter and the number of oscillator shells.

Bibliography

[1] J. Gasser and H. Leutwyler, Annals Phys. **158** (1984) 142; Nucl. Phys. B **250** (1985) 465.

[2] V. Bernard, N. Kaiser and U.-G. Meißner, Int. J. Mod. Phys. E **4** (1995) 193 [arXiv:hep-ph/9501384].

[3] G. 't Hooft, Nucl. Phys. B **72** (1974) 461.

[4] G. 't Hooft, Phys. Rept. **142** (1986) 357.

[5] U. Löring, K. Kretzschmar, B. C. Metsch and H.-R. Petry, Eur. Phys. J. A **10** (2001) 309 [arXiv:hep-ph/0103287].

[6] U. Löring, B. C. Metsch and H.-R. Petry, Eur. Phys. J. A **10** (2001) 395 [arXiv:hep-ph/0103289].

[7] U. Löring, B. C. Metsch and H.-R. Petry, Eur. Phys. J. A **10** (2001) 447 [arXiv:hep-ph/0103290].

[8] E. E. Salpeter and H. A. Bethe, Phys. Rev. **84** (1951) 1232.

[9] E. E. Salpeter, Phys. Rev. **87** (1952) 328.

[10] R. Ricken, M. Koll, D. Merten and B. C. Metsch, Eur. Phys. J. A **18** (2003) 667 [arXiv:hep-ph/0302124].

[11] D. Merten, U. Löring, K. Kretzschmar, B. Metsch and H.-R. Petry, Eur. Phys. J. A **14** (2002) 477 [arXiv:hep-ph/0204024].

[12] T. Van Cauteren, D. Merten, T. Corthals, S. Janssen, B. Metsch, H.-R. Petry and J. Ryckebusch, Eur. Phys. J. A **20** (2004) 283 [arXiv:nucl-th/0310058].

[13] S. Migura, PhD thesis, University of Bonn, in progress.

[14] M. Kotulla *et al.*, Phys. Rev. Lett. **89** (2002) 272001 [arXiv:nucl-ex/0210040].

[15] S. Eidelman *et al.*, Phys. Lett. B592, 1 (2004).

[16] Chr. Haupt, "Elektromagnetische Momente der Baryonen im Rahmen der Bethe-Salpeter Gleichung", Diploma thesis, University of Bonn, TK-02-06 (2002).

[17] D. Lurié, *Particles and Fields*, Interscience Publishers, Bristol (1968).

[18] F. J. Dyson, Phys. Rev. **75** (1949) 1736.

[19] U. Löring, "A Covariant Quark Model of Baryons with Instanton-induced forces", PhD thesis, University of Bonn, TK-01-02, (2001).

[20] G. 't Hooft, Phys. Rev. D **14** (1976) 3432 [Erratum-ibid. D **18** (1978) 2199].

[21] M. A. Shifman, A. I. Vainshtein and V. I. Zakharov, Nucl. Phys. B **163** (1980) 46.

[22] M. E. Peskin and D. V. Schroeder, "An Introduction to Quantum Field Theory", Westview Press (1995).

[23] I. Eschrich *et al.* [SELEX Collaboration], Phys. Lett. B **522** (2001) 233 [arXiv:hep-ex/0106053].

[24] M. I. Adamovich *et al.* [WA89 Collaboration], Eur. Phys. J. C **8** (1999) 59.

[25] B. Kubis and U.-G. Meißner, Eur. Phys. J. C **18** (2001) 747 [arXiv:hep-ph/0010283].

[26] K. Berger, R. F. Wagenbrunn and W. Plessas, Phys. Rev. D **70** (2004) 094027 [arXiv:nucl-th/0407009].

[27] J. B. Zhang, P. O. Bowman, D. B. Leinweber, A. G. Williams and F. D. R. Bonnet [CSSM Lattice collaboration], Phys. Rev. D **70** (2004) 034505 [arXiv:hep-lat/0301018].

[28] H. D. Politzer, Nucl. Phys. B **117** (1976) 397.

[29] R. Beck [Crystal Ball and A2 Collaborations], "Recent results and future plans from MAMI", *Prepared for 32nd International Workshop on Gross Properties of Nuclei and Nuclear Excitation: Probing Nuclei and Nucleons with Electrons and Photons (Hirschegg 2004), Hirschegg, Austria, 11-17 Jan 2004*

[30] B. M. K. Nefkens *et al.*, Phys. Rev. D **18** (1978) 3911.

[31] A. Bosshard *et al.*, Phys. Rev. D **44** (1991) 1962.

[32] N. B. Wallace *et al.*, Phys. Rev. Lett. **74** (1995) 3732.

[33] H. T. Diehl *et al.*, Phys. Rev. Lett. **67** (1991) 804.

[34] D. A. Varshalovich, A. N. Moskalev, V. K. Khersonskii, *Quantum Theory of Angular Momentum*, World Scientific Publishing Co. Pte. Ltd., Singapur, first reprint(1989).

[35] L. C. Biedenharn, H. Van Dam, *Quantum Theory of Angular Momentum*, Academics Press, New York and London (1965).

[36] J. Friedrich and T. Walcher, Eur. Phys. J. A **17** (2003) 607 [arXiv:hep-ph/0303054].

[37] J. Bermuth *et al.*, Phys. Lett. B **564** (2003) 199 [arXiv:nucl-ex/0303015].

[38] G. Warren *et al.* [Jefferson Lab E93-026 Collaboration], Phys. Rev. Lett. **92**, 042301 (2004) [arXiv:nucl-ex/0308021].

[39] B. Plaster *et al.* [Jefferson Laboratory E93-038 Collaboration], Phys. Rev. Lett. **91**, 122002 (2003) [arXiv:nucl-ex/0511025].

[40] S. Capstick and B. D. Keister, Phys. Rev. D **51**, 3598 (1995) [arXiv:nucl-th/9411016].

[41] V. V. Frolov *et al.*, Phys. Rev. Lett. **82** (1999) 45 [arXiv:hep-ex/9808024].

[42] F. Foster and G. Hughes, Rept. Prog. Phys. **46** (1983) 1445.

[43] S. Stein *et al.*, Phys. Rev. D **12** (1975) 1884.

[44] W. Bartel *et al.*, Phys. Lett. B **28** (1968) 148.

[45] L. Tiator, D. Drechsel, S. Kamalov, M. M. Giannini, E. Santopinto and A. Vassallo, Eur. Phys. J. A **19** (2004) 55 [arXiv:nucl-th/0310041].

[46] M. Ferraris, M. M. Giannini, M. Pizzo, E. Santopinto and L. Tiator, Phys. Lett. B **364** (1995) 231.

[47] I. G. Aznauryan, V. D. Burkert, G. V. Fedotov, B. S. Ishkhanov and V. I. Mokeev, Phys. Rev. C **72** (2005) 045201 [arXiv:hep-ph/0508057].

[48] U. Löring, "Instantoneffekte in einem kovarianten Quarkmodell der Baryonen", Diploma thesis, University of Bonn, TK-97-03 (1997).

[49] D. Merten, "Hadron Form Factors and Decays", PhD thesis, University of Bonn, TK-02-03 (2002)

Danksagung

Mein Dank geht zunächst an Prof. Dr. Herbert-R. Petry für die Überlassung des Themas aber auch für Anregungen und Ratschläge, welche nicht unwesentlich zum Gelingen dieser Arbeit beigetragen haben. Auch Herrn Priv.-Doz. Dr. Bernard C. Metsch bin ich zu Dank für mancherlei Vorschläge und Diskussionen aber auch für die Durchsicht des Manuskriptes verpflichtet. Herrn Prof. Dr. Ulf-G. Meißner danke ich für die Übernahme des Koreferates. Herrn Prof. Dr. Reinhard Beck und Herrn Prof. Dr. Ulrich Klein als fachnahe bzw. fachangrenzende Mitglieder der Promotionskommission gebührt ebenfalls mein Dank.

Ich habe die Atmosphäre im ehemaligen Institut für theoretische Kernphysik und der jetzigen Theorieabteilung des Helmholtz-Institutes für Strahlen- und Kernphysik immer als freundlich und sehr angenehm empfunden. Besonders bin ich meinem Kollegen Herrn Sascha Migura für fachliche, manchmal auch außerfachliche Gespräche dankbar.

Der Deutschen Forschungsgemeinschaft danke ich für finanzielle Unterstützung im Rahmen des Sonderforschungsbereiches/Transregio 16 “Subnuclear Structure of Matter”, ebenso wie der Wilhelm und Else Heraeus-Stiftung für Förderbeiträge zur Teilnahme an den Frühjahrstagungen der Deutschen Physikalischen Gesellschaft.

Schließlich bedanke ich mich ganz herzlich bei meinen Eltern für die Unterstützung während meines Studiums und der Promotion.